1981

Tubular electrodes in flow injection analysis

Peter Lawrence Meschi
Iowa State University

MESCHI, PETER LAWRENCE

TUBULAR ELECTRODES IN FLOW INJECTION ANALYSIS

Iowa State University PH.D. 1981

PLEASE NOTE:

In all cases this material has been filmed in the best possible way from the available copy. Problems encountered with this document have been identified here with a check mark __√__.

1. Glossy photographs or pages _____
2. Colored illustrations, paper or print _____
3. Photographs with dark background _____
4. Illustrations are poor copy _____
5. Pages with black marks, not original copy _____
6. Print shows through as there is text on both sides of page _____
7. Indistinct, broken or small print on several pages ✓
8. Print exceeds margin requirements _____
9. Tightly bound copy with print lost in spine _____
10. Computer printout pages with indistinct print _____
11. Page(s) _____ lacking when material received, and not available from school or author.
12. Page(s) _____ seem to be missing in numbering only as text follows.
13. Two pages numbered _____. Text follows.
14. Curling and wrinkled pages _____
15. Other _____

Tubular electrodes in flow injection analysis

by

Peter Lawrence Meschi

A Dissertation Submitted to the

Graduate Faculty in Partial Fulfillment of the

Requirements for the Degree of

DOCTOR OF PHILOSOPHY

Department: Chemistry
Major: Analytical Chemistry

Approved:

Signature was redacted for privacy.

In Charge of Major Work

Signature was redacted for privacy.

For the Major Department

Signature was redacted for privacy.

For the Graduate College

Iowa State University
Ames, Iowa

1981

TABLE OF CONTENTS

LIST OF FIGURES

LIST OF TABLES

I. INTRODUCTION

Flow Injection Analysis (FIA) has been recently introduced as a new approach to automated chemical analysis (1). In FIA, a small volume of sample is injected into a fluid stream which contains a chemical reagent. The fluid stream carries the sample through the analyzer where, by means of a suitable transducer, the product of the reaction between the analyte in the sample and the reagent in the fluid stream produces an electrical signal proportional to the concentration of the analyte. FIA has been most successfully applied to simple colorimetric procedures, although the technique is being adapted to more complex means of detection. Principles, applications, and trends in Flow Injection Analysis have been discussed in a recent review article by Ruzicka and Hansen (2).

This thesis is primarily concerned with the use of a flow-through, tubular electrode as an amperometric detector for FIA. The use of an electrochemical detector is of mutual benefit for the continued development of FIA and electroanalytical chemistry. Electrochemical detection offers simplicity to FIA in that the analyte can often be detected directly without the reaction of the sample with a reagent. This eliminates the problem associated with designing the apparatus so that there is enough time for the reaction to occur before the sample reaches the detector. Electrochemical detection also offers selectivity in that only electroactive species are detected. Selectivity is particularly important in the analysis of complex samples and can be controlled to some extent by the choice of the potential of the electrode and the mode of detection (3). FIA with electrochemical detection has

some advantages over more conventional methods of electrochemical analysis, i.e., polarography, where the sample is manually introduced and removed from the electrochemical cell. With FIA, the electrochemical analysis of a large number of samples can be automated and performed in a short time ($\sim$100-200 samples h^{-1}) with moderately high precision. Also, electrochemistry is performed on a small volume of sample; typically, 0.100 mL of sample or less is used in FIA while at least 10-25 mL of sample is required for a voltammetric cell.

The amperometric response of a flow-through electrode in FIA differs from the response of a flow-through electrode in more typical applications. Usually, in electroanalytical applications, a sample containing a uniform concentration of analyte is passed through the electrode at a constant flow rate for an extended length of time producing an amperometric response that is constant and proportional to the concentration of the analyte in the sample. This amperometric response is referred to as a "steady-state current" since the response of the electrode does not vary with time. In FIA, the sample is dispersed, because of the small volume of sample and the motion of the fluid stream, to a degree that a steady-state current is never achieved. The amperometric response of the electrode appears as a peak-shaped function of time, the height of which is taken to be proportional to the concentration of the analyte in the sample. The short time and small volume of sample in FIA are benefits of measuring a nonsteady-state signal. However, a nonsteady-state signal is dependent on the extent of the dispersion of the sample and factors which affect dispersion also affect the amperometric response of the

electrode. The extent of dispersion must be the same for each sample if the results of the analysis are to be accurate.

Unfortunately, to date, the effect of the dispersion of the sample on the response of the electrochemical detector has been overlooked. The characteristics of an electrode are determined for the case of a steady-state current and the assumption is made that the electrode will behave in a similar fashion for FIA. In the research reported in this thesis, the effect of dispersion on the amperometric response of a tubular electrode was studied. Equations describing the dispersion of a sample in FIA were developed and applied to tubular electrodes to predict the amperometric and coulometric response of the electrode to a dispersed sample. In this thesis, the theory is compared to experimental results. The factors that influence the response of the electrode, the limitations of the theory, and the relative merits of the use of peak current and peak area as analytical measurements are discussed. The steady-state behavior of the tubular electrode is also described and a comparison between the experimental and theoretical behavior of the tubular electrode is made.

II. INSTRUMENTATION AND APPARATUS

A. Electronic Instrumentation

A block diagram of the electronic instrumentation is shown in Figure II-1. Four modules comprised the instrument: a Timing Module, a Potential Control Module, a Waveform Generator, and a Data Acquisition Module. The instrument was designed with an emphasis on versatility of operation. By making the appropriate connections between modules and the adjustment of the controls on the modules, a variety of DC and pulsed-potential electrochemical techniques were performed.

1. Timing Module

The Timing Module generated a sequence of pulses which controlled and coordinated the potential of the working electrode and the measurement of cell current in voltammetric and amperometric experiments. The duration of each pulse was variable and independent of the duration of other pulses. The control of an event was not inherently delegated to a particular pulse by the design of the module but assigned to a pulse by the operator through connections made external to the module. These features provided flexibility in the control and timing of events.

A block diagram of the Timing Module is shown in Figure II-2. The module was designed to produce a sequence of seven pulses. Each pulse was generated by a monostable circuit constructed from a 555 Timer integrated circuit (Figure II-3). The monostable was compatible with the family of digital circuits known as TTL and responded to, and produced, digital signals corresponding to TTL logic levels (HI = +5 V,

Figure II-1. Block diagram of pulse voltammograph

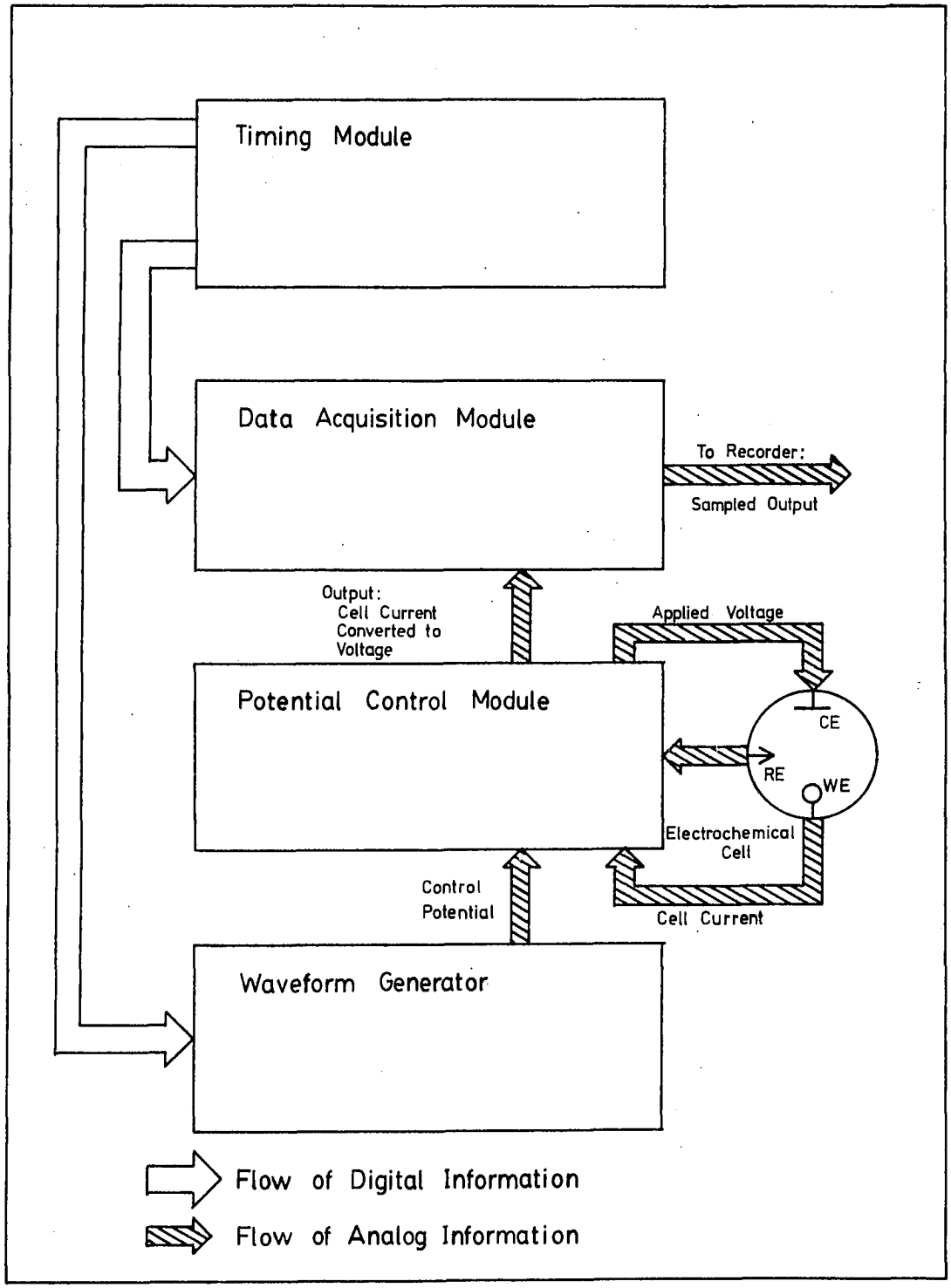
Timing Module
Data Acquisition Module
To Recorder:
Sampled Output
Output:
Cell Current
Converted to
Voltage
Applied Voltage
Potential Control Module
CE
RE
WE
Electrochemical
Cell
Control
Potential
Cell Current
Waveform Generator
Flow of Digital Information
Flow of Analog Information

Figure II-2. Block diagram of Time Module

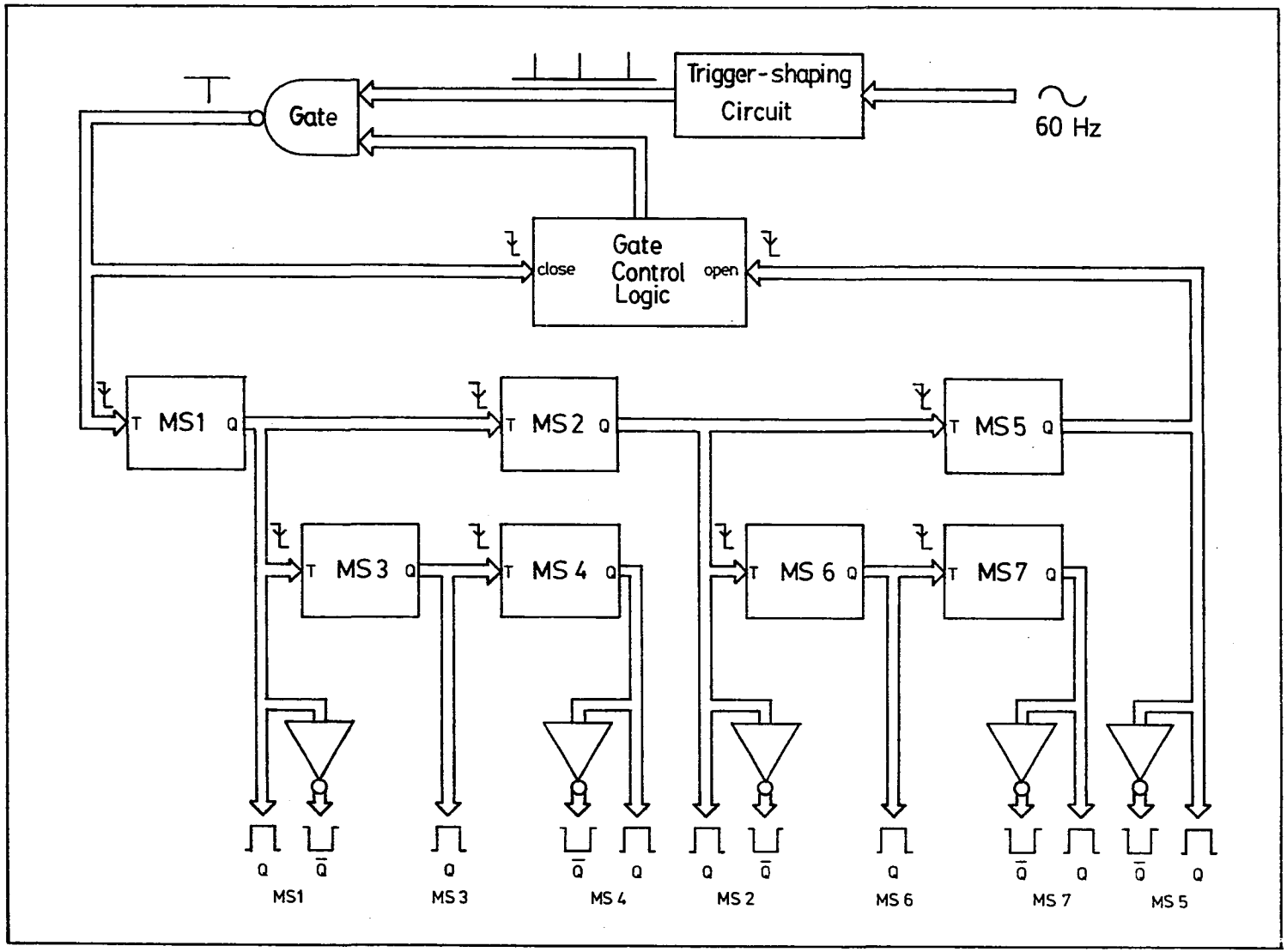
Trigger-shaping Circuit
60 Hz
Gate
close
Gate Control Logic
open
T MS1 Q
T MS2 Q
T MS5 Q
T MS3 Q
T MS4 Q
T MS6 Q
T MS7 Q
Q
Q̄
MS1
MS3
MS4
MS2
MS6
MS7
MS5

Figure II-3. Diagram of 555 Timer in monostable configuration

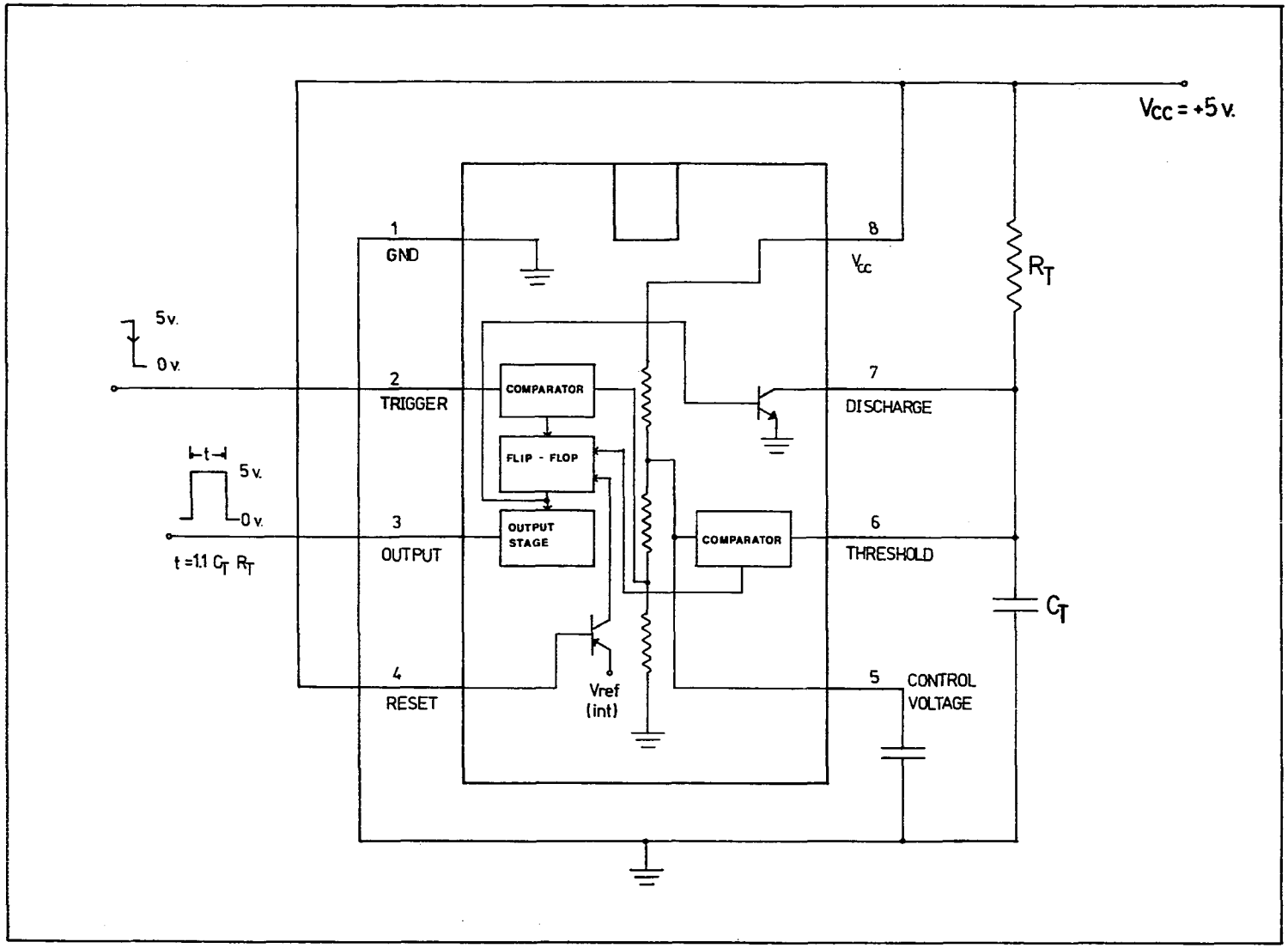
Vcc = +5 v.
1
GND
8
Vcc
RT
5v.
0 v.
2
TRIGGER
COMPARATOR
7
DISCHARGE
FLIP - FLOP
t
5 v.
0 v.
3
OUTPUT
OUTPUT STAGE
COMPARATOR
6
THRESHOLD
t = 1.1 CT RT
CT
4
RESET
Vref (int)
5
CONTROL VOLTAGE

LO = 0 V). A HI-to-LO transition at the trigger terminal of the monostable initiated a LO-to-HI transition at the output terminal. The duration of the HI level, i.e., the pulse width, was determined by the values of an external resistance, R_t, and an external capacitance, C_t, as shown by Equation II-1.

$$\text{Pulse width} = 1.1\ R_tC_t \tag{II-1}$$

For each monostable, R_t was 9.09 kΩ in series with a 100-kΩ, 10-turn potentiometer. The potentiometers were equipped with 10-turn digital dials. The dial setting, D, indicated the effective resistance, R_p, of the potentiometer as a percentage of the nominal resistance, R_n, as shown by Equation II-2.

$$D/100 = R_p/R_n \tag{II-2}$$

The timing resistance, R_t, was the sum of the 9.09-kΩ resistance, R_s, in series with R_p. The pulse width, T, as a function of the dial setting is shown in Equation II-3.

$$T = 1.1(R_n/100)C_tD + 1.1\ R_sC_t \tag{II-3}$$

The capacitance, C_t, was selected from five capacitors by way of a rotary switch. With this arrangement, the pulse width of each monostable could be varied from 0.1 ms to 12.0 s over five ranges of C_t.

Because of the large tolerances allowed in the manufacturing of capacitors, each range of each monostable was calibrated to permit the accurate setting of the pulse width. A Heath Universal Digital Instrument was used to measure the pulse width at several dial settings, D, for each range. Since Equation II-3 is linear, the pulse width was plotted

as a function of D and was fitted to a straight line by using the method of linear least squares. The pulse width for a particular set of C_t and D could then be calculated from Equation II-4

$$T = M_{ms,c}D + B_{ms,c} \qquad \text{(II-4)}$$

where $M_{ms,c}$ was the slope of the least-squares fit and $B_{ms,c}$ was the intercept. The subscripts ms and c indicate that each set of M and B values is unique for one range of one monostable. Values of $M_{ms,c}$ and $B_{ms,c}$ are listed in Table II-1.

The sequences of pulses produced by the monostables were organized into three groups. The main sequence was comprised of monostables MS 1, MS 2, and MS 5. The remaining four monostables were arranged into two subsequences with monostables MS 3 and MS 4 in one group and monostable MS 6 and MS 7 in the other. Within a sequence, the trigger terminal of a monostable was connected to the output terminal of the preceding monostable. The HI-to-LO transition at the end of a pulse initiated a new pulse at the output of the following monostable. Thus, once the first monostable in a sequence had been triggered, the following monostables were activated in order of succession upon the termination of the pulse from the preceding monostable.

The subsequences of the pulse trains were branches of the main sequence. The trigger terminal of monostable MS 3, the first monostable of the first subsequence, was connected to the output terminal of monostable MS 1. The trigger terminal of monostable MS 6, the first monostable of the second subsequence, was connected to the output terminal of

Table II-1. Timing constants for the Data Acquisition Module

C_t			Monostables						
μF	Range		MS 1	MS 2	MS 3	MS 4	MS 5	MS 6	MS 7
0.01	1	$M_{ms,c}$ (ms)	0.01073	0.01110	0.01168	0.01085	0.01118	0.01089	0.01141
		$B_{ms,c}$ (ms)	0.0960	0.1004	0.1044	0.0966	0.1005	0.0961	0.1017
0.10	2	$M_{ms,c}$ (ms)	0.1086	0.1122	0.1111	0.1129	0.1157	0.1111	0.1119
		$B_{ms,c}$ (ms)	0.976	1.017	1.007	1.017	1.050	0.990	0.995
1.00	3	$M_{ms,c}$ (ms)	1.071	1.050	1.083	1.111	1.116	1.093	1.089
		$B_{ms,c}$ (ms)	9.56	9.45	9.69	9.79	10.08	9.64	9.65
10.0	4	$M_{ms,c}$ (s)	0.01184	0.01054	0.01043	0.01154	0.01095	0.01200	0.01155
		$B_{ms,c}$ (s)	0.1057	0.0939	0.0946	0.1017	0.0982	0.1051	0.1008
100.0	5	$M_{ms,c}$ (s)	0.1142	0.1130	0.1148	0.1179	0.1162	0.1139	0.1159
		$B_{ms,c}$ (s)	1.021	1.017	1.028	1.049	1.050	1.032	1.028

monostable MS 2. As with a sequence, each subsequence was activated by the output of the preceding monostable.

The cycle of operation was initiated by an external signal at the trigger terminal of monostable MS 1. Trigger signals were produced from a 60-Hz sine wave to help eliminate noise from 60-Hz radiation. The trigger signals comprised a series of pulses which were spaced 16.7 ms apart and had a pulse width of 40 ns. Since the trigger signals had a constant relationship to the phase of the 60-Hz wave, the pulses from the monostables had a constant relationship to the phase of any 60-Hz background noise. The measurement of current, which was controlled by a pulse, was made over the same portion of the 60-Hz wave during each cycle of operation. Changes in values of the current due to the random sampling of the 60-Hz noise were, therefore, eliminated.

The cycle of operation was generally longer than one 60-Hz cycle. To prevent the restarting of the main sequence before the end of the preceding cycle, a NAND gate and logic circuitry were used to control the triggering of monostable MS 1. The trigger-shaping circuit was connected to an input terminal of the NAND gate. The other input terminal of the NAND gate was connected to the logic circuit. A trigger signal could pass through the NAND gate only when the signal from the logic circuit was HI. At the beginning of a cycle of operation, all monostables in the main sequences were deactivated and the gate was open. The first trigger signal to pass through the gate initiated the cycle and informed the logic circuit that the cycle had started. The logic circuit closed the gate to prevent the passage of more trigger signals. The termination of

the pulse from monostable MS 5 informed the logic circuit that the cycle had been completed. The logic circuit then opened the gate. The next trigger signal started the cycle of operation over again. The time relationships between the trigger signals, operation of the gate, and the output of the monostables are summarized in Figure II-4.

Electrical pulses controlled operations of the instrument by the activation of digitally driven analog switches located in the other modules. The monostables of the main sequence were used to control the generation of the potential waveform for voltammetric and amperometric experiments. The monostables of the first and second subsequences were used to control the measurement of current after changes in the potential of the electrode produced by monostables MS 2 and MS 5, respectively. The first monostable in each subsequence was employed to produce a time delay between the beginning of a potential step and the measurement of current. The measurement of current was affected by the second monostable of the subsequence. Analog switches were closed by either a HI or LO level signal depending on the design of the switch. Inverted output, in addition to the noninverted output, was provided for all monostables with the exception of monostables MS 3 and MS 6.

2. Potential Control Module

Housed in the Potential Control Module was a three-electrode potentiostat. The potentiostat maintained a potential difference between the reference and working electrodes in the electrolysis cell equal to a signal voltage applied to the input terminal of the potentiostat. By passing the cell current through the counter and working

Figure II-4. Timing chart

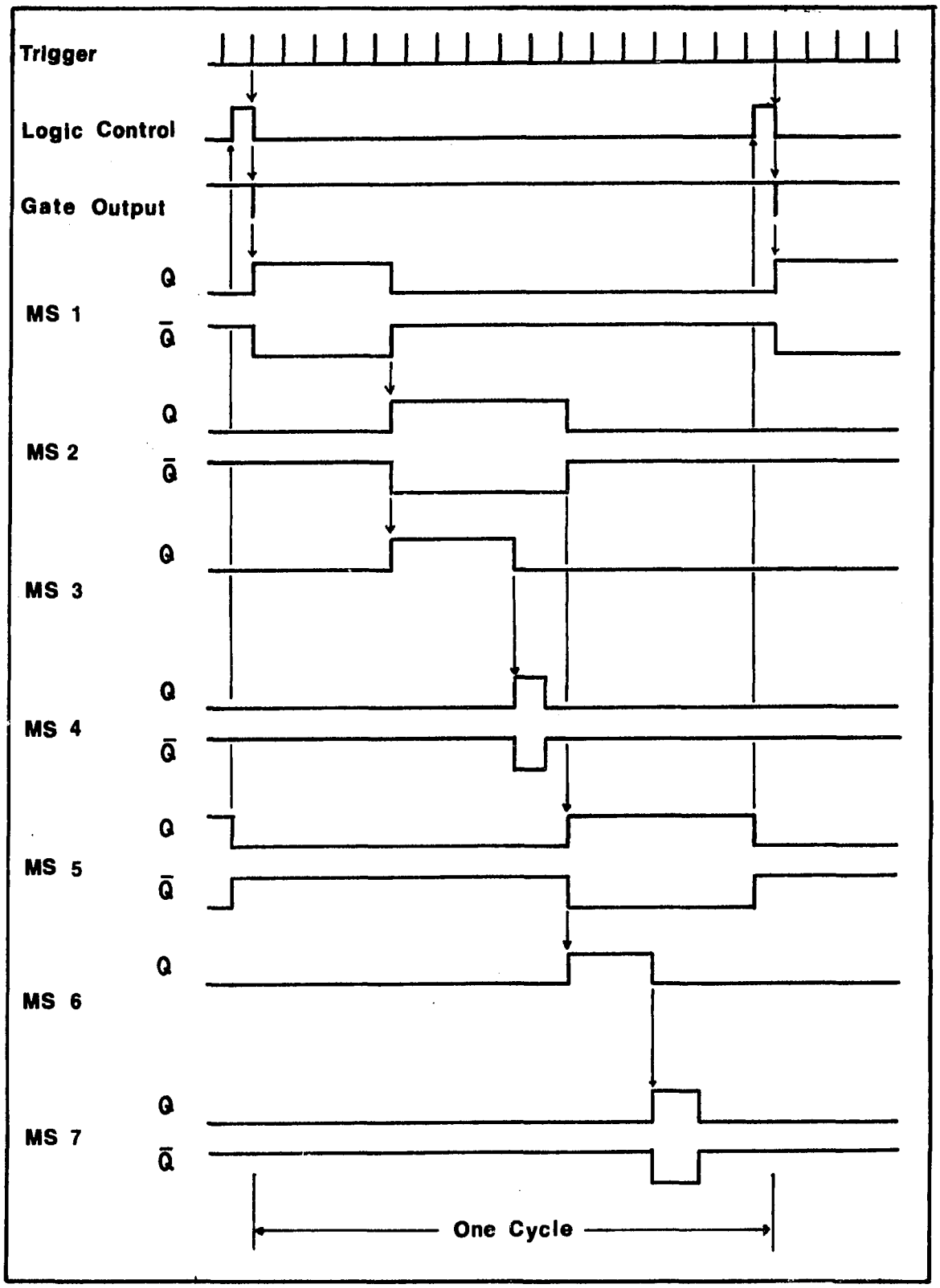
Trigger
Logic Control
Gate Output
MS 1
Q
$\bar{Q}$
MS 2
Q
$\bar{Q}$
MS 3
Q
Q
MS 4
$\bar{Q}$
Q
MS 5
$\bar{Q}$
Q
MS 6
Q
MS 7
$\bar{Q}$
One Cycle

electrodes, the potential was maintained without drawing appreciable current through the reference electrode; thus, errors in the control of potential due to the IR drop across the junction of the reference electrode with the cell were minimized. Cell current was measured by a current-to-voltage converter connected to the working electrode. Circuitry to compensate for constant background current and to integrate the output of the current-to-voltage converter were also included in the Potential Control Module. The circuits in the Potential Control Module were constructed from operational amplifiers according to conventional designs. Details of the design and construction of the Potential Control Module are found in Reference 4.

3. Waveform Generator

The Waveform Generator supplied the voltage signal to the Potential Control Module. The Waveform Generator contained a triangular-waveform generator and three sources of constant voltage. The triangular-waveform generator and each of the voltage sources were connected by analog switches to the input of a summing amplifier. Under the direction of the Timing Module, the analog switches were opened and closed in various sequences and combinations. The potentials at the inputs of the summing amplifier were combined and appeared at the output of the Waveform Generator as a complex waveform. For cyclic voltammetry, a triangular waveform was required. For amperometry, only a signal of constant voltage was required. These simple waveforms were produced by grounding the control input of the analog switch of the triangular-waveform

generator or one of the constant voltage sources. Details of the design and construction of the Waveform Generator are found in Reference 4.

4. Data Acquisition Module

The Data Acquisition Module contained a sample-and-hold circuit. A schematic diagram of the circuit is shown in Figure II-5. The circuit was adapted from a design found in the literature (5).

In experiments where the potential of the electrode was stepped, the cell current changed rapidly as a function of time. The sample-and-hold circuit served as an interface between the current-to-voltage converter and a recording device. The circuit obtained the instantaneous signal at a given time after application of the potential step, and then retained that value until the next sampling period.

The major components of the sample-and-hold circuit were two dual SPST analog switches (AD7513), two operational amplifiers (AD540 and AD503), and a 10.0-μF capacitor. In the output section of the circuit, the 10.0-μF capacitor was connected to the noninverting input terminal of the AD503. The AD503 was used as a potential follower The potential follower served as a high-impedance buffer between the capacitor and a recording device. A recording device could then measure the potential across the capacitor at the output of the follower without causing an appreciable loss of charge from the capacitor and a degradation of the signal. The input section consisted of the AD540 operational amplifier. The AD540 provided a high-impedance input for the sample-and-hold circuit and a low-impedance current source to charge the capacitor. Signal sources were connected to the noninverting input of the AD540.

Figure II-5. Schematic of Data Acquisition Module

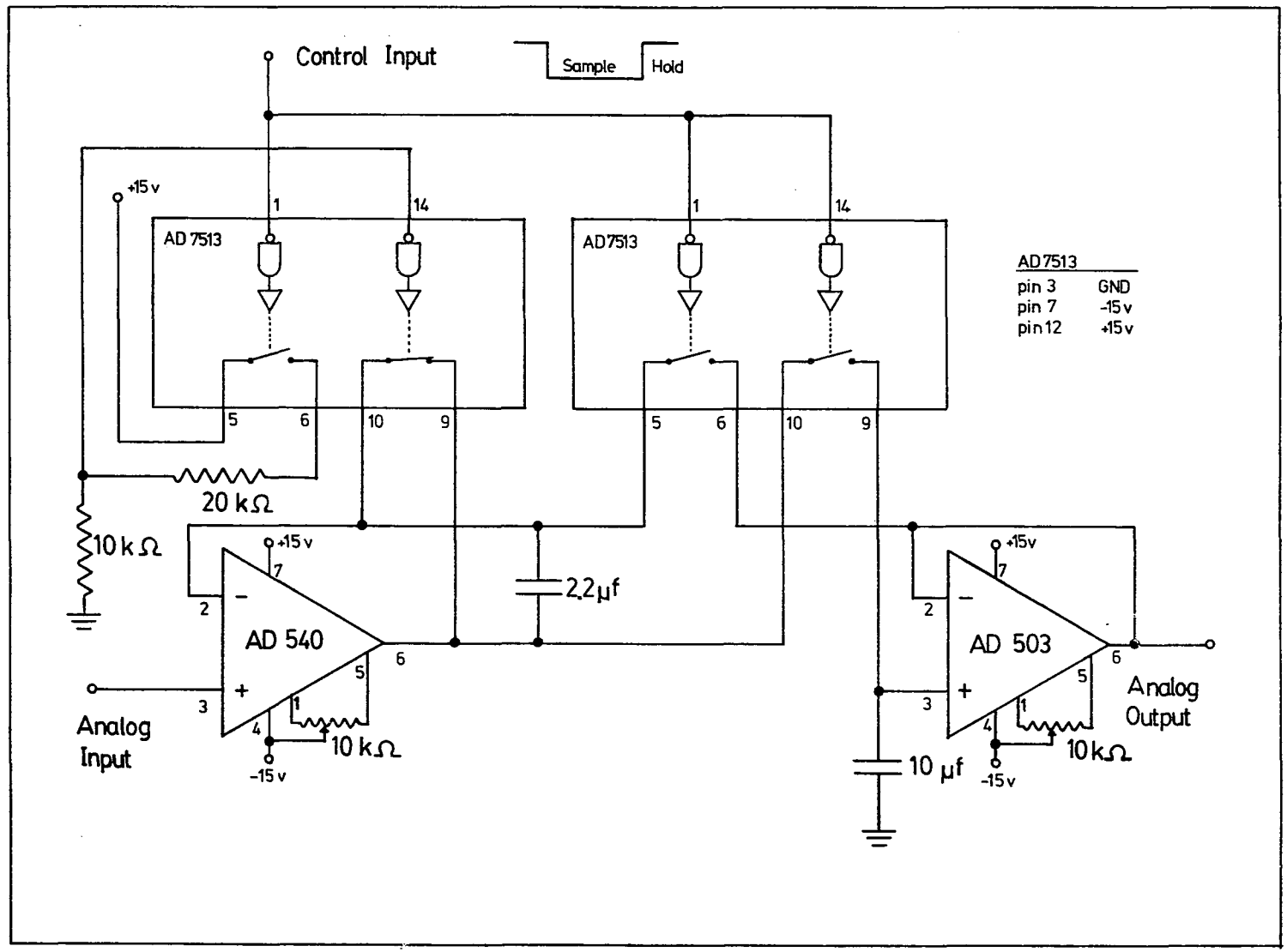
Control Input
Sample
Hold
+15 v
AD 7513
AD7513
1
14
5
6
10
9
AD7513
pin 3 GND
pin 7 -15 v
pin 12 +15 v
20 kΩ
10 kΩ
+15 v
AD 540
2
3
4
5
6
7
Analog Input
10 kΩ
-15 v
2.2µf
AD 503
Analog Output
10 µf

The input and output sections were electrically joined by analog switches. The connection depended on the logic signal at the control input. A LO signal closed the switches to form the "sample" configuration of the circuit. The output of the potential follower was fed back to the inverting input of the AD540. The output terminal of the AD540 was connected to the capacitor and the noninverting input of the potential follower. In this configuration, the AD540 kept the voltage at the output of the sample-and-hold circuit equal to the voltage of the input signal. In the process of maintaining this balance, the 10.0-μF capacitor was charged to the voltage of the input signal. The AD540 was capable of supplying 25 mA of current. This insured the rapid charging of the capacitor and the rapid "tracking" of the input signal inspite of the large capacitor. The 2.2-μF capacitor, connected across the feedback loop, dampened the oscillations and removed high-frequency noise. At the end of the sampling period, a HI logic signal at the control input opened the feedback loop. The capacitor and the output of the follower were then isolated from the AD540 and the input signal. The capacitor retained the last voltage of the sampling period. This voltage remained at the output of the sample-and-hold circuit until the next sampling period. The loss of potential during the holding period was minimized by choosing a capacitor of high quality and of large capacitance, and by using an operational amplifier with a low input bias current.

All solid state components were purchased from Analog Devices, Inc., Norwood, MA. The 10.0-μF capacitor was from Electronics Associates, Inc., Long Branch, NJ. All other components were obtained from local suppliers.

B. Flow Systems

In an experiment where the amperometric response of a flow-through electrode is studied as a function of the flow rate of the fluid stream, the ideal flow system would have the following qualities:

1) The flow system should maintain a constant flow rate throughout an experiment.

2) The flow rate should be easy to regulate and be reproducible from day to day.

3) The flow rate should be steady with a minimum of pulsations.

4) The flow system should have a large eluent reservoir to minimize interruptions during an experiment.

5) The flow system should have a high degree of reliability.

Whether or not a flow system has the above qualities ultimately depends on the design and quality of the pump used in the construction of the flow system. For the experiments in this thesis, three flow systems were developed. One system was based on syringe pumps, another system used a reciprocating pump, and a third system utilized a peristaltic pump.

1. Flow System I

Flow System I, shown schematically in Figure II-6, was constructed from two syringe pumps from Pine Instrument Co., Grove City, PA. These pumps were manufactured with Teflon pistons in precision-bore (1.0-in i.d.) Pyrex cylinders. Each cylinder had a capacity of 100 mL. Leakage of solution at the piston-cylinder interface was prevented by two

Figure II-6. Flow System I

A. Eluent reservoir

B. Syringe pumps

C. Glass T-tube

D. 2-way slider valves

E. T-connector

F. Electrode

G. Potentiostat

H. Recorder

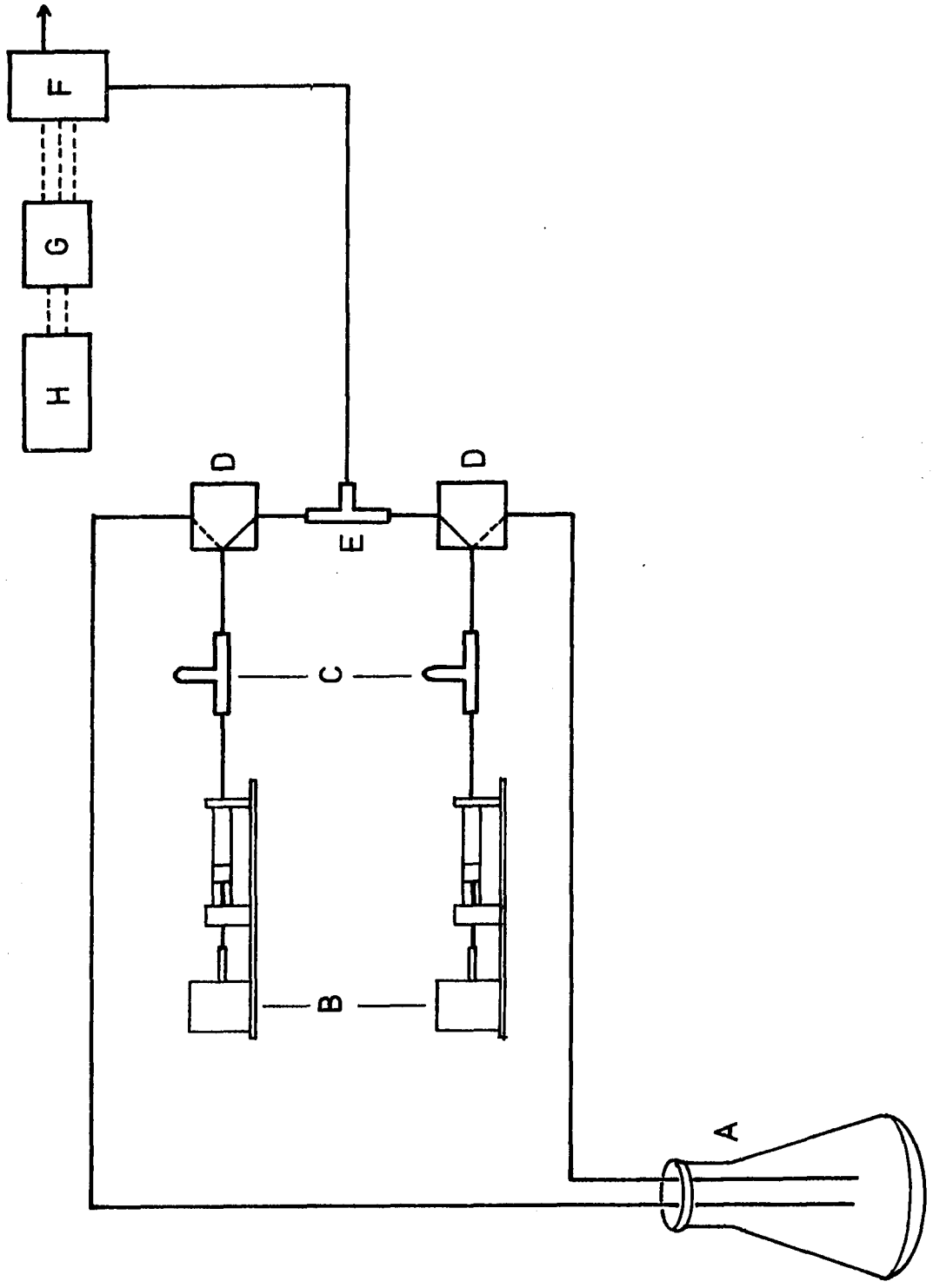
F
G
H
D
D
E
C
B
A

compression seals made from Fetfe, an inert and pliable fluoroelastomer from Ace Glass, Inc., Vineland, NJ. The piston was driven by an electric motor through a screw drive. Flow rate was controlled by the speed of the motor which was set by a 10-turn potentiometer. Motor speed was kept constant by a negative-feedback circuit through a signal from a tachometer mounted on the drive shaft. Each pump produced flow rates of 0.1 - 1.0 mL min^{-1}. When the pumps were operated in parallel, flow rates up to 2.0 mL min^{-1} were obtained. No calibration of the flow rate was necessary. The flow rate was read directly from the dial of the potentiometer. Connections were made with Teflon tubing (0.79-mm i.d.) and polypropylene fittings. The tubing, fittings, valves, and tee were from Altex Scientific, Inc., Berkeley, CA.

The general operating characteristics of the flow system were excellent. Constant flow rates were obtained almost immediately after starting the pumps. Flow rates were easy to adjust and were reproducible from day to day. The limited capacity (100 mL) of the pumps was, however, a distinct drawback. The actual working volume of each pump was 50-60 mL. At the moderate flow rate used in this research, the pumps had to be refilled every 1.0-1.5 h. Refilling the pumps involved shutting the system off, switching the pumps from the detector to the eluent reservoir, then manually cranking the pistons back to their starting position. In addition to the inconvenience of filling the pumps, the operator had to be constantly aware of the volume of the solution remaining in each pump to avoid running out at an inopportune time. The system was best suited to short experiments and was used in the

study of the amperometric response of the tubular electrode under steady-state conditions.

2. Flow System II

Flow System II (Figure II-7) was assembled to overcome the shortcomings of Flow System I. This system incorporated a Milton Roy Model CK Instrument miniPump® purchased from Laboratory Data Control, Riviera Beach, FL. Flow was produced by two reciprocating pistons. Liquid was drawn from the reservoir during the back stroke of each piston and discharged into the flow system on the forward stroke. To smooth the delivery of eluent, the pistons were designed to operate 180° out of phase with each other. Flow rate was controlled by adjustment of the length of the stroke of the pistons and could be varied from 0-6 mL min^{-1}. The length of the stroke was manually adjusted through a micrometer and read as a percentage of the maximum length of the stroke. Flow rates were calibrated by measurement of the volume of a solution (20-30 mL) delivered into a 50 mL buret during a specified time period.

A Model 709 pulseDampener®, also from Laboratory Data Control, was used to smooth the pulsing flow from the pump. The pulse dampener was constructed with an adjustable spring-loaded bellows. Maximum dampening occurred when the spring tension on the bellows equaled the back pressure of the flow system. The bellows were designed to operate at 200-1200 psi. In order to provide sufficient back pressure, 40 ft of 0.10-in i.d. x 1/16-in o.d. stainless steel tubing, Alltech Associates, Arlington Heights, IL, was used as a flow restrictor. Connections between the pump, pulse dampener, and flow restrictor were made with

Figure II-7. Flow System II

A. Eluent reservoir

B. Piston pump

C. Pulse dampener

D. Pressure gauge

E. Flow restrictor

F. Sample-injection valve

G. Sample loop

H. Electrode

I. Potentiostat

J. Recorder

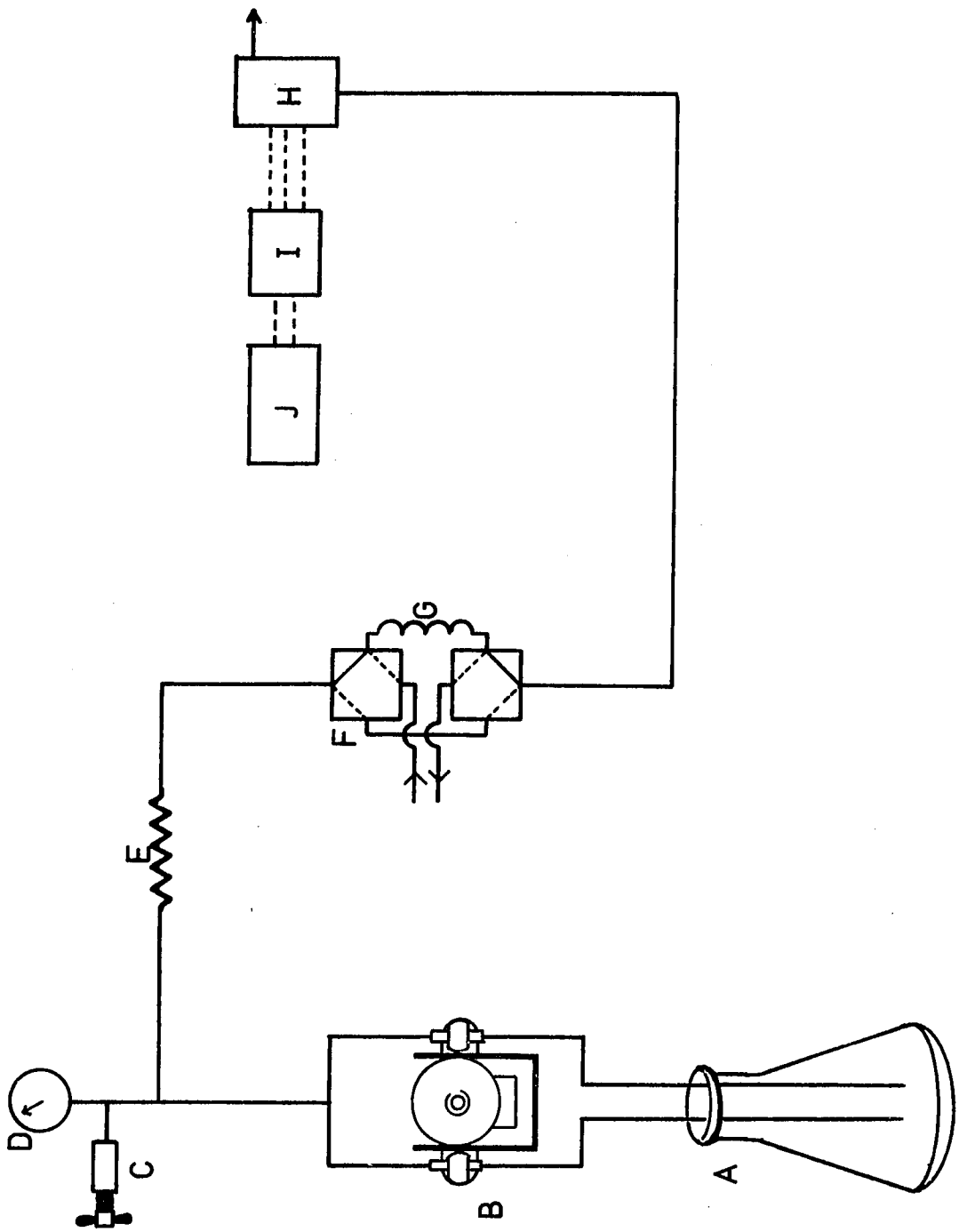
H
I
J
G
F
E
D
C
B
A

0.050-in i.d. x 1/16-in o.d. stainless steel tubing and stainless steel Swagelok fittings, also from Alltech Associates.

Altex Teflon tubing was used for the inlet lines to the pump (1.5-mm i.d. x 1/8-in o.d.) and for all plumbing downstream from the flow restrictor (0.79-mm i.d. x 1/16-in o.d.). Connections of the Teflon tubing to the pump and the flow restrictor were made with Swagelok fittings. All other connections were made with Altex fittings. The sample-injection valve was also from Altex.

The characteristics of Flow System II were very good. Flow rates were constant, easy to set, and reproducible. Pulsations in the flow were minimized to an acceptable level, even though they could not be entirely eliminated. The principal advantage of Flow System II was the large eluent reservoir. A 2-L reservoir was used which contained enough eluent for an entire day. Although the initial adjustment of the pulse dampener frequently required up to 30 min, the system functioned all day without further attention. Flow System II was practical for long experiments and was used in the study of dispersion in Flow Injection Analysis.

3. Flow System III

Flow System III, shown in Figure II-8, was based on a Minipuls 2-HP4 peristaltic pump from Gilson Medical Electronics, Inc., Middleton, WI. Eluent was supplied to the pump from a 2-L reservoir. The rate of flow depended on the rotation speed of the pump and the diameter of the manifold-tube and was continuously adjustable over a large range of flow rates for a given diameter of the manifold-tube by controlling the speed

Figure II-8. Flow System III

A. Eluent reservoir

B. Peristaltic pump

C. Glass T-tube

D. Needle valve

E. Sample loop

F. Sample-injection valve

G. Electrode

H. Potentiostat

I. Recorder

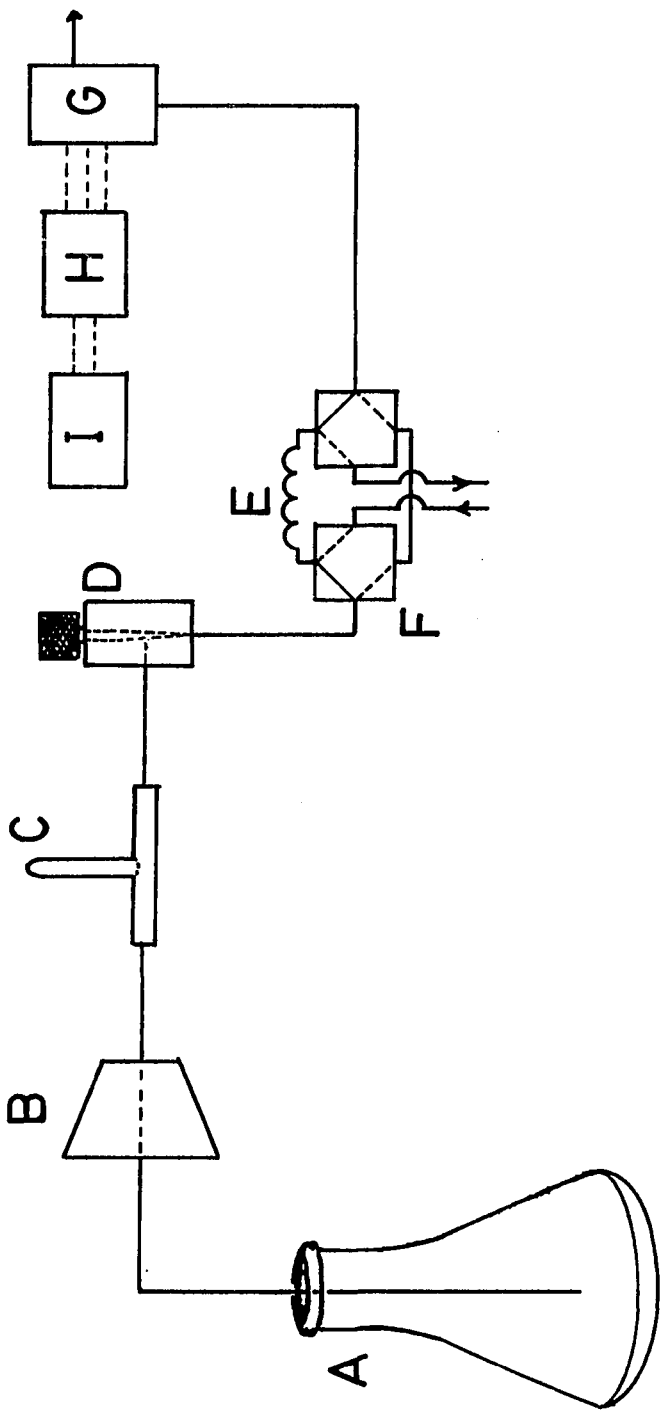
G
H
I
E
F
D
C
B
A

of the pump. For the studies described in this thesis, two ranges of flow rates were required: the flows from two 0.76-mm i.d. vinyl manifold-tubes were combined to provide flow rates in the range 0.4 - 2.6 mL min^{-1}, and a 2.29-mm i.d. vinyl manifold-tube was used to produce flow rates in the range 1 - 9 mL min^{-1}. Flow rate was calibrated by the same procedure used to calibrate the flow rate of Flow System II. Pulsations in the fluid stream were dampened by an inverted glass T-tube and an adjustable needle valve. The glass T-tube contained an air bubble ($\sim$0.5 mL) in the stem. Pulsations were minimized when the back pressure generated by the needle valve was great enough to divert a small amount of the fluid stream into the stem of the T-tube during the high-pressure portion of the pulsations. The needle valve was constructed by the Chemistry Shop at Iowa State University and has been described elsewhere (6). All connections were made with Teflon tubing (0.79-mm i.d.) and Altex tube-end fittings. The sample injection valve was from Altex.

The quality of the fluid stream produced by Flow Stream III was similar to the quality of the fluid stream produced by Flow System II. Flow System III was, however, easier to operate and maintain than Flow System II. The only disadvantage of Flow System III was that only approximate flow rates could be set according to a calibration curve. Flow rate was primarily determined by the speed of the pump which was accurately set through a dial; however, the pressure of the rollers against the manifold-tube, the wear in the manifold-tube, and the back pressure of the flow system also affected the flow rate, and these parameters varied from day to day. After the flow rate was set and the

pulsations were dampened, the flow rate was measured to determine an accurate value. Typically, the variation in the flow rate from the initial setting was ±0.2 mL min^{-1} for the smaller manifold-tube and ±0.3 mL min^{-1} for the larger manifold-tube Whether or not this is a drawback depends on the study being conducted. In general, Flow System III was excellent for Flow Injection Analysis. Flow System III was used in the later steady-state experiments and dispersion experiments.

C. Electrodes

Two tubular electrodes were used in this study. Both were constructed in the Chemistry Shop at Iowa State University.

Electrode I, shown in Figure II-9, was constructed from a platinum disk with dimensions 1/4-in o.d. x 0.149-cm thickness. A 0.096-cm i.d. tubular channel was drilled through the center of the disk to form the surface of the electrode. Prior to assembly, the flat surfaces of the disk were covered with a thin film of fingernail polish. The nail polish was applied to help guard against contact with solution which might seep into the platinum-Teflon interface of the assembled detector. A platinum wire was used to align the bore of the electrode with the upper and lower halves of the electrolysis cell.

Electrode II was constructed according to the design in Figure II-10. A square piece of platinum, 0.25 in x 0.25 in x 0.159-cm thickness, was cast in an Epoxy disk and pressed into a 1-in i.d. cup machined into a piece of glass-filled Teflon used to construct the lower portion of the

Figure II-9. Electrode I

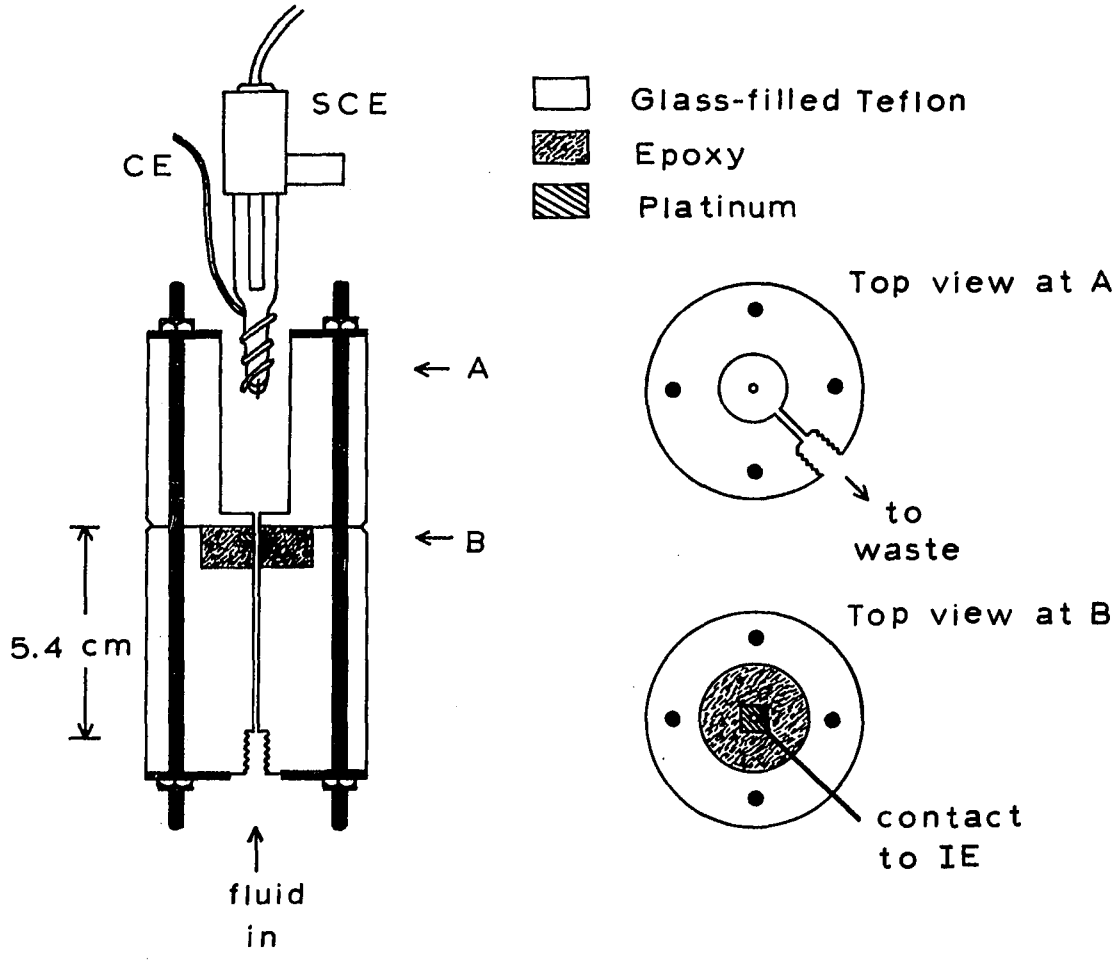
SCE
CE
A
B
5.4 cm
fluid
in
Glass-filled Teflon
Epoxy
Platinum
Top view at A
to
waste
Top view at B
contact
to IE

Figure II-10. Electrode II

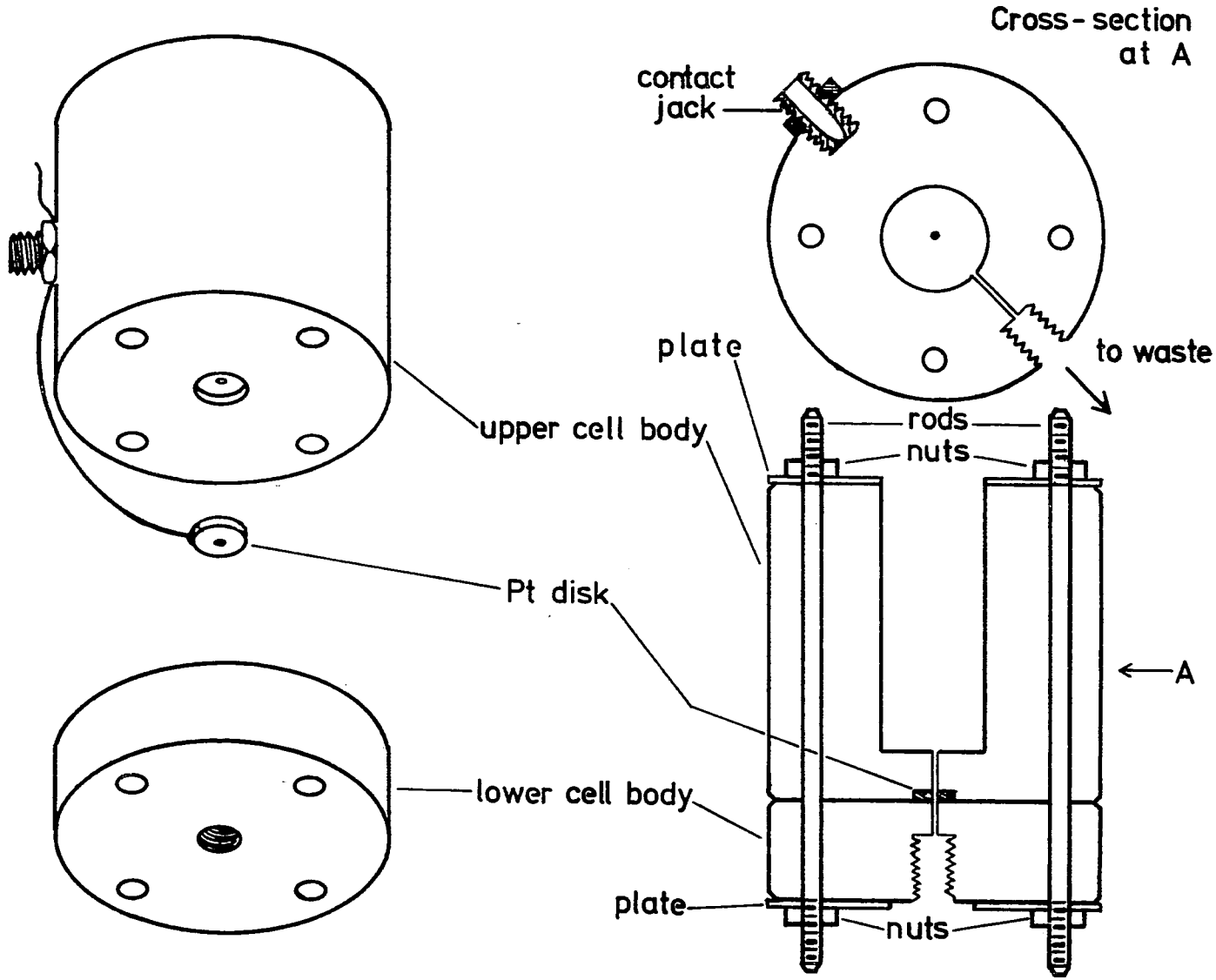
Cross-section
at A
contact
jack
plate
to waste
rods
nuts
upper cell body
Pt disk
A
lower cell body
plate
nuts

detector. The tubular channel was drilled to 0.0794-cm i.d. after assembly of the electrode.

The electrolysis cells were completed with a fiber-junction calomel electrode (Model 39270), Beckman Instruments, Inc., Fullerton, CA, for the reference electrode, and a coil of 21-ga Pt wire for the counter electrode. In both designs, waste liquid was removed from the upper compartment of the cell by aspiration.

Electrode I was used in the initial studies of steady-state current. The performance of Electrode I was excellent when properly sealed; however, the seal was not durable and had to be reformed every 2-3 days. The characteristics of the electrode varied with the quality of the seal. Electrode II was designed to overcome the problems of sealing associated with Electrode I. Judging from the features of voltammograms, Electrode II was not as well-sealed as the best assemblies of Electrode I, but the quality of the seal for Electrode II was very good nonetheless. Electrode II was very stable and was used for months before deterioration was noticed. Apparently, the epoxy used in casting Electrode II was slightly permeable to solutions. The life span of the electrode was increased by storing the electrode in a desiccator. Electrode II was used in most of the experiments described in this thesis.

III. THE EVALUATION OF THE STEADY-STATE RESPONSE OF A TUBULAR ELECTRODE

A. Introduction

In a recent publication, Blaedel and Iverson have postulated the existence of a component of the steady-state current at a tubular electrode which is independent of fluid flow rate (7). My experience with analytical applications of tubular electrodes and an examination of their published data have led me to conclude that the postulation of Blaedel and Iverson was based on a mathematical artifact of inaccurate data analysis. In this thesis, I propose an alternate interpretation of the results of Blaedel and Iverson in the hope of correcting misconceptions in the literature about the analytical response of tubular electrodes.

The solution to the equation of convective-diffusional mass transfer to the inner surface of a tubular electrode is given by Equation III-1 and is presently the accepted basis for the consideration of the amperometric response of a tubular electrode (8-11).

$$I_{ss} = 5.43nFD^{2/3}L^{2/3}v_f^{1/3}C_o \qquad \text{(III-1)}$$

In Equation III-1:

I_{ss} = mass transport limited, steady-state current (C s^{-1});

n = number of electrons involved in the electrochemical reaction per molecule of electroactive specie (eq mol^{-1});

F = the faraday (C eq^{-1});

D = coefficient of diffusion of electroactive specie (cm^2 s^{-1});

L = length of the electrode (cm);

v_f = volume flow rate of the solution through the electrode ($cm^3\ s^{-1}$);

C_o = bulk concentration of the electroactive specie in the sample ($mol\ cm^{-3}$).

Although the dependence of I_{ss} on various experimental parameters predicted by Equation III-1 has been verified for several experimental systems, the accuracy of Equation III-1 may be limited under certain conditions because of the practical difficulty of constructing an experimental system which satisfies all the mathematical assumptions made in the derivation of Equation III-1. In the derivation, the following assumptions were made:

1) The parabolic laminar flow profile is approximated by a linear equation in the region of the diffusion layer at the surface of the electrode.

2) Cylindrical diffusion to the inner surface of the tubular electrode is approximated as linear diffusion.

3) Mass transport from axial diffusion is negligible compared to the mass transport by convection.

4) The fraction of analyte consumed by the reaction at the electrode is negligible so that the boundary condition $C = C_o$ applies at the axis of the tubular electrode.

The approximations listed above for the derivation of Equation III-1 have been tested by Flanagen and Marcoux (12). In their study, the amperometric response of a tubular electrode was calculated by a

computational method known as digital simulation without reliance on the assumptions. When the results of the simulation were compared with currents derived from Equation III-1, Flanagen and Marcous found the assumptions to be valid only when LD/v_f was less than 10^{-6}. For values of LD/v_f greater than 10^{-6}, the errors in Equation III-1 increased as the failure of the assumptions increased in severity. The error was small for values of LD/v_f between 1.0×10^{-6} and 1.0×10^{-4} but increased rapidly for LD/v_f greater than 5.0×10^{-4}. Tubular electrodes as commonly applied for analysis are described by LD/v_f values of 1.0×10^{-4} to 1.0×10^{-2}. Based on the criterion of Flanagen and Marcoux, Equation III-1 is valid only for the shortest electrodes when operated at relatively high flow rates (e.g., $L = 0.16$ cm, $D = 1.0 \times 10^{-5}$ cm^2 s^{-1}, $v_f = 10$ mL min^{-1}). The amperometric response for long electrodes and low flow rates deviates significantly from Equation III-1.

There are many causes for deviation of the observed response of practical tubular electrodes from the theoretical predictions of Equation III-1 other than the limitations inherent in the derivation of the equation. The assumption of laminar flow is easily negated by the turbulence produced at irregularities in the wall of the tubular channel, particularly at the interface of the inlet channel with the electrode surface. Capillary leakage may also occur at this interface and analyte diffusing into the interfacial space undoubtedly is electrolyzed with a response different than predicted by Equation III-1. A more serious limitation on the theory, which is well within the control of the analyst, is the result of the selection of an electrode potential which

is not within the region for a mass-transport limited reaction. The reversibility of electrode reactions is frequently decreased by adsorption of impurities from solution during the electroanalytical application, and deviation of the actual response from the theoretical is increased as the flux of the electroactive species is made larger, i.e., higher v_f and C_o. These causes for deviation are easy to idealize in theory, but difficult to eliminate in practice.

In my experience, deviations of the response of the electrode from predicted behavior are common. Compliance of the experimental amperometric response to Equation III-1 should never be assumed and should be verified for each electrode under the specific operating conditions characteristic of the particular application.

The customary proof of the compliance of a tubular electrode with Equation III-1 is a linear plot of the experimental values of plotted I_{ss} versus $v_f^{1/3}$ (7,13,14). Blaedel and Iverson studied the response of a tubular electrode for v_f in the range 1-10 mL min^{-1}. Plots of I_{ss} versus $v_f^{1/3}$ were apparently linear; however, lines generated from the data by linear least-squares calculations did not extrapolate to zero for $v_f = 0$. The response of the electrode was concluded to be of the form

$$Y = A + Bv_f^{1/3} \qquad \text{(III-2)}$$

where B is the slope of the plot and A is the intercept. The component of the current represented by $Bv_f^{1/3}$ was taken to be the mass transport limited steady-state current, I_{ss}, as described by Equation III-1. The intercept, A, was postulated to represent a flow-rate independent

current, I_{ind}. I_{ind} was observed to be a linear function of C_o for a given set of determinations; however, I_{ind} was also found to vary from day to day and to be dependent on the method of electrode pretreatment. Since the current was dependent on C_o, but independent of flow rate, the source of I_{ind} was concluded to be the axial diffusion of the analyte to the electroactive surface at the ends of the tubular electrode. The slopes of the straight lines calculated by Blaedel and Iverson by the least-squares method (B in Equation III-2) were found to be inversely related to the intercept. Furthermore, all lines calculated by Blaedel and Iverson intersected at v_f = 1 mL min^{-1} when extrapolated to v_f = 0 mL min^{-1}.

The weak point in Blaedel and Iverson's treatment of the data was their assumption that I_{ss} is a linear function of $v_f^{1/3}$. Rather than utilize Equation III-1, the amperometric response of their electrode is described better by an empirical form of Equation III-1 given below.

$$I_{ss} = nFAK_1 v_f^{\alpha} C_o \qquad \text{(III-3)}$$

In Equation III-3, A is the area of the electrode (cm^2), K_1 is a proportionality constant ($s^{(\alpha-1)}\ cm^{(1-3\alpha)}$), and α is the value of the exponent for the flow rate. The exponent α in Equation III-3 should be determined experimentally from the slope of a plot of log I_{ss} versus log v_f. Published values of α obtained in this manner vary from 0.320 to 0.362 (9,14-17). I have determined values as low as 0.234 for an electrode which had not been polished, but typical values are in the range 0.280 to 0.340. Though in reasonable agreement with theory, these values deviate

enough from the theoretical value of 1/3 to cause significant impact on the intercept for experimental results plotted on the basis of an assumed value of α.

When the steady-state amperometric response of an electrode whose flow-rate dependence is v_f^{α} is plotted versus $v_f^{1/3}$ ($\alpha \neq 1/3$), the plot is a curve, not a straight line. Because of the small deviation of the experimental value of α from theory, the curvature is slight and not easily detected by visual examination. The plots of I_{ss} versus $v_f^{1/3}$ appear to be linear due to the small number and limited range of the values of flow rate examined, particularly when theory has preconditioned the researcher to expect linearity. The application of a least-squares calculation to the data imposes linearity on the plot and disguises the true relationship between I_{ss} and v_f. Although the linear fit is a good approximation for the function over the range of v_f normally tested, the linear equation fails to represent the behavior of the electrode adequately outside the range of v_f tested, especially as v_f approaches zero. For an electrode responding to Equation III-3, the slope of the tangent to a plot of I_{ss} versus $v_f^{1/3}$ will be $3\alpha nFAK_1 v_f^{\alpha-1/3} C_o$. The plot of I_{ss} versus $v_f^{1/3}$ will be a straight line, independent of v_f only for $\alpha = 1/3$. For small deviations of α from 1/3, the plot will appear to be adequately fitted by a straight line for large v_f with a slope which is nearly proportional to α. The curvature of the plot of I_{ss} versus $v_f^{1/3}$ from the straight line which fits the data at large v_f will be greatest in the region $v_f \rightarrow 0$ mL min^{-1}, where data are usually not obtained because of the difficulty in controlling

the flow rate. Because the slope of the linear fit of the data is proportional to α for large values of v_f, and since all straight lines must intersect at $v_f = 1$ mL min^{-1}, the intercept of the calculated line will be positive for $\alpha < 1/3$ and negative for $\alpha > 1/3$. This is all consistent with the data reported by Blaedel and Iverson.

I conclude that I_{ind} is an anomalous consequence of the inappropriate extrapolation of a linear least-squares fit to nonlinear data and not due to the presence of a flow-rate independent current. In the sections that follow, I provide a recalculation of the results of Blaedel and Iverson and the results of my own experiments to support my contention.

B. Recalculation of Blaedel and Iverson's Data

There are four features of the experimental results of Blaedel and Iverson that are important in developing my argument.

1) Both positive and negative intercepts were obtained for plots of I_{ss} versus v_f (Tables I and II in Reference 7).

2) The intercept was a linear function of C_o (Figure 3 in Reference 7).

3) An inverse relationship was observed between the values of slope and intercept (Tables I and II in Reference 7).

4) All fitted lines intersected at $v_f^{1/3} = 1$ $mL^{1/3}$ $min^{-1/3}$ (Figure 2 in Reference 7).

Features 1 and 2 are the essential basis for the postulation of Blaedel and Iverson for the existence of I_{ind}. Features 3 and 4 will be used specifically to support my argument that the conclusion of Blaedel and

Iverson is the result of an incorrect assumption concerning the dependence of I_{ss} on v_f. The recalculation of Blaedel and Iverson's data based on my model of the behavior of an electrode accounts for all four features listed above.

To support my argument, I have reproduced the features of the experimental results of Blaedel and Iverson by assuming the general response of the electrode as given by Equation III-4

$$I_{ss} = K_1' v_f^{\alpha} C_o \qquad \text{(III-4)}$$

where K_1' equals $nFAK_1$ of Equation III-3. I then calculated slopes and intercepts of plots of I_{ss} versus $v_f^{1/3}$ using the method of linear least squares. The values of K_1', C_o, and v_f were taken from Blaedel and Iverson's paper (7) so that a direct comparison could be made between their published results and my calculations.

1. The determination of K_1'

The value of K_1' for my simulation was determined from Figure 2 in Reference 7. Figure 2 contains a plot of I_{ss} versus $v_f^{1/3}$ for electrodes submitted to different procedures. According to my interpretation, each pretreatment resulted in a slightly different value of α.

When Equation III-4 is plotted as a function of $v_f^{1/3}$, Equation III-4 can be written as

$$I_{ss} = K_1' C_o v_f^{\beta} v_f^{1/3} \qquad \text{(III-5)}$$

where β is the deviation of the exponential power of v_f from 1/3; $\beta = \alpha - 1/3$.

Since the α values in Figure 2 of Reference 7 are unknown, Equation III-5 is solved for K_1' by using the value of I_{ss} corresponding to $v_f = 1$. For $v_f = 1$, v_f^{α} is equal to 1 for all values of α. Thus, Equation III-5 becomes

$$I_{ss} = K_1' C_o [1\ mL^{\alpha}\ min^{-\alpha}] \qquad \text{(III-6)}$$

This property of v_f^{α} accounts for Feature 4 of Blaedel and Iverson's data as stated previously.

For the actual calculation of K_1', I_{ss} at $v_f^{1/3} = 1$ was estimated from Figure 2 of Reference 7 to be 60 nA for C_o equal to 4 μM. By substituting these values in Equation III-6, I calculate

$$K_1' = 15\ nA\ min^{\alpha}\ \mu M^{-1}\ mL^{-\alpha}$$

The values of K_1' can also be obtained by the analysis of the data in Table 1 of Reference 7. Table 1 presents the data of Figure 2 in the linear form of

$$I_{ss} = S v_f^{1/3} + I_{ind} \qquad \text{(III-7)}$$

where S is the slope of the plot which was taken by Blaedel and Iverson to be equal to $5.43nFD^{2/3}L^{2/3}C_o$. If Equation III-7 is a good approximation of the response of the electrode in the region of $v_f = 1$, then Blaedel and Iverson's representation of the amperometric response can be translated into my representation as shown in Equation III-8.

$$I_{ss} = S v_f^{1/3} + I_{ind} = K_1' C_o v_f^{\beta} v_f^{1/3} \qquad \text{(III-8)}$$

Again, at $v_f = 1$, $v_f^{1/3} = v_f^{\beta} = 1$ and Equation III-8 becomes Equation III-9.

$$I_{ss} = S[1\ mL^{1/3}min^{-1/3}] + I_{ind} = K_1'C_o[1\ mL^{\alpha}\ min^{-\alpha}] \qquad (III-9)$$

Substituting the average values of S and I_{ind} from Table 1 of Reference 7 into Equation III-9,

$$K_1' = 60.1\ nA$$

For $C_o = 4\ \mu M$, $K_1' = 15.03\ nA\ min^{\alpha}\ \mu M^{-1}\ mL^{-\alpha}$ which is in excellent agreement with the value calculated directly from Figure 2.

To simulate the features of Figure 2, I calculated I_{ss} using Equation III-10 for α's in the range of 0.280 - 0.360 in 0.005 increments with the inclusion of $\alpha = 1/3$.

$$I_{ss} = 60(nA\ min^{\alpha}\ mL^{-\alpha})v_f^{\alpha} \qquad (III-10)$$

The experimental values of flow rate used by Blaedel and Iverson were estimated from Figure 2 in Reference 7 to be 1, 2, 3, 4, 6, 8, and 9 mL min^{-1}. The results of the calculations are listed in Table III-1.

2. Calculations of slope and intercept for simulated data

The next step is to show that if the simulated data in Table III-1 were plotted versus $v_f^{1/3}$, then a least-squares fit of the data would produce Blaedel and Iverson's slopes and intercepts for values of $\alpha \neq 1/3$.

The equations used by Blaedel and Iverson to calculate the slope (B) and the intercept (A) of a least-squares fit are found in Reference 18

Table III-1. I_{ss} for various α and v_f as calculated from Equation III-10

	I_{ss} (nA)						
	v_f (mL min^{-1})						
α	1	2	3	4	6	8	9
0.280	60.0	72.9	81.6	88.5	99.1	107.4	111.0
0.285	60.0	73.1	82.1	89.1	100.0	108.5	112.2
0.290	60.0	73.4	82.5	89.7	100.9	109.7	113.4
0.295	60.0	73.6	83.0	90.3	101.8	110.8	114.7
0.300	60.0	73.9	83.4	90.0	102.7	112.0	116.0
0.305	60.0	74.1	83.9	91.6	103.6	113.1	117.3
0.310	60.0	74.4	84.3	92.2	104.6	114.3	118.6
0.315	60.0	74.6	84.8	92.9	105.5	115.5	119.9
0.320	60.0	74.9	85.3	93.5	106.5	116.7	121.2
0.325	60.0	75.2	85.7	94.2	107.4	117.9	122.5
0.330	60.0	75.4	86.2	94.8	108.4	119.2	123.9
1/3	60.0	75.6	86.5	95.2	109.0	120.0	124.8
0.335	60.0	75.7	86.7	95.5	109.4	120.4	125.3
0.340	60.0	75.9	87.2	96.1	110.3	121.7	126.6
0.345	60.0	76.2	87.7	96.8	111.3	122.9	128.0
0.350	60.0	76.5	88.1	97.5	112.3	124.2	129.5
0.355	60.0	76.7	88.6	98.1	113.3	125.5	130.9
0.360	60.0	77.0	89.1	98.8	114.4	126.8	132.3

with corrections published in Reference 19. The equations are listed below with Blaedel and Iverson's original notation.

$$B = \frac{\Sigma xy - (\Sigma x)(\Sigma y)/N}{S_{xx}} \qquad \text{(III-11)}$$

$$A = \bar{y} - B\bar{x} \qquad \text{(III-12)}$$

In Equations III-11 and III-12:

N = number of data points;

$\bar{y} = \Sigma y/N$;

$\bar{x} = \Sigma x/N$;

$S_{xx} = \Sigma x^2 - (\Sigma x)^2/N$.

For a plot of I_{ss} versus $v_f^{1/3}$, $y = I_{ss}$ and $x = v_f^{1/3}$.

The slopes and intercepts can be computed more accurately if Equations III-11 and III-12 are rewritten and simplified using the parameters of my model. In rewriting the equations, the following substitutions are made:

$$\Sigma x = \Sigma v_f^{1/3}$$

$$\Sigma y = \Sigma I_{ss} = \Sigma K_1' C_o v_f^{\alpha} = K_1' C_o \Sigma v_f^{\alpha}$$

$$\Sigma xy = K_1' C_o \Sigma v_f^{\alpha} v_f^{1/3} = K_1' C_o \Sigma v_f^{\alpha+1/3}$$

$$\Sigma x^2 = \Sigma v_f^{2/3}$$

$$(\Sigma x)^2 = (\Sigma v_f^{1/3})^2$$

Equation III-11 becomes Equation III-13

$$B = \left[\frac{\Sigma v_f^{\alpha+1/3} - \frac{1}{N}\Sigma v_f^{1/3}\Sigma v_f^{\alpha}}{\Sigma v_f^{2/3} - \frac{1}{N}(\Sigma v_f^{1/3})^2}\right] K_1' C_o \qquad \text{(III-13)}$$

and Equation III-12 becomes Equation III-14

$$A = \left[\frac{\Sigma v_f^{\alpha}}{N} - \left(\frac{\Sigma v_f^{\alpha+1/3} - \frac{1}{N}\Sigma v_f^{1/3}\Sigma v_f^{\alpha}}{\Sigma v_f^{2/3} - \frac{1}{N}(\Sigma v_f^{1/3})^2}\right)\frac{\Sigma v_f^{1/3}}{N}\right] K_1' C_o$$

$$= \left[\frac{1}{N}\left(\frac{\Sigma v_f^{\alpha}\Sigma v_f^{2/3} - \Sigma v_f^{\alpha+1/3}\Sigma v_f^{1/3}}{\Sigma v_f^{2/3} - \frac{1}{N}(\Sigma v_f^{1/3})^2}\right)\right] K_1' C_o \qquad \text{(III-14)}$$

Interesting implications can be drawn from Equations III-13 and III-14. The dependence of the slope and intercept on N and v_f indicates that the number of data points used in the calculation, and the values of v_f chosen, influences the results of the calculation. This implies that the results of the calculations are affected by the nature of the data as well as the values of the data. Also, for $\alpha = 1/3$,

$$B = \left[\frac{\Sigma v_f^{2/3} - \frac{1}{N}(\Sigma v_f^{1/3})^2}{\Sigma v_f^{2/3} - \frac{1}{N}(\Sigma v_f^{1/3})^2}\right] K_1' C_o = [1] K_1' C_o$$

and

$$A = \left[\frac{\Sigma v_f^{1/3}}{N} - [1]\frac{\Sigma v_f^{1/3}}{N}\right] K_1' C_o = [0] K_1' C_o = 0$$

However, for $\alpha \neq 1/3$, if the same N and set of v_f's are used throughout a concentration study, the slope and intercept will be a linear function of C_o. This explains Blaedel and Iverson's observation that the intercept of the linear fit to the experimental data was proportional to C_o.

The slope and intercept of a linear fit was calculated for the data in Table III-1 for each value of α using Equations III-13 and III-14. The results are shown in Table III-2. Values of I_{ss}, as calculated from Equation III-10, are shown in Figure III-1 as a plot of I_{ss} versus $v_f^{1/3}$ for α = 0.300, 1/3, and 0.360. There is considerable similarity between the lines in Figure III-1 of this thesis and the lines in Figure 1 of Reference 7, particularly between the plot for α = 0.300 in Figure III-1 and Curve II-C in Figure 1. The plots in Figure III-1 appear to be linear for all values of α used in the calculation, and one might conclude from mere inspection of the plots that each corresponds to a tubular electrode whose response is in compliance with theory.

A comparison of Blaedel and Iverson's experimental results and the data in Table II-2 shows several important correlations:

1) The magnitude of the calculated slopes and intercepts agree with Blaedel and Iverson's data over the range of α used.
2) The relationship between slope and intercept are the same for a given α in both studies. For example, for a slope of 50 nA min^{α} $mL^{-\alpha}$, the intercept is $\sim$9.7 nA in both studies.
3) Both the results of my calculations, and Blaedel and Iverson's data, show an inverse relationship between the slope and the intercept. As the slope increases, the intercept becomes more negative.
4) In both studies, negative intercepts are observed for values of slopes > 60 nA which corresponds to values of α > 1/3.

Table III-2. Results of the least-square fit for a plot of I_{ss} versus $v_f^{1/3}$ for the data in Table III-1

α	Slope (nA $min^{1/3}$ mL^{-1})	Intercept (nA)
0.280	47.1	13.4
0.285	48.2	12.2
0.290	49.4	11.0
0.295	50.6	9.8
0.300	51.7	8.6
0.305	52.9	7.3
0.310	54.2	6.1
0.315	55.4	4.8
0.320	56.6	3.5
0.325	57.9	2.2
0.330	59.1	0.9
1/3	60.0	0.0
0.335	60.4	-0.4
0.340	61.7	-1.8
0.345	63.0	-3.1
0.350	64.4	-4.6
0.355	65.7	-6.0
0.360	67.1	-7.4

Figure III-1. Recalculated values of steady-state current from data in Reference 7

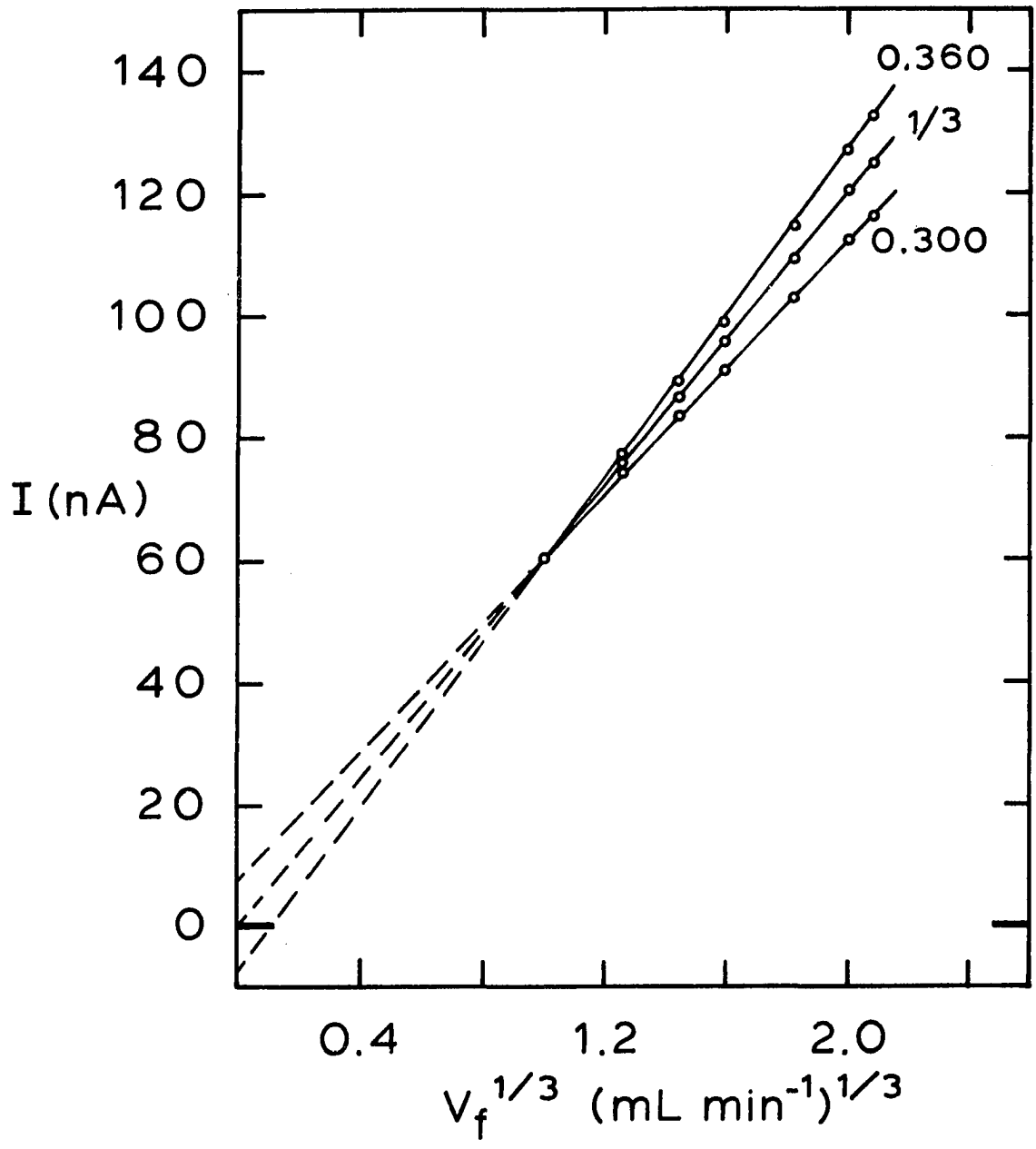
140
120
100
80
I (nA)
60
40
20
0
0.360
1/3
0.300
0.4
1.2
2.0
$V_f^{1/3}$ (mL min^{-1})$^{1/3}$

These correlations are best illustrated in Figure III-2 where a quantitative comparison is made between my results, and Blaedel and Iverson's data. In Figure III-2, the slope is plotted as a function of intercept. The results of my calculations are represented as a line which corresponds to values of α in the range 0.280 - 0.344. Blaedel and Iverson's data were taken from Tables I and II of Reference 7, and are represented by the open circles and triangles. The agreement between the calculated line and the data of Blaedel and Iverson is excellent.

Taking into consideration the correlations discussed above and the concentration dependence of Equation III-14, the day-to-day variation in the slope and intercept and the dependence of the slope and intercept on the pretreatment of the electrode are easily explained if the true value of α, which correctly describes the behavior of the electrode, fluctuates about the value of 1/3.

C. Experimental

1. Instrumentation and apparatus

The instrumentation and apparatus used in this study are discussed in Chapter II. Most experiments were performed with Flow System III using Electrode II as a detector. Where noted, Electrode I was used with Flow System I.

2. Preparation of solutions

A solution of 0.10 M H_2SO_4 and a solution of 0.10 M H_2SO_4 containing 5.0×10^{-4} M KI were used in this study. The 0.10 M H_2SO_4 was prepared

Figure III-2. Correlation of slope ($dI_{ss}/dv_f^{1/3}$) with I_{ind}

o - Data from Table I, Reference 7

Δ - Data from Table II, Reference 7

--- - Calculated from Equation III-10

for α = 0.280 - 0.344

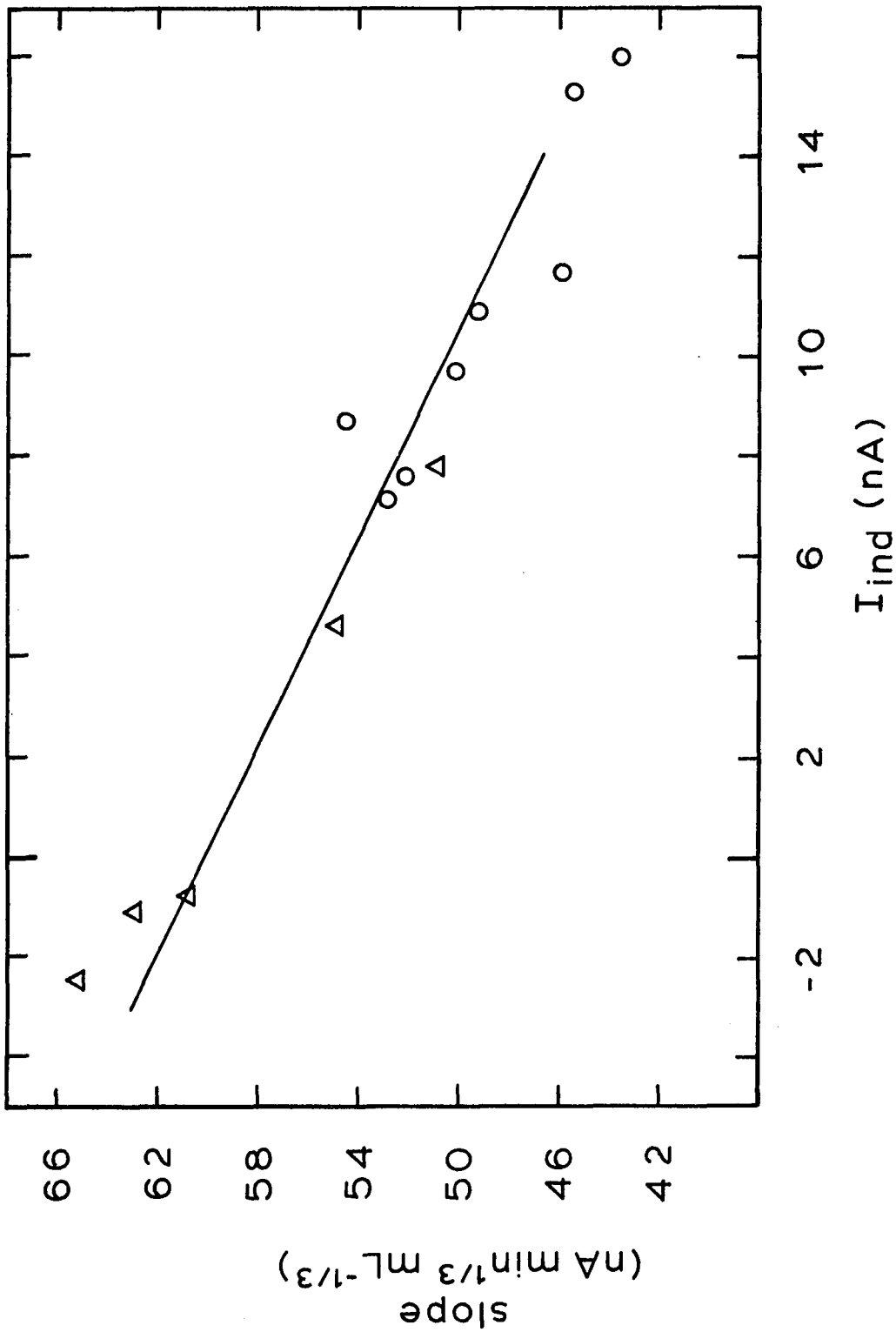
slope
(nA min^1/3 mL^-1/3)
66
62
58
54
50
46
42
-2
2
6
10
14
I_ind (nA)

by diluting 11.2 mL of concentrated H_2SO_4 to 2 L with deionized water. A stock solution of 5.0×10^{-2} M KI was made by dissolving 8.3023 g of KI in deaerated 0.10 M H_2SO_4 and then diluting to 1 L with 0.10 M H_2SO_4. A 10 mL aliquot of the stock solution was diluted to 1 L with 0.10 H_2SO_4 to make the working solution of 5.0×10^{-4} M KI. The working solution was deaerated and kept under a nitrogen atmosphere to prevent the oxidation of iodide by dissolved oxygen.

3. Procedures

The electrodes were preconditioned in the conventional voltammetric manner by repeated scans of the applied potential between the limits -0.2 V and 1.0 V versus SCE until consecutive current-potential curves for solutions containing iodide were reproducible. The limiting-current plateau for the anodic wave for iodide was in the range 0.7-0.9 V versus SCE and the measurement of I_{ss} was made at a potential of 0.8 V versus SCE.

The sensitivity of the detector was generally observed to decrease slightly over an extended period of use (several hours) or upon storage overnight. The sensitivity was restored by polishing the inner surface of the tubular electrode prior to the voltammetric pretreatment. Polishing was with 1 μm Metadi diamond paste from Buehler Ltd., Evanston, IL. The paste was applied to a 22-ga Pt wire which was drawn back and forth in the tubular channel of the detector. The paste was cleaned from the channel with a stream of distilled water flowing at high pressure.

D. Results and Discussion

Values of I_{ss} are shown in Table III-3. This includes data obtained without the benefit of the polishing procedure applied just prior to the measurement of I_{ss} (Exp. A) as well as data for the same electrode obtained following the polishing procedure (Exp. B). Plots made of I_{ss} versus $v_f^{1/3}$ shown in Figure III-3 (open circles) appear to be linear and the slopes and the intercepts of the plots are given in Table III-3. The values of α are significantly less than 1/3 for the data given in Table III-3. The linear least-squares fit to the plots gives intercepts which deviate significantly from zero. The experimental value of α, determined from plots of log I_{ss} versus log v_f, are also given in Table III-3, as well as the slopes and intercepts for the linear fits to plots of I_{ss} versus v_f^{α} using experimental values of α. The confidence limits (90%) and the coefficient of correlation (R) are given in Table III-3 for the intercept and the slope of each plot for each experiment. A comparison of the confidence limits for the plots of I_{ss} versus $v_f^{1/3}$ to the corresponding plots of I_{ss} versus v_f^{α} shows that there is less relative uncertainty in the value of the slopes for the plots of I_{ss} versus v_f^{α}. The value of the intercept is also much smaller for the plots of I_{ss} versus v_f^{α} and can be considered to be zero when compared to the range of the confidence limits. The increase in sensitivity which results from polishing the electrode is probably caused by removal of adsorbed material which blocks the active surface area. The value of α is low, however, even after polishing. Tubular electrodes are difficult to polish adequately; thus, the low values of α may be attributed to the

Table III-3. Experimental values of I_{ss} and the results of least-squares calculations

Exp. A	V_f (mL min^{-1})	I_{ss}[a] (μA)	Exp. B	V_f (mL min^{-1})	I_{ss}[a] (μA)
	1.66	15.96		1.70	16.16
	2.51	17.77		2.53	18.13
	3.90	19.79		3.89	20.57
	5.21	21.28		5.24	22.36
	6.07	21.73		6.08	23.21
	6.96	22.34		6.93	24.05
	7.93	23.18		7.85	24.85
	8.93	23.82		8.83	25.60
I_{ss} vs. $V_f^{1/3}$:					
slope ($\mu A min^{1/3} mL^{-1/3}$)		8.66±0.43			10.83±0.31
intercept		5.95±0.74			3.39±0.54
R		0.9976			0.9993
log I_{ss} vs. log V_f:					
slope (α)		0.234±0.003			0.280±0.002
R		0.9987			0.9997
I_{ss} vs. V_f^{α}:					
slope ($\mu A min^{\alpha} mL^{-\alpha}$)		14.20±0.57			13.93±0.28
intercept (μA)		0.12±0.84			0.095±0.44
R		0.9987			0.9997

[a] I_{ss} corrected for background observed in absence of iodide.

Figure III-3. Plots of experimental values of I_{ss}

A. Unpolished electrode

o - $\alpha = 1/3$

Δ - $\alpha = 0.234$

B. Polished electrode

o - $\alpha = 1/3$

Δ - $\alpha = 0.280$

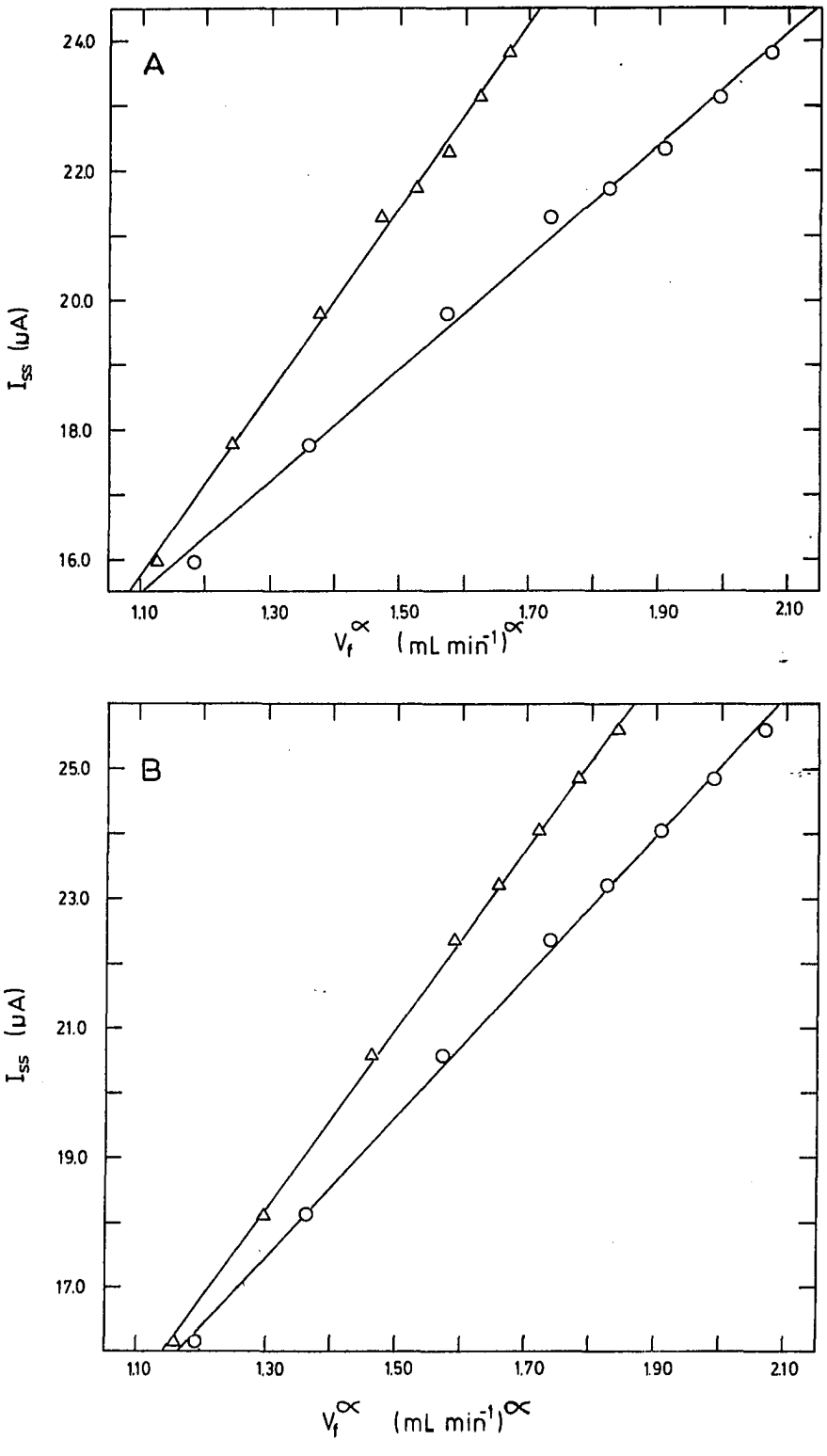
A
B
24.0
22.0
20.0
18.0
16.0
25.0
23.0
21.0
19.0
17.0
I_{ss} (uA)
1.10
1.30
1.50
1.70
1.90
2.10
V_f^{α} $(mL\ min^{-1})^{\alpha}$

effects of electrode kinetics which at the higher flow rates causes the value of the current to be less than the mass-transport limited value.

For other cases observed in my experimental work, the nonzero intercepts of the linear least-squares fit to the plots of I_{ss} versus $v_f^{1/3}$ were significant only when the experimental values of α were not equal to 1/3. Some examples are reported in Table III-4. The data for Table III-4 were acquired using Electrode I with measurement of I_{ss} at a flow rate of 0.5, 1.0, 1.5, and 2 0 mL min^{-1} for a solution of 5.0 x 10^{-4} M KI. Fingernail polish was applied to the flat surfaces of the platinum disk of Electrode I prior to assembly to help guard against contact with solution which might seep into the platinum-Teflon interface of the assembled detector. The importance of a good seal to the performance of Electrode I is shown in Figures III-4 and III-5. In Figure III-4, the voltammogram of the oxidation of iodide taken with a well-sealed electrode is shown. The voltammetric features of the voltammogram are well defined: the curve in the region of the mass-transport limited current is flat and broad, the rising portion of the curve is sharp indicating a reversible reaction, and there is no evidence of any appreciable background current or process. The voltammogram in Figure III-4 corresponds to Experiment 4 in Table III-4. The voltammogram in Figure III-5 is characteristic of an electrode that is not properly sealed. The voltammogram in Figure III-5 was recorded the day before the voltammogram in Figure III-4 was recorded. In the interim, the electrode was disassembled and resealed. The most notable feature of the voltammogram in Figure III-5 is the large sloping background current. Because of this background current, the voltammetric

Table III-4. The results of least-squares calculations for various experiments using Electrode I

Experiment	1	2	3	4	5	6
I_{ss} vs. $v_f^{1/3}$:						
Slope ($\mu A\ min^{1/3}\ mL^{-1/3}$)	12.43	10.20	10.51	11.49	9.73	11.85
Intercept (μA)	-1.54	0.26	-0.00_3	0.26	1.46	0.11
log I_{ss} vs. log v_f						
Slope (α)	0.374	0.325	0.333	0.327	0.290	0.329
I_{ss} vs. v_f^{α}						
Slope ($\mu A\ min^{\alpha}\ mL^{-\alpha}$)	11.07	10.46	10.52	11.74	11.22	12.00
Intercept (μA)	-0.21	0.00_3	-0.02	0.02	-0.01	-0.03

Figure III-4. Voltammogram from a well-sealed electrode for the oxidation of I^- in 0.10 M H_2SO_4

Electrode I

$C_{I^-} = 5.0 \times 10^{-4}$ M

Flow rate = 1.0 mL min^{-1}

Scan rate = 3 0 V min^{-1}

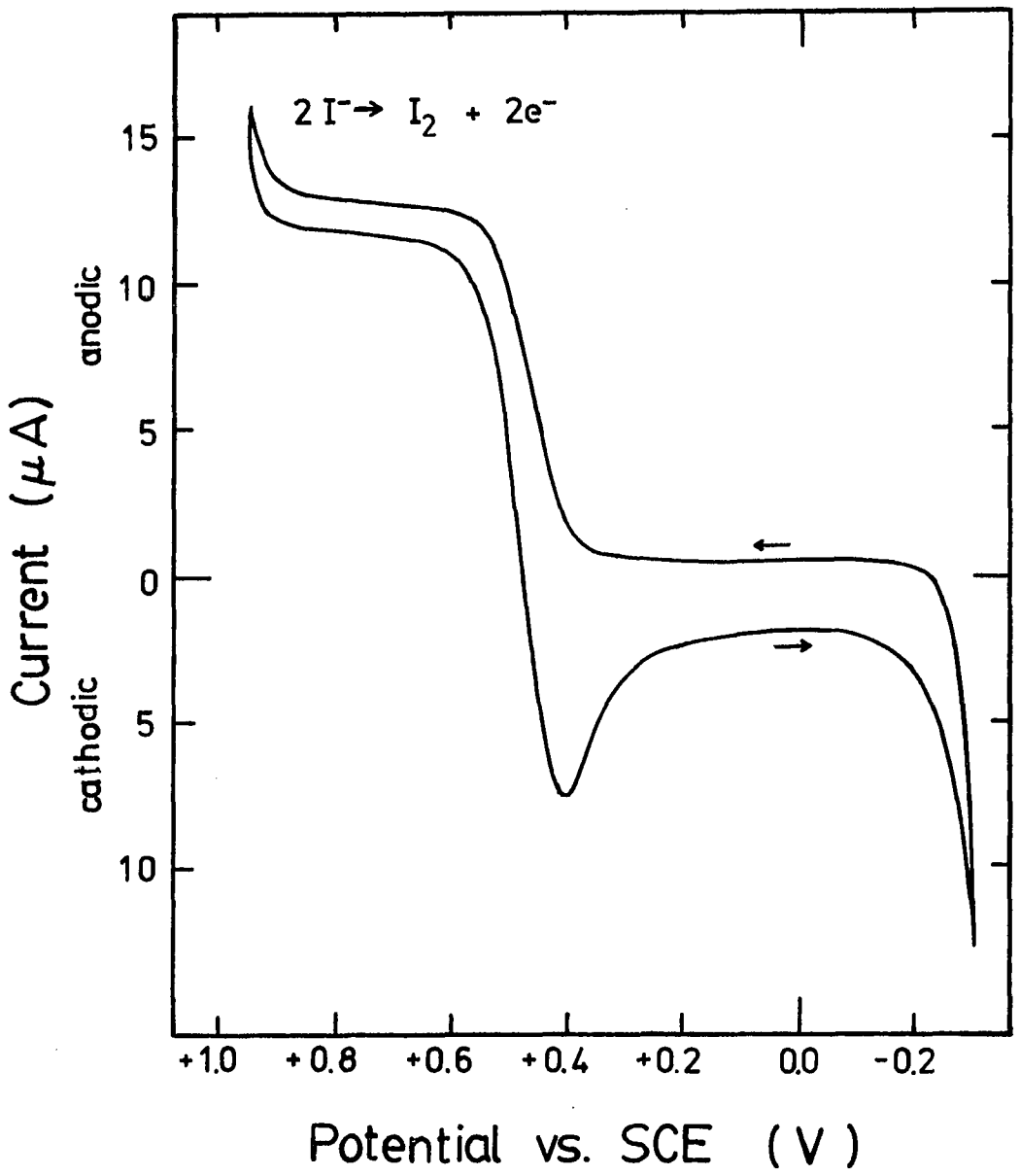
2 I⁻→ I₂ + 2e⁻
15
10
5
0
5
10
anodic
cathodic
Current (μA)
+1.0
+0.8
+0.6
+0.4
+0.2
0.0
-0.2
Potential vs. SCE (V)

Figure III-5. Voltammogram from a leaky electrode for the oxidation of I^- in 0.10 M H_2SO_4

Electrode I

$C_{I^-} = 5.0 \times 10^{-4}$ M

Flow rate = 1.0 mL min^{-1}

Scan rate = 3.0 V min^{-1}

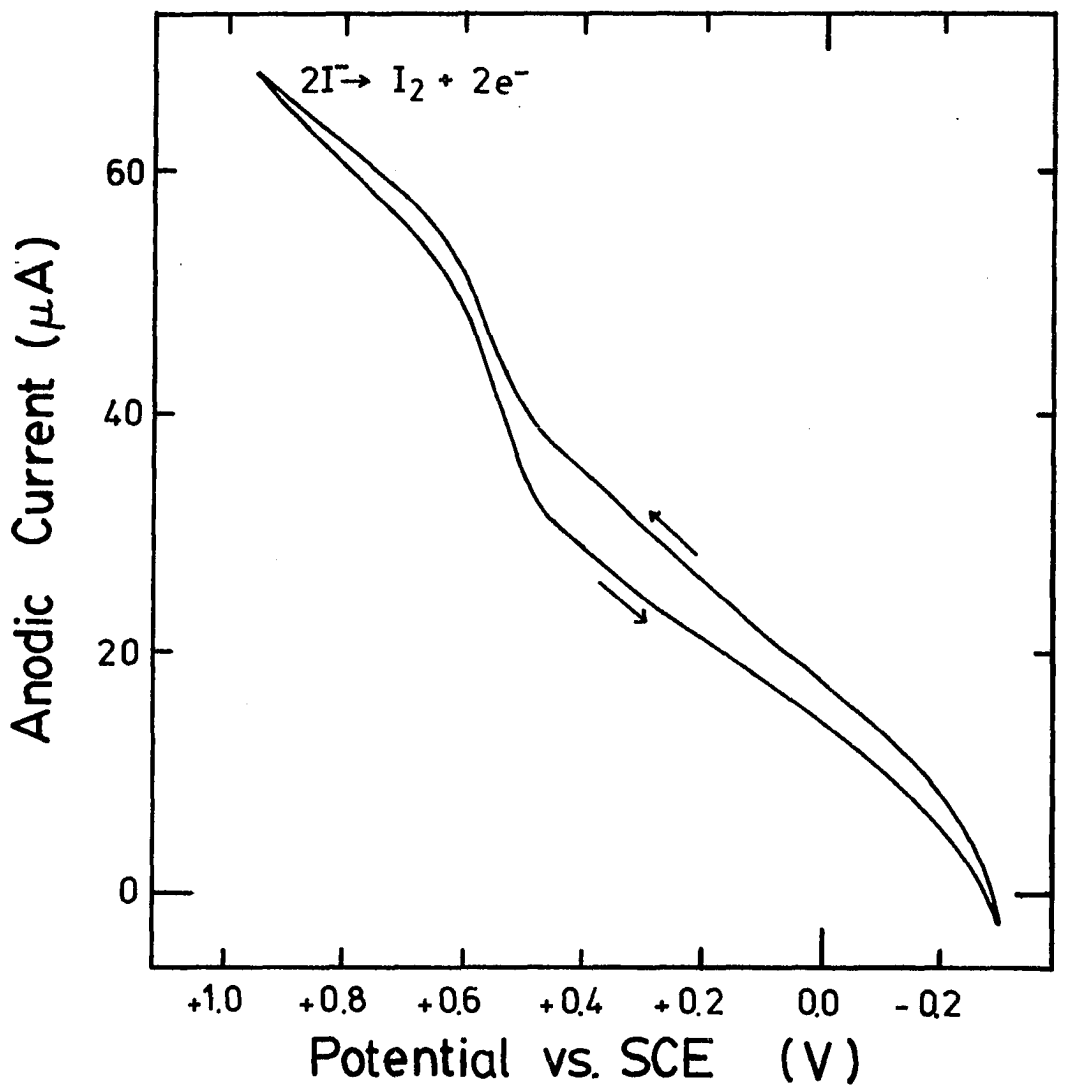
2I⁻→ I₂ + 2e⁻
60
40
20
0
Anodic Current (μA)
+1.0
+0.8
+0.6
+0.4
+0.2
0.0
-0.2
Potential vs. SCE (V)

features of the curve become distorted and are not as well defined as in Figure III-4. The behavior of the background current appears to be analogous to the behavior of a resistor in a simple DC circuit in which Ohm's law is obeyed. This is attributed to the high resistance of the solution in a capillary leak. Generally, the background current of a sealed electrode is stable and can be measured in the absence of the analyte. The value of the background current can then be used as a correction in the measurement of I_{ss}. The measurement of I_{ss} for the electrode of Figure III-5 was impossible due to the slow and steady decay of the background current as a constant potential. Because of its decay, the value of the background current was different for each measurement of I_{ss} which made a correction impossible. The electrode of Figure III-4 is an extreme case; however, perfectly sealed electrodes are difficult to construct and to maintain and most electrodes leak to some degree. If leakage occurs to the extent that the background current is unstable and significant when compared to the value of I_{ss} being measured, then errors in the measurement of I_{ss} will be reflected in the values of the intercept and slope for the least-squares fit of a plot of I_{ss} versus $v_f^{1/3}$.

E. Conclusion

The validity of the concept of a flow-rate independent component of the steady-state current in tubular electrodes which has been proposed as making a significant contribution to the total current, even for moderately large v_f, _e.g._, > 1 mL min^{-1}, has been brought into

serious question. The concept was originally proposed to explain the nonzero intercepts obtained for linear extrapolations of plots of I_{ss} versus v_f^{α} which were made with the assumption that α was equal to the theoretical value of 1/3. The actual value of α describing the response of practical electrodes may vary significantly from 1/3 and should be calculated from plots of log I_{ss} versus log v_f. Plots of I_{ss} versus v_f^{α} which are constructed using the experimental value of α have an intercept which is virtually zero within the uncertainty of the data. I speculate that these findings for tubular electrodes are also applicable to the interpretation of plots of I_{ss} versus $v_f^{1/2}$ for flow-through detectors constructed from planar electrodes (20,21). Nonzero intercepts for linear extrapolations of those plots have also been explained as the result of a significant flow-rate independent current.

IV. THE CURRENT-TIME RESPONSE OF A TUBULAR ELECTRODE IN FLOW INJECTION ANALYSIS

A. Introduction

A natural application of tubular electrodes is the determination of an electroactive species in a fluid stream. In early applications, the solutions to be analyzed were passed through the electrode with experimental conditions chosen so that steady-state currents were observed (22-30). The relationship between the electrical current and the concentration of the analyte for the steady-state application is described by Equation III-1.

$$I_{ss} = 5.43nFD^{2/3}L^{2/3}v_f^{1/3}C_o \qquad \text{(III-1)}$$

In more recent applications, tubular electrodes have been used as detectors in Liquid Chromatography (LC) (31-38) and in Flow Injection Analysis (FIA) (37-41). In these applications, a sample of the solution to be analyzed is introduced into a continuous stream of a nonelectroactive reagent. The sample is carried to the electrode by the fluid stream. Passage of the sample through the electrode produces a current which is a "peak-shaped" function of time The maximum of the current-time curve (32,33,35,38) and the area under the current-time curve (31, 32,34,37,38,41) have been found to be proportional to the concentration of the analyte in the sample.

The applications of tubular electrodes to FIA and LC differ from steady-state applications in that the dispersion of the analyte plays an

important role in the amperometric response of the electrode. As the sample is carried toward the electrode, the analyte in the sample is dispersed either by chromatographic processes (in LC) or by differences in the rate of axial mass transport caused by the nonuniformity of the radial flow-profile (in FIA). Because of dispersion, the concentration of the analyte in the flow stream is neither uniform nor equal to the original concentration of the analyte in the sample. Both the axial and radial distribution of the analyte are affected by dispersion; thus, factors which influence dispersion consequently influence the amperometric response of the electrode.

The relationship between the dispersion of a sample injected into a fluid stream and the amperometric response of a tubular electrode has not been investigated in previous studies reported in the chemical literature. In previous works, the behavior of the tubular electrode in a dispersive system was described in general terms by the equation for the steady-state current (Equation III-1) (3,4,31,32,37,39,42). The tacit implication was that the peak current, the current at the maximum of the current-time curve, is analogous to a steady-state current. This led to the assumption that parameters which affect the steady-state current will also affect the peak current in the same manner.

The comparison of the amperometric response of a tubular electrode in a dispersive system to the steady-state current has several drawbacks:

(1) The steady-state equation does not describe the time-dependence of the amperometric response of an electrode in a dispersive system.

(2) The equation for the steady-state amperometric response does not predict the proper proportionality constant relating the peak current to the concentration of the analyte in the sample.

(3) In FIA, the amperometric response of the electrode depends on the volume of the sample, V_S, and the volume of the flow system between the injector and the electrode, V_R. In chromatography, the amperometric response of the electrode depends on the volume of the sample, V_S, and factors which affect the partitioning of the analyte between the fluid stream and the column. The steady-state equation does not take these parameters into account.

(4) The steady-state equation cannot be integrated in a satisfactory manner to predict the charge passed through the electrode during the electrolysis of the injected sample.

(5) The dispersion of a sample in a fluid stream and the mass transport of the analyte to the surface of an electrode are both dependent on the flow rate, v_f. This is reflected in the observed relationship between the peak current and flow rate. The steady-state equation expresses only the flow-dependency of the mass transport to the surface of the electrode and does not consider the contribution of dispersion.

In the past, points 1 through 4 were recognized as limitations of the steady-state equation (3,32) and were readily apparent when the steady-state equation was compared to experimental results. Point 5

illustrates a case where the comparison of steady-state current to peak current was insidious. Routine laboratory experience taught that peak current was a function of flow rate. Since the steady-state equation predicted a dependence of the current on the cube root of the flow rate, peak current was assumed to have the same relationship. If experimental results deviated from the predicted relationship, the differences were attributed to problems with the electrode or to the electrochemistry. Although these misconceptions were not usually discussed formally, they were prevalent for a number of years (3).

This is a particular problem in the development of electrochemical detectors for Liquid Chromatography. Flow Injection Analysis is often used prior to the application of chromatography to characterize the behavior of the electrode and the electrochemistry of the analyte (3,4,37, 38,42-44). The column is removed from the flow system and the injector is connected to the electrode with a piece of tubing. Since no analysis is actually performed, a more appropriate name for this technique would be "Flow Injection Amperometry". The thought is as follows: In the absence of a column, the signal from the electrode is analogous to a steady-state current and can be used to study the behavior of the electrode and the electrochemistry without complications due to the flow system. Actually, one type of dependency on the flow system is unintentionally exchanged for another type.

A desirable objective would be to develop a general theory of dispersion to explain the current response of an electrode in Liquid Chromatography and in Flow Injection Analysis. Theories on band

broadening in Liquid Chromatography (45,46) and on dispersion in Flow Injection Analysis (47-53) have been published. These works are based on models which assume that the signal from a detector in a dispersive system is a gaussian-shaped function of time. The dispersion is expressed in terms of empirical parameters such as HETP, the height equivalent to a theoretical plate; N, the number of imaginary mixing stages in a flow stream; t_i, the mean residence time in an imaginary mixing stage; and W_0, the width of the peak when extrapolated back to the moment of injection. The results provide useful qualitative information about factors which influence dispersion; but, the relationship between real parameters and dispersions is always expressed in terms of empirical parameters. Because of the heavy reliance on an assumed mass distribution and on the use of empirical parameters, the models above do not provide enough information to describe the amperometric response of an electrode accurately.

This thesis focuses on the amperometric response of the tubular electrode in Flow Injection Analysis as a first step in developing a general theory concerning the amperometric response of an electrode in a dispersive system. The problem of dispersion in Flow Injection Analysis was chosen because of the general lack of knowledge in the area and because of the relative simplicity of this problem when compared to the problem of dispersion in Liquid Chromatography. Hopefully, the results of this study can later be extended to include the effects of dispersion in Liquid Chromatography.

In this study, a theory of dispersion in fluid streams based upon a physical model of dispersion is developed, and equations describing the current-time curve, the peak current and the area under the current-time curve for a tubular electrode are derived. The theory is compared to the results of an experiment in which the amperometric and pulse-amperometric responses of a tubular electrode were recorded for various values of V_R, V_S, and v_f. Factors that influence the dispersion and amperometric response of the electrode, the limitations of the theory, and the relative merits of peak current and peak area as analytical measurements are discussed. Although this study deals specifically with the tubular electrode, general results which are applicable to electrodes of different geometries and to other types of detectors are also presented.

B. Theoretical Considerations

1. Dispersion of a mass in a fluid stream

After being injected into a fluid stream, the analyte in a liquid sample is transported by convection and diffusion. Since not all portions of the sample are transported in an identical fashion in the stream, a redistribution of the analyte occurs. The net effect of the redistribution is the dispersion of the analyte into the neighboring regions of the fluid stream.

The process of dispersion in a stream flowing through a straight tube under laminar conditions is illustrated in Figure IV-1. The velocity of the fluid at any point in the tube, U_r, is a function of

Figure IV-1. Distribution of the mean concentration of an analyte in a fluid stream

A. Initial mass distribution

B. Dispersed mass distribution

A. INITIAL MASS DISTRIBUTION

t=0

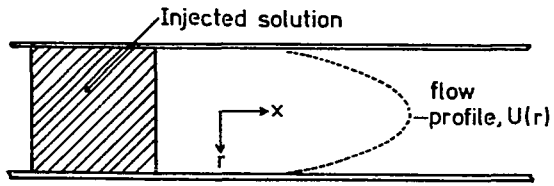

LONGITUDINAL CROSS-SECTION

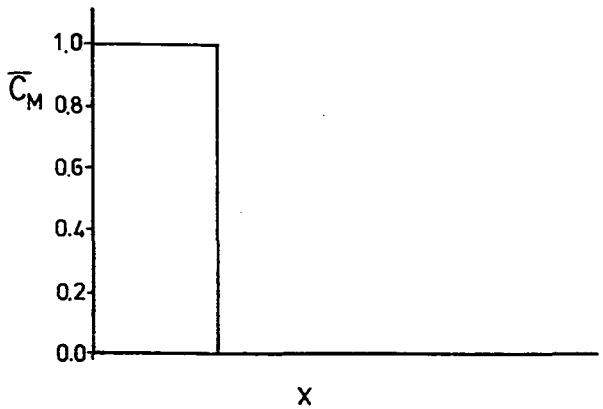

B. DISPERSED MASS DISTRIBUTION

t > 0

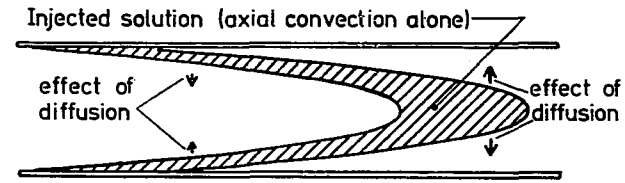

LONGITUDINAL CROSS-SECTION

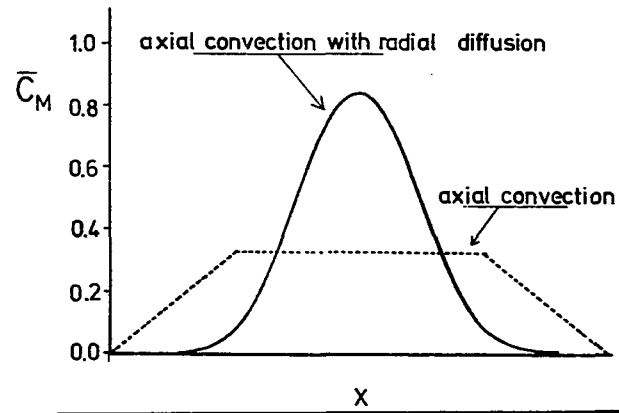

the radial distance, r, from the axis of the tube as described by the Poiseuille equation (Equation IV-1).

$$U_r = U_o(1 - r^2/a^2) \qquad \text{(IV-1)}$$

In Equation IV-1, a is the radius of the tube and U_o is the maximum fluid velocity which exists at the axis of the tube, i.e., r = 0. At the walls of the tube, r = a and $U_r = 0$. The distribution of U_r across the diameter of the tube has the shape of a parabola as shown in Figure IV-1. Immediately upon placing the sample in the fluid stream, i.e., t = 0, the analyte is assumed to be homogeneous throughout the region of the tube occupied by the sample and at a concentration equal to the original concentration of the analyte in the sample. C_o. The distribution of the analyte at t = 0 is shown in Figure IV-1A by the diagram showing the longitudinal cross-section of the stream and by the plot of the normalized mean concentration of the analyte over the radial cross-section, $\bar{C}_m$, versus the distance along the axis of the tube, x. After the injection, different regions of the sample are carried by the stream at different rates because of the radial nonuniformity of the velocity of the stream. The sample near the axis of the tube is carried faster than the sample near the walls of the tube. If axial convection was the only mode of mass transport, then the material in the sample would be spread along the tube and confined to a parabola-shaped region in the fluid stream as shown in the diagram of the longitudinal cross-section in Figure IV-1B.

The dispersion of the sample is, however, complicated by the radial diffusion of the sample from the parabola-shaped region. The inequalities in the rates of axial mass transport causes the development of a

radial concentration gradient. Diffusion occurs in a direction parallel to concentration gradients and has the effect of decreasing the severity of the gradient. Within the fluid stream, under laminar flow, diffusion is the only mechanism for transport of the analyte in a radial direction; the radial fluid velocity is zero for laminar flow. Analyte concentrated in the faster moving regions of the sample diffuses outward to slower moving regions of the fluid stream, while analyte concentrated in the slower moving regions of the sample diffuses inward to faster moving regions of the fluid stream. This movement of the analyte is represented by arrows in the diagram of the longitudinal cross-section in Figure IV-1B. The effects of radial diffusion seem at first almost contradictory. Radial diffusion mixes the components of the sample into the fluid stream but also restricts the axial dispersion of the sample through the movements described above. The extent to which radial diffusion affects the mass distribution of a sample depends upon the relative rates of axial convection and radial diffusion. Changes in radial variations in concentration due to axial convection must be slower than changes due to radial diffusion if diffusion is to have an appreciable effect on the mass distribution. The effect of radial diffusion is shown in Figure IV-1B in the comparison of the mass distribution of a sample dispersed by axial convection alone to the mass distribution of a sample dispersed by a combination of axial convection and radial diffusion.

While both axial convection and radial diffusion affect the mass distribution within a tube, radial diffusion plays a particularly

important role in the current-time response of a tubular electrode to a dispersed mass. Radial diffusion brings the analyte to the surface of the electrode making a reaction possible. The current at an electrode is proportional to the rate at which the analyte diffuses across the stagnant layer of fluid at the surface of the electrode where U_r is virtually zero. This stagnant layer of fluid is known as the diffusion layer. Since the diffusion layer is very thin, the electrode is sensitive only to the concentration of the analyte near the surface of the electrode. This is in contrast to the more common spectrophotometric detector which responds to the total mass in the cross-section of the tube. The concentration of the analyte near the surface of the electrode depends largely on radial diffusion because of the role of radial diffusion in establishing the radial concentration profile across the tube. In the limiting case of dispersion of the sample by high axial convection and low radial diffusion (mass distribution for convection alone is shown in Figure IV-1B), the mass in the first portion of the sample to pass through the detector would be concentrated in the center of the fluid stream and away from the surface of the electrode. The electrode would be "blind" to this portion of the sample. Radial diffusion is, therefore, necessary to bring the mass from the early part of the sample to the surface of the electrode.

2. Mathematical description of dispersion

For the system described above, the concentration of an analyte, C, as a function of axial distance, x, radial distance, r, and time, t, is given by Equation IV-2

$$\frac{\partial C}{\partial t} = D\left(\frac{\partial^2 C}{\partial r^2} + \frac{1}{r}\frac{\partial C}{\partial r} + \frac{\partial^2 C}{\partial x^2}\right) - U_o\left(1 - \frac{r^2}{a^2}\right)\frac{\partial C}{\partial x} \qquad \text{(IV-2)}$$

where D is the coefficient of diffusion of the analyte. The solution of Equation IV-2 with the appropriate boundary conditions gives the value of C for all values of r, x, and t, and, hence, describes the mass distribution of the sample within the fluid stream. A complete solution of the problem of the dispersion of a sample of finite volume has been published by Gill and Sankarasubramanian (54). However, due to the complexity of their treatment, an alternative, approximate solution will be offered in this thesis. This solution has been derived by other workers for a variety of applications (55-57), but has yet to be applied to Flow Injection Analysis with amperometric detection.

The fundamental work on the theory of the dispersion of matter in a fluid stream was published by Sir Geoffrey Taylor (58-60). The results of his work have been applied in many fields. For example, his findings have been applied to the dispersion of an indicator in the blood stream (61-64), to the longitudinal mixing of fluids in a pipe (65,66), to the dispersion of mass in a tubular chemical reactor (67-69), and to the theory of gas and liquid chromatography (70-72). The above is by no means a definitive list of applications. Often the application of Taylor's contribution to a field is disguised. In the case if dispersion in FIA (47-53), Taylor's findings are at the heart of the treatment although the emphasis on the variance of the mass distribution, instead of on a solution of Equation IV-2, could lead a reader to think otherwise.

In his original analysis of the problem of dispersion, Taylor offered an approximate solution to Equation IV-2 which was obtained by making the following assumptions:

1) Changes in the concentration in the axial direction due to convection are much greater than the changes due to diffusion; thus, the term $D \frac{\partial^2 C}{\partial x^2}$ in Equation IV-2 may be neglected.

2) Changes in the concentration due to convection are slow compared to the time required for diffusion to minimize radial variations in concentration.

These assumptions are easily restated: The axial mass transport is controlled by convection and the radial mass transport is controlled by diffusion. Under these conditions, Taylor found that the mean concentration of a substance, C_m, is dispersed relative to a plane, which moves with the average velocity of the fluid stream U_m, by a process analogous to molecular diffusion. Instead of a coefficient of diffusion, the proportionality constant is a coefficient of dispersion, K. Mathematically, the process is described by Equation IV-3.

$$\frac{\partial C_m}{\partial t} = K \frac{\partial^2 C_m}{\partial x'^2} \qquad \text{(IV-3)}$$

In Equation IV-3:

$$K = \frac{a^2 U_m^{\,2}}{48\, D}\,; \qquad \text{(IV-4)}$$

$$C_m = \frac{2}{a^2} \int_0^a r\, C(r) dr; \qquad \text{(IV-5)}$$

$$U_m = \frac{2}{a^2} \int_0^a r\,U(r)dr; \qquad \text{(IV-6)}$$

$$x' = x - U_m t. \qquad \text{(IV-7)}$$

The modified distance, x', is the axial coordinate in the moving frame of reference and x is the axial coordinate in the stationary frame of reference. The problem of dispersion in a three-dimensional system can now be treated in the same manner as the problem of linear diffusion and, therefore, is greatly simplified.

For the case of the dispersion of a sample of finite volume, we can assume that the sample is initially confined to a region of the fluid stream - $h \leq x' \leq +h$ and that, for $t > 0$, the sample is dispersed relative to the plane at $x' = 0$ as described by Equation IV-3 (Figure IV-2). The dispersion of the sample can be solved by considering the initial distribution to be an infinite number of line sources and by superposing the solution of the line sources (73). The solution for dispersion from a line source is

$$C_m = \frac{M}{2a^2\pi^{3/2}K^{1/2}t^{1/2}} \exp\{-x^2/4Kt\} \qquad \text{(IV-8)}$$

where M is the mass of the sample concentrated initially on the line (58). If the sample of finite volume is divided into an infinite number of lines of width ds', the mass of sample on each line would be

$$M = \pi a^2 C_o\, ds' \ . \qquad \text{(IV-9)}$$

Figure IV-2. Dispersion of a sample relative to a moving frame of reference

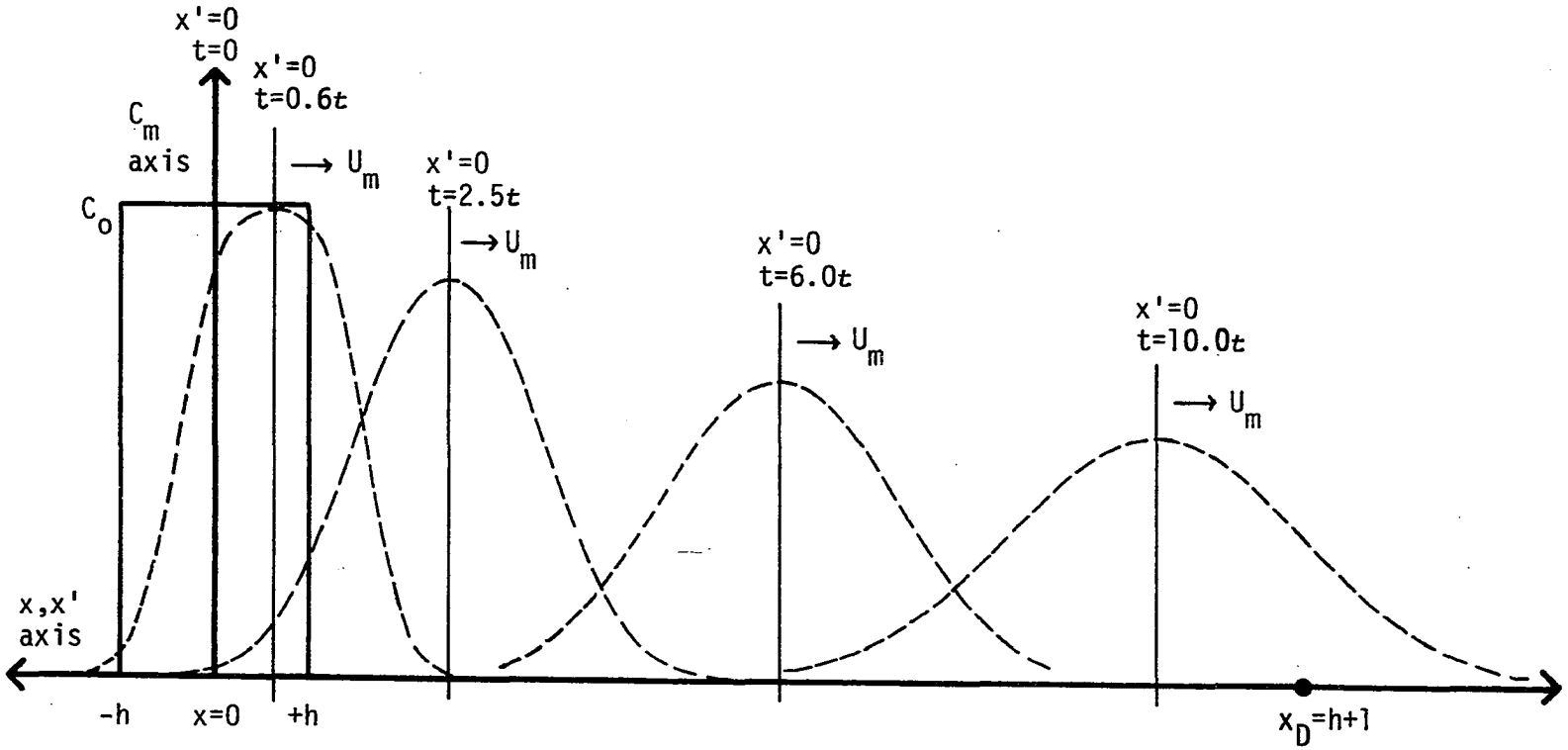
x'=0
t=0
x'=0
t=0.6t
C_m
axis
$\rightarrow U_m$
x'=0
t=2.5t
C_o
$\rightarrow U_m$
x'=0
t=6.0t
$\rightarrow U_m$
x'=0
t=10.0t
$\rightarrow U_m$
x,x'
axis
-h
x=0
+h
x_D=h+1

For an arbitrary point P' whose distance from a line source is s' (Figure IV-3), the concentration at point P' due to the dispersion of mass from the line source is

$$\frac{C_o ds'}{2\pi^{1/2} K^{1/2} t^{1/2}} \exp\{-s'^2/4Kt\} \qquad \text{(IV-10)}$$

at time t. The total concentration at P' is the sum of the contributions from all of the line sources and can be expressed as the integral

$$C_m(x',t) = \int_{x'-h}^{x'+h} \frac{C_o}{2\pi^{1/2} K^{1/2} t^{1/2}} \exp\{-s'^2/4Kt\}\, ds' \; . \qquad \text{(IV-11)}$$

The solution to the integral in Equation IV-11 is expressed in terms of the error function erf{z} where

$$\text{erf}\{z\} = \frac{2}{\pi^{1/2}} \int_0^z \exp\{-n^2\}\, dn \; . \qquad \text{(IV-12)}$$

If

$$n = \frac{s'}{2\, K^{1/2}\, t^{1/2}} \qquad \text{(IV-13)}$$

and

$$dn = \frac{ds'}{2\, K^{1/2}\, t^{1/2}} \; , \qquad \text{(IV-14)}$$

Figure IV-3. Initial distribution of the sample as an infinite number of line sources

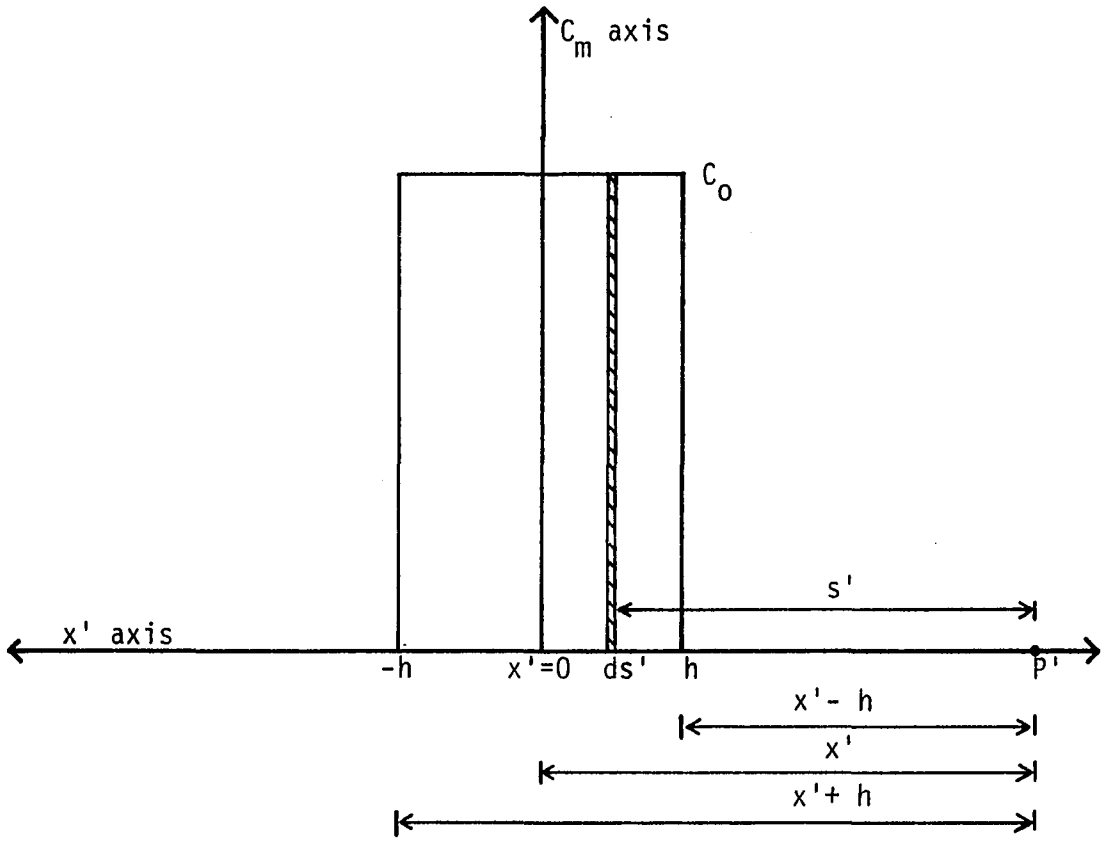
C_m axis
C_o
s'
x' axis
-h
x'=0
ds'
h
p'
x'- h
x'
x'+ h

Equation IV-11 becomes

$$C_m(x',t) = \frac{C_o}{\pi^{1/2}} \int_{\frac{x'-h}{2K^{1/2}t^{1/2}}}^{\frac{x'+h}{2K^{1/2}t^{1/2}}} \exp\{-n^2\}\, dn \qquad \text{(IV-15)}$$

By rewriting Equation IV-15 as shown in Equation IV-16,

$$C_m(x',t) = \frac{C_o}{2}\left[\frac{2}{\pi^{1/2}}\int_0^{\frac{x'+h}{2\sqrt{Kt}}} \exp\{-n^2\}\, dn - \frac{2}{\pi^{1/2}}\int_0^{\frac{x'-h}{2\sqrt{Kt}}} \exp\{-n^2\}\, dn\right], \qquad \text{(IV-16)}$$

the solution to Equation IV-11 becomes apparent upon the examination of Equation IV-12 and $C_m(x',t)$ is given by Equation IV-17.

$$C_m(x',t) = \frac{C_o}{2}\left[\operatorname{erf}\left\{\frac{h+x'}{2\sqrt{Kt}}\right\} + \operatorname{erf}\left\{\frac{h-x'}{2\sqrt{Kt}}\right\}\right] \qquad \text{(IV-17)}$$

Equation IV-17 describes dispersion in the moving frame of reference and in linear dimensions. A more useful form of the solution is desired which expresses the mean concentration of the sample within a tubular electrode as a function of time, t, the sample volume, V_S, the volume of the flow system, V_R, and the volume flow rate, v_f. In the stationary frame of reference, the electrode is positioned at a point along the axis of the flow system, X_D, such that

$$X_D = h + l \qquad \text{(IV-18)}$$

where l is the distance between the injector and the electrode (Figure IV-2). From Equation IV-7, the distance between the plane $x' = 0$ and X_D is

$$x' = X_D - U_m t = h + l - U_m t \quad . \tag{IV-19}$$

By substituting the right side of the expression above for x' in Equation IV-17, the mean concentration at the electrode becomes

$$C_m(X_D,t) = \frac{C_o}{2}\left[\text{erf}\left\{\frac{2h + l - U_m t}{2\sqrt{Kt}}\right\} + \text{erf}\left\{\frac{U_m t - l}{2\sqrt{Kt}}\right\}\right] . \tag{IV-20}$$

To express the mean concentration at the electrode in terms of V_S, V_R, and v_f, the following substitutions are made:

$$h = \frac{V_S}{2\pi a^2} \quad ; \tag{IV-21}$$

$$l = \frac{V_R}{\pi a^2} \quad ; \tag{IV-22}$$

$$U_m = \frac{1}{\pi a^2}\int_0^a 2\pi r U(r)dr = \frac{v_f}{\pi a^2} \quad . \tag{IV-23}$$

The final form of the solution for $C_m(X_D,t)$ is given by Equation IV-24.

$$C_m(X_D,t) = \frac{C_o}{2}\left[\text{erf}\left\{\frac{V_S + V_R - v_f t}{2\pi a^2\sqrt{Kt}}\right\} + \text{erf}\left\{\frac{v_f t - V_R}{2\pi a^2\sqrt{Kt}}\right\}\right] \tag{IV-24}$$

Equation IV-24 has broader applications than one would expect judging from Taylor's initial assumptions. The results of experimental work (55,56,58,62-64,74) and of numerical solutions (54,57,63,64,74-76) are in good agreement with Taylor's solution at high flow rates and for large values of time. Under these conditions, assumptions 1 and 2 are met. Subsequent studies have removed some of the restrictions placed on Taylor's original solution by extending Taylor's work to include the effects of axial diffusion (77), the time-dependency of the coefficient of dispersion, K, (54,78), and the effect of curvature of the flow system (79,80) on the process of dispersion. The extended solutions are generally not in a form that is convenient to use; however, they demonstrate that the process of dispersion is "diffusive" in nature (Equation IV-3) and that only the form of the coefficient of dispersion, K, (Equation IV-4) is changed upon removing Taylor's restrictions. Equation IV-24 can be used effectively to describe the dispersion of a system for which Taylor's assumptions are not valid provided K is determined experimentally.

In FIA, Taylor's solution is generally applicable if the curvature of the tubing is not extensive or the residence time of the sample in the fluid stream is not too small. Deviations from Taylor's solution, as they apply to FIA, are discussed in more detail in Chapter IV, Section D.

3. Amperometric response of a tubular electrode to a dispersed mass

The electrical current at a tubular electrode depends on the concentration of the analyte at the outer boundary of the diffusion layer rather than on the mean concentration of the analyte as given by

Equation IV-24. Knowledge of the radial distribution of the concentration is necessary, therefore, to describe fully the current response of a tubular electrode.

The concentration as a function of radius is given in Taylor's solution by Equation IV-25 (60) where z is the normalized radius and equal to r/a.

$$C(z) = C_m + \frac{a^2 U_m}{4D}\left(-\frac{1}{3} + z^2 - \frac{1}{2}z^4\right)\frac{\partial C_m}{\partial x} \qquad \text{(IV-25)}$$

By substituting Equation IV-24 for C_m and the first derivative of Equation IV-24 with respect to V_R ($\partial C_m/\partial V_R$) for $\partial C_m/\partial x$ into Equation IV-25, the concentration at the electrode as a function of radius can be expressed as in Equation IV-26.

$$C(X_D,z,t) = C_o\left[\frac{1}{2}\left[\operatorname{erf}\left\{\frac{V_S+V_R-v_f t}{2\pi a^2\sqrt{Kt}}\right\} + \operatorname{erf}\left\{\frac{v_f t-V_R}{2\pi a^2\sqrt{Kt}}\right\}\right] + \frac{v_f}{8\pi^{3/2}D\sqrt{Kt}}\left(-\frac{1}{3} + z^2 - \frac{1}{2}z^4\right)\cdot\left[\exp\left\{-\left(\frac{V_S+V_R-v_f t}{2\pi a^2\sqrt{Kt}}\right)^2\right\} - \exp -\left(\frac{v_f t-V_R}{2\pi a^2\sqrt{Kt}}\right)^2\right]\right] \qquad \text{(IV-26)}$$

To represent the concentration at the outer boundary of the diffusion layer, the position of an effective diffusion layer is expressed as a normalized radius and substituted into Equation IV-26. If the effective thickness of the diffusion layer δ for a tubular electrode is

$$\delta = \left(\frac{aLD}{U_o}\right)^{1/3}; \qquad \text{(IV-27)}$$

the diffusion layer occurs at the normalized radius d as given by Equation IV-28.

$$d = 1 - \frac{\delta}{a} = 1 - \left(\frac{LD}{U_o a^2}\right)^{1/3} \qquad \text{(IV-28)}$$

The substitution of the value of d for z in Equation IV-26 gives the concentration at the diffusion layer, $C(X_D,d,t)$.

The mean concentration at the electrode, $C_m(X_D,t)$, and the concentration at the diffusion layer, $C(X_D,d,t)$, were calculated from Equations IV-24, IV-26, and IV-28, for the following conditions:

$V_S = 0.157$ mL

$V_R = 1.963$ mL

$v_f = 0.47$ mL min^{-1}

$K = 5$ cm^2 s^{-1}

$D = 1.04 \times 10^{-5}$ cm^2 s^{-1}

$a = 0.05$ cm

$L = 0.159$ cm

A comparison of $C_m(X_D,t)$ and $C(X_D,d,t)$ is shown in Figure IV-4. The concentration at the diffusion layer, $C(X_D,d,t)$, lags the mean concentration. Early in the peak, the concentration at the diffusion layer is less than the mean concentration, while later in the peak, the concentration at the diffusion layer becomes greater than the mean concentration. The differences are minimal in the center region with $C(X_D,d,t)$ becoming equal to $C_m(X_D,t)$ at some point near the maxima of both curves. The lag is caused by the inability of radial diffusion to produce a uniform radial concentration in the forward and rear

Figure IV-4. Comparison of $C_m(X_D,t)$ and $C(X_D,d,t)$

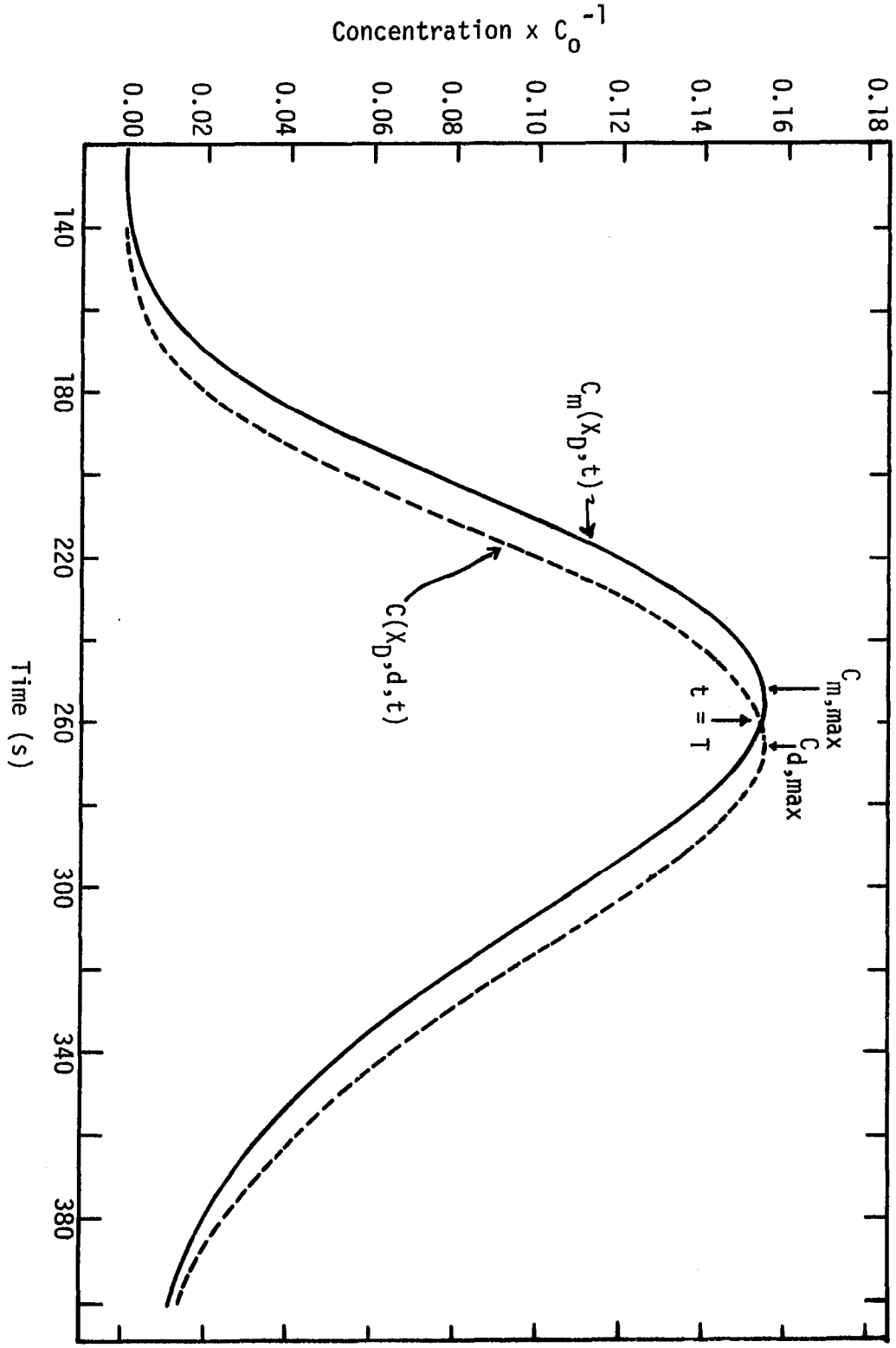
Concentration x C_o^{-1}
0.00
0.02
0.04
0.06
0.08
0.10
0.12
0.14
0.16
0.18
Time (s)
140
180
220
260
300
340
380
$C_m(X_D,t)$
$C(X_D,d,t)$
$C_{m,max}$
$C_{d,max}$
t = T

regions of the mass distribution. This is illustrated in Figure IV-5 where the concentration at the electrode is shown as a function of radius for several times in the concentration-time curve of Figure IV-4. The difference between $C_m(X_D,t)$ and $C(X_D,d,t)$ causes a subtle difference between the response of a spectrophotometric detector and that of an amperometric detector. The signal from a spectrophotometric detector follows the mean concentration, while the amperometric detector responds to the concentration at the outer boundary of the diffusion layer. In previous studies, the theory of dispersion has been tested by techniques that respond to the mean concentration. The use of a tubular electrode to verify the theory of dispersion is a more rigorous test of the theory of the radial distribution.

The current at a tubular electrode can be related to the concentration at the diffusion layer by the steady-state equation. If the electrode is very short compared to the length of tubing over which the sample is dispersed, then variation in concentration along the electrode will be negligible. The amperometric response of the tubular electrode under conditions of sample dispersion in a fluid stream is assumed to be at virtual "instantaneous steady-state" as given by Equation IV-29.

$$i(t) = 5.43nFD^{2/3}L^{2/3}v_f^{1/3}C(X_D,d,t) \qquad \text{(IV-29)}$$

By substituting Equation IV-26 into Equation IV-29, the current at the electrode for Flow Injection Analysis is expressed as a function of V_S, V_R, v_f, and t.

Figure IV-5. Concentration of the analyte at the electrode as a function of the radius of the tube

Time (cf. Figure IV-4)

A. t = 230 s

B. t = 260 s

C. t = 320 s

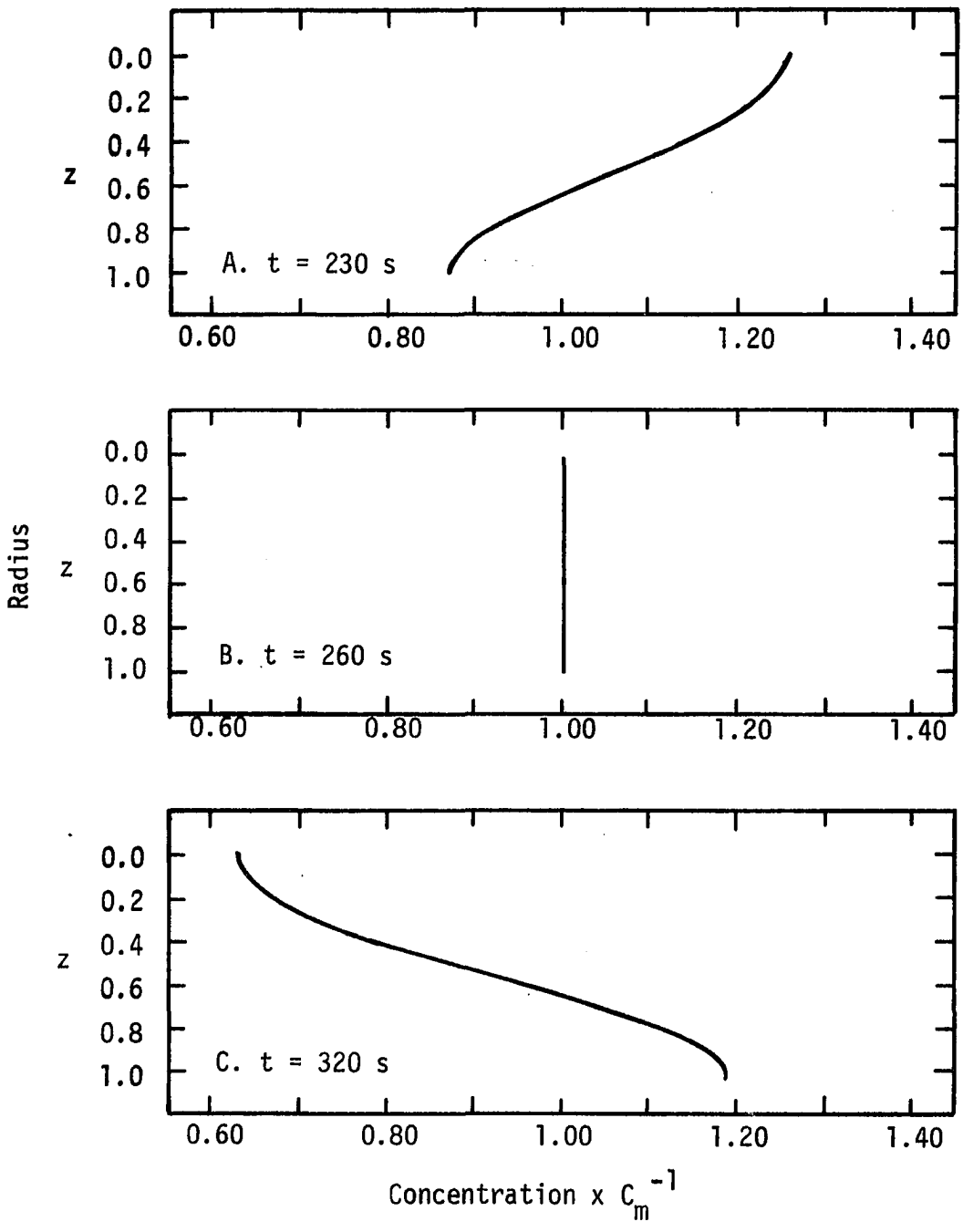
A. t = 230 s
B. t = 260 s
C. t = 320 s
z
0.0
0.2
0.4
0.6
0.8
1.0
0.60
0.80
1.00
1.20
1.40
Radius
Concentration x C_m^{-1}

$$i(t) = 5.43nFD^{2/3}L^{2/3}v_f^{1/3}C_o[\frac{1}{2}[\mathrm{erf}\{\frac{V_S+V_R-v_ft}{2\pi a^2\sqrt{Kt}}\} + \mathrm{erf}\{\frac{v_ft-V_R}{2\pi a^2\sqrt{Kt}}\}] + \frac{v_f}{8\pi^{3/2}D\sqrt{Kt}}(-\frac{1}{3} + d^2 - \frac{1}{2}d^4) \cdot [\exp -(\frac{V_S+V_R-v_ft}{2\pi a^2\sqrt{Kt}})^2\} - \exp\{-(\frac{v_ft-V_R}{2\pi a^2\sqrt{Kt}})^2\}]] \quad \text{(IV-30A)}$$

The terms outside of the brackets in Equation IV-30A form the expression for the steady-state current, I_{ss}; i.e., the electrical current produced by passing a solution of the sample at constant concentration, C_o, directly through the electrode. The substitution of I_{ss} into Equation IV-30A emphasizes the effect of dispersion on the response of the electrode in FIA.

$$i(t) = I_{ss}[\frac{1}{2}[\mathrm{erf}\{\frac{V_S+V_R-v_ft}{2\pi a^2\sqrt{Kt}}\} + \mathrm{erf}\{\frac{v_ft-V_R}{2\pi a^2\sqrt{Kt}}\}] + \frac{v_f}{8\pi^{3/2}D\sqrt{Kt}}(-\frac{1}{3} + d^2 - \frac{1}{2}d^4)[\exp\{-(\frac{V_S+V_R-v_ft}{2\pi a^2\sqrt{Kt}})\} - \exp\{-(\frac{v_ft-V_R}{2\pi a^2\sqrt{Kt}})^2\}]] \quad \text{(IV-30B)}$$

Equation IV-30B provides an expression applicable to electrodes of other geometries when d is calculated by Equation IV-31.

$$d = 1 - \frac{\delta}{a} = 1 - \frac{nFADC_o}{aI_{ss}} \quad \text{(IV-31)}$$

Equations IV-30A and IV-30B, while fully describing the current-time response of the electrode, are restricted to cases where Taylor's

assumptions are valid because of the reliance of the mathematical solution on a well-defined radial distribution. The expression for the current-time response of the electrode can be simplified to a more useful form by restricting the solution to the current at the maximum of the current-time peak. This will not only make the solution more general, but will also produce the equation for a quantity that is useful to the analytical chemist.

The peak current occurs approximately when the origin of the moving frame of reference arrives at the electrode. The examination of Figure IV-2 and Equation IV-17 shows that the maximum mean concentration in the moving frame of reference is at the origin (x'=0) and that the maximum mean concentration can be expressed as given by Equation IV-32.

$$C_m(x'=0,t) = C_o \operatorname{erf}\{\frac{h}{2\sqrt{Kt}}\} = C_o \operatorname{erf}\{\frac{V_S}{4\pi a^2\sqrt{Kt}}\} \qquad \text{(IV-32)}$$

The first derivative of Equation IV-32 with respect to axial distance, $\partial C_m/\partial x'$, is zero; thus, at the maximum, the concentration along the radius is uniform and equal to C_m.

$$C(x'=0,z,t) = C_m(x'=0,t) + \frac{a^2 U_m}{4D}(-\frac{1}{3} + z^2 - \frac{1}{2}z^4)(0) = C_m(x'=0,t) \qquad \text{(IV-33)}$$

The origin of the moving frame of reference arrives at the electrode after traversing the distance h+1 at a velocity U_m. The time for this journey is T and equal to

$$T = \frac{h+1}{U_m} = \frac{0.5\ V_S+V_R}{v_f} \quad . \qquad \text{(IV-34)}$$

The arrival of the origin (x'=0) at the electrode is closely associated with the observed maximum in the recorded current-time curve (Figure IV-4). The response of the electrode to C_m for x'=0 and t=T is, therefore, a good approximation for the peak current (Equation IV-35).

$$i_p = 5.43nFD^{2/3}L^{2/3}v_f^{1/3}C_m(x'=0,T) \qquad \text{(IV-35)}$$

With the substitution of Equations IV-32 and IV-34, Equation IV-35 can be written in several forms.

$$i_p = 5.43nFD^{2/3}L^{2/3}v_f^{1/3}C_o\,\mathrm{erf}\left\{\frac{V_S}{4\pi a^2\sqrt{KT}}\right\} \qquad \text{(IV-36A)}$$

$$i_p = 5.43nFD^{2/3}L^{2/3}v_f^{1/3}C_o\,\mathrm{erf}\left\{\frac{V_S}{4\pi a^2}\sqrt{\frac{v_f}{K(0.5V_S + V_R)}}\right\} \qquad \text{(IV-36B)}$$

Similar to Equation IV-30A, Equations IV-36A and IV-36B can also be expressed in a more general form in terms of the steady-state current, I_{ss}, as given by Equations IV-37A and IV-37B.

$$i_p = I_{ss}\,\mathrm{erf}\left\{\frac{V_S}{4\pi a^2\sqrt{KT}}\right\} \qquad \text{(IV-37A)}$$

$$i_p = I_{ss}\,\mathrm{erf}\left\{\frac{V_S}{4\pi a^2}\sqrt{\frac{v_f}{K(0.5V_S + V_R)}}\right\} \qquad \text{(IV-37B)}$$

The relationship between the true maximum in the current-time peak and the maximum as represented by the equations above is shown in Figure IV-4. The true maximum can be calculated from Equation IV-30A by substituting into Equation IV-30A the time at which the derivative of

Equation IV-30A with respect to time, $\frac{di(t)}{dt}$, is equal to zero. The calculation of the true maximum is tedious and does not readily give information about the relationships among the various parameters. Equations IV-35 through IV-37B are good approximations to the true maximum, are easy to calculate, and readily show the approximate dependence of i_p upon V_S, V_R, and v_f. Since they depend solely on C_m, Equations IV-35 through IV-37B can be used in the case where K is determined experimentally and radial distribution of concentration is not known. Equations IV-37A and IV-37B are also applicable to pulse voltammetry.

The expression for i_p can be further simplified for high dispersion by an approximation for the error function. For numerical values of x less than 0.2, the approximation for the error function shown below is accurate as verified in Table IV-1.

$$\text{erf}\{x\} = 2x/\pi^{1/2} \qquad \text{(IV-38)}$$

Table IV-1. Approximate numerical values of erf{x}

x	erf{x}	$2x/\pi^{1/2}$	error
0.0	0.000	0.000	0.0%
0.1	0.112	0.113	0.9%
0.2	0.223	0.226	1.3%
0.4	0.428	0.451	5.3%
0.6	0.604	0.677	12.1%
1.0	0.843	1.128	33.8%

On the basis of the approximation, Equations IV-36A through IV-37B can be written as

$$i_p = 5.43nFD^{2/3}L^{2/3}v_f^{1/3}C_o\left(\frac{V_S}{2\pi^{3/2}a^2\sqrt{KT}}\right) \qquad \text{(IV-39A)}$$

$$i_p = 5.43nFD^{2/3}L^{2/3}v_f^{1/3}C_o\left[\frac{V_S}{2\pi^{3/2}a^2}\sqrt{\frac{v_f}{K(0.5V_S + V_R)}}\right] \qquad \text{(IV-39B)}$$

$$i_p = I_{ss}\left(\frac{V_S}{2\pi^{3/2}a^2\sqrt{KT}}\right) \qquad \text{(IV-39C)}$$

and

$$i_p = I_{ss}\,\frac{V_S}{2\pi^{3/2}a^2}\sqrt{\frac{v_f}{K(0.5V_S + V_R)}} \qquad \text{(IV-39D)}$$

respectively. Again, Equations IV-39A and IV-39B are specific for a tubular electrode, while Equations IV-39C and IV-39D are more general and are applicable to electrodes of other geometries and to pulse amperometry.

4. Coulometric response of a tubular electrode to a dispersed mass

An important analytical measure of the quantity of the analyte injected into a fluid stream is the area under the current-time peak. This area is the charge in coulombs, Q_p, which has passed through the electrode during the electrolysis of the sample and is represented by the integral in Equation IV-40.

$$Q_p = \int_0^\infty i(t)dt \qquad \text{(IV-40)}$$

Intuitively, Q_p is expected to be independent of dispersion, and dependent only on the concentration of the analyte and the volume of the sample injected. The relationship between Q_p and the experimental parameters can be postulated for the hypothetical case in which there is no dispersion of an injected sample. If a sample of concentration C_o is injected into a fluid stream, the response of the electrode in the absence of dispersion would be a square wave, the height of which would be a steady state current. The width of the square wave would be the residence time of the sample in the electrode, t_r, and equal to the length of the sample zone divided by the flow rate. The charge passed through the electrode is, therefore, the product of Q_p, the steady state current, I_{ss}, and the residence time, t_r, and can be expressed in several ways as given by Equation IV-41.

$$Q_p = I_{ss}\, t_r = I_{ss}\, \frac{2h}{U_m} = I_{ss}\, \frac{V_S}{v_f} \qquad \text{(IV-41)}$$

Since the steady-state current is a function of flow rate, the relationships in Equations IV-41 are best written as

$$Q_p = \frac{kC_o V_S}{v_f^{1-\alpha}} \qquad \text{(IV-42)}$$

when

$$I_{ss} = k v_f^{\alpha} C_o \,.$$

For a tubular electrode where

$$k = 5.43nFD^{2/3}L^{2/3}$$

and

$$\alpha = 1/3,$$

Equation IV-42 becomes Equation IV-43.

$$Q_p = \frac{5.43nFD^{2/3}L^{2/3}V_SC_o}{v_f^{2/3}} \qquad \text{(IV-43)}$$

When Q_p is assumed to be independent of dispersion, the expression for Q_p is dependent on the sample volume, V_S, and the volume flow rate, v_f, but not on the other parameters of the flow system which affect the dispersive process.

To prove that Q_p is independent of dispersion, a more rigorous analysis is required. As stated in Equation IV-40, Q_p is the integral of the current function with respect to time evaluated between the limits of t=0 and t=∞. From Equation IV-30B, the charge Q_p due to a sample injected into a fluid stream is expressed as the integral shown below.

$$Q_p = I_{ss}\int_o^\infty \left[\frac{1}{2}\left[\mathrm{erf}\left\{\frac{V_S+V_R-v_ft}{2\pi a^2\sqrt{Kt}}\right\} + \mathrm{erf}\left\{\frac{v_ft-V_R}{2\pi a^2\sqrt{Kt}}\right\}\right]\right.$$
$$+ \frac{v_f}{8\pi^{3/2}D\sqrt{Kt}}\left(-\frac{1}{3} + d^2 - \frac{1}{2}d^4\right)\left[\exp\left\{-\left(\frac{V_S+V_R-v_ft}{2\pi a^2\sqrt{Kt}}\right)^2\right\}\right.$$
$$\left.\left. - \exp\left\{-\left(\frac{v_ft-V_R}{2\pi a^2\sqrt{Kt}}\right)^2\right\}\right]\right] dt \qquad \text{(IV-44)}$$

The solution to Equation IV-44 was obtained by Dr. Glenn Leucke, Department of Mathematics, Iowa State University, and will be presented here in several steps. For convenience, the integral in Equation IV-44 is divided into integrals A and B such that

$$A = \int_0^\infty \left[\operatorname{erf}\left\{\frac{V_S+V_R-v_f t}{2\pi a^2\sqrt{Kt}}\right\} + \operatorname{erf}\left\{\frac{v_f t-V_R}{2\pi a^2\sqrt{Kt}}\right\}\right]dt \qquad \text{(IV-45)}$$

and

$$B = \int_0^\infty \frac{1}{\sqrt{Kt}}\left[\exp\left\{-\left(\frac{V_S+V_R-v_f t}{2\pi a^2\sqrt{Kt}}\right)^2\right\} - \exp\left\{-\left(\frac{v_f t-V_R}{2\pi a^2\sqrt{Kt}}\right)^2\right\}\right]dt \; . \qquad \text{(IV-46)}$$

With this notation, Equation IV-44 becomes

$$Q_p = I_{ss}\left[\frac{1}{2}A + \frac{v_f}{8\pi^{3/2}D}\left(-\frac{1}{3} + d^2 - \frac{1}{2}d^4\right)B\right] \; . \qquad \text{(IV-47)}$$

In the solution of Integral A, the following substitutions are made to simplify the notation:

$b = V_R$

$c = V_S+V_R$

$f = 2\pi a^2\sqrt{K}$

$g = v_f$

Integral A is now written as Equation IV-48.

$$A = \int_0^\infty \left[\operatorname{erf}\left\{\frac{c-gt}{ft^{1/2}}\right\} + \operatorname{erf}\left\{\frac{gt-b}{ft^{1/2}}\right\}\right]dt \qquad \text{(IV-48)}$$

The error function is an odd function; hence, erf{-x} = -erf{x}. As a consequence, Equation IV-48 can be written as

$$A = \int_0^\infty [\mathrm{erf}\{\frac{gt-b}{ft^{1/2}}\} - \mathrm{erf}\{\frac{gt-c}{ft^{1/2}}\}]dt \qquad \text{(IV-49)}$$

If the substitutions

$$\alpha(t) = \frac{gt-b}{ft^{1/2}}$$

and

$$\beta(t) = \frac{gt-c}{ft^{1/2}}$$

are made, Equation IV-49 becomes Equation IV-50.

$$A = \int_0^\infty [\mathrm{erf}\{\alpha(t)\} - \mathrm{erf}\{\beta(t)\}]dt \qquad \text{(IV-50)}$$

By definition of the error function

$$\mathrm{erf}(x) = \frac{2}{\pi^{1/2}} \int_0^x \exp\{-y^2\}dy,$$

Equation IV-50 can be written as Equation IV-51.

$$A = \frac{2}{\pi^{1/2}} \int_0^\infty \left[\int_0^{\alpha(t)} \exp\{-y^2\}dy - \int_0^{\beta(t)} \exp\{-y^2\}dy \right] dt \qquad \text{(IV-51)}$$

Since $\alpha(t)$ is greater than $\beta(t)$, the integrals representing the error functions can be combined and A can be expressed as a double integral (Equation IV-52).

$$A = \frac{2}{\pi^{1/2}} \int_0^{\infty} \int_{\beta(t)}^{\alpha(t)} \exp\{-y^2\} dy dt = \int_R \int \exp\{-y^2\} dy dt \qquad \text{(IV-52)}$$

The symbol R in Equation IV-52 is the space between the two curves $y=\beta(t)$ and $y=\alpha(t)$ (Figure IV-6).

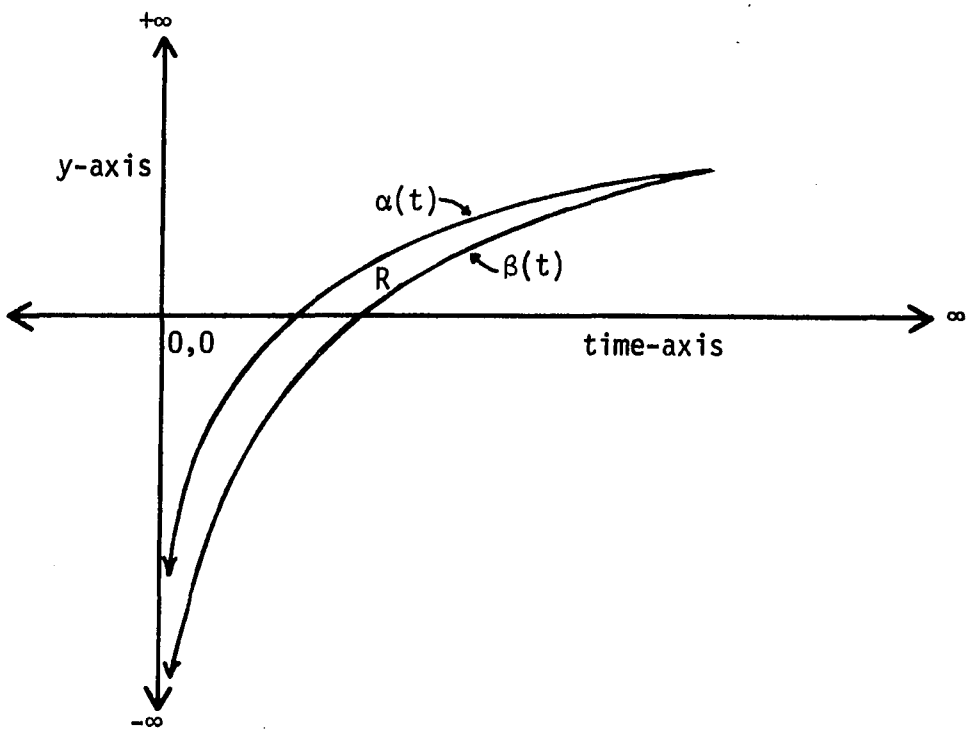

Figure IV-6. Functions $\alpha(t)$ and $\beta(t)$

Equation IV-52 can be evaluated by reversing the order of integration. When the order of integration is reversed, new limits of integration must be determined. The new limits of the internal integral must define the boundaries of region R with t as the dependent variable instead of y. These limits can be found by solving the equations $y=\alpha(t)$ and $y=\beta(t)$ for t. For the time being, these limits will be designated as $\alpha^{-1}(y)$ and $\beta^{-1}(y)$, respectively. The new limits of y must be wide enough to include all of region R and, therefore, can be set at $-\infty$ and ∞. After rearranging Equation IV-52, Integral A becomes

$$A = \frac{2}{\pi^{1/2}} \int_{-\infty}^{\infty} \int_{\alpha^{-1}(y)}^{\beta^{-1}(y)} \exp\{-y^2\} dt dy \qquad \text{(IV-53)}$$

The evaluation of the internal integral in Equation IV-53 is as follows:

$$\int_{\alpha^{-1}(y)}^{\beta^{-1}(y)} \exp\{-y^2\} dt = \exp\{-y^2\} t \Big|_{\alpha^{-1}(y)}^{\beta^{-1}(y)} = \exp\{-y^2\}[\beta^{-1}(y) - \alpha^{-1}(y)] \qquad \text{(IV-54)}$$

Equation IV-53 becomes

$$A = \frac{2}{\pi^{1/2}} \int_{-\infty}^{\infty} \exp\{-y^2\}[\beta^{-1}(y) - \alpha^{-1}(y)] dy \qquad \text{(IV-55)}$$

Before Equation IV-55 can be solved, the values of $\alpha^{-1}(y)$ and $\beta^{-1}(y)$ must be derived. By definition,

$$y = \alpha(t) = \frac{g}{b}\sqrt{t} - \frac{b}{f}\frac{1}{\sqrt{t}} \quad . \tag{IV-56}$$

Equation IV-56 can be rearranged to the form

$$\frac{g}{b}(\sqrt{t})^2 - y(\sqrt{t}) - \frac{b}{f} = 0 \tag{IV-57}$$

which is a quadratic equation, the solution of which is Equation IV-58.

$$\sqrt{t} = \frac{y \pm \sqrt{y^2 + 4\frac{gb}{f^2}}}{\frac{2g}{f}} \tag{IV-58}$$

Since $ab>0$, $\frac{g}{b}>0$, and $\sqrt{t} \geq 0$, the only solution of concern is

$$\sqrt{t} = \frac{y + \sqrt{y^2 + 4\frac{gb}{f^2}}}{\frac{2g}{f}} \quad .$$

Hence,

$$t = \left[\frac{y + \sqrt{y^2 + 4\frac{gb}{f^2}}}{\frac{2g}{f}}\right]^2 = \alpha^{-1}(y) \quad . \tag{IV-59}$$

If the same procedure is followed for

$$y = \beta(t) = \frac{g}{b}\sqrt{t} - \frac{c}{f}\frac{1}{\sqrt{t}} \quad ,$$

the solution for $\beta^{-1}(y)$ is

$$\beta^{-1}(y) = \left[\frac{y + \sqrt{y^2 + \frac{4gc}{f^2}}}{\frac{2g}{f}} \right]^2 . \qquad \text{(IV-60)}$$

The difference $\beta^{-1}(y) - \alpha^{-1}(y)$ is now calculated.

$$\beta^{-1}(y) - \alpha^{-1}(y)$$

$$= \frac{f^2}{4g^2} \left[y^2 + 2y \sqrt{y^2 + 4\frac{gc}{f^2}} + y^2 + \frac{4gc}{f^2} - y^2 - 2y \sqrt{y^2 + 4\frac{gb}{f^2}} - y - \frac{4gb}{f^2} \right]$$

$$= \frac{f^2}{4g^2} \left[2y\left(\sqrt{y^2 + \frac{4gc}{f^2}} - \sqrt{y^2 + \frac{4gb}{f^2}}\right) + \frac{4g}{f^2}(c-b) \right] \qquad \text{(IV-61)}$$

By substituting Equation IV-61 into Equation IV-55, Integral A becomes

$$A = \frac{f^2}{2\pi^{1/2}} \int_{-\infty}^{\infty} \exp\{-y^2\} \left[2y\left(\sqrt{y^2 + \frac{4gc}{f^2}} - \sqrt{y^2 + \frac{4gb}{f^2}}\right) \right] dy$$

$$+ \frac{f^2}{2\pi^{1/2} g^2} \int_{-\infty}^{\infty} \exp\{-y^2\} \left[\frac{4g(c-b)}{f^2} \right] dy \qquad \text{(IV-62)}$$

The term

$$2y\left(\sqrt{y^2 + \frac{4gc}{f^2}} - \sqrt{y^2 + \frac{4gb}{f^2}}\right)$$

is an odd function, i.e., $F(-y) = -F(y)$; thus, the solution of the first integral in Equation IV-62 is zero. Equation IV-62 becomes

$$A = \frac{2(c-b)}{\pi^{1/2} g} \int_{-\infty}^{\infty} \exp\{-y^2\} dy = \frac{2(c-b)}{g} \quad . \tag{IV-63}$$

The final solution of Integral A, after substituting back to the original parameters, is

$$A = \frac{2\ V_S}{v_f} \quad . \tag{IV-64}$$

To aid in the evaluation of Integral B, the following substitutions are made:

$$b = \frac{V_S + V_R}{2\pi a^2 \sqrt{K}}$$

$$c = \frac{v_f}{2\pi a^2 \sqrt{K}}$$

$$f = \frac{V_R}{2\pi a^2 \sqrt{K}}$$

$$g = \frac{1}{\sqrt{K}}$$

$$x = \sqrt{t}$$

$$2xdx = dt$$

Integral B is now written as Equation IV-65.

$$B = 2g \int_0^\infty [\exp\{-(\frac{b}{x} - cx)^2\} - \exp\{-(cx - \frac{f}{x})^2\}]dx \qquad \text{(IV-65)}$$

By expanding the term in the bracket for each exponential, Equation IV-65 becomes

$$B = 2g \int_0^\infty [\exp\{-(\frac{b^2}{x^2} + 2bc - c^2x^2)\} - \exp\{-(c^2x^2 + 2cf - \frac{f^2}{x^2})\}]dx$$

$$= 2g \exp\{2bc\} \int_0^\infty \exp\{-\frac{b^2}{x^2} - c^2x^2\}dx$$

$$+ 2g \exp\{2cf\} \int_0^\infty \exp\{-c^2x^2 - \frac{f^2}{x^2}\}dx \qquad \text{(IV-66)}$$

The variable is now changed to

$$y = cx .$$

With the change in variable,

$$dx = \frac{dy}{c} ,$$

$$\frac{b}{x} = \frac{bc}{y} ,$$

and

$$\frac{f}{x} = \frac{fc}{y} .$$

Since c is greater than zero, Integral B becomes

$$B = \frac{2g}{c} \exp\{2bc\} \int_0^\infty \exp\{-y^2 - \frac{(bc)^2}{y^2}\} dy$$

$$+ \frac{2g}{c} \exp\{2cf\} \int_0^\infty \exp\{-y^2 - \frac{(fc)^2}{y^2}\} dy \qquad \text{(IV-67)}$$

From a table of integrals (81),

$$\int_0^\infty \exp\{-x^2 - (a/x)^2\} dx = \frac{\pi^{1/2}}{2} \exp\{-2a\}$$

The solution to Equation IV-67 is, therefore,

$$B = \frac{2g}{c} \exp\{2bc\} \cdot \frac{\pi^{1/2}}{2} \exp\{-2bc\}$$

$$- \frac{2g}{c} \exp\{2cf\} \cdot \frac{\pi^{1/2}}{2} \exp\{-2cf\} = \frac{g\pi^{1/2}}{c} - \frac{g\pi^{1/2}}{c} \qquad \text{(IV-68)}$$

with final solution to Integral B as

$$B = 0 \quad . \qquad \text{(IV-69)}$$

By substituting the solution of Integral A and Integral B into Equation IV-47, the charge Q_p becomes

$$Q_p = I_{ss}\left[\frac{1}{2} \cdot \frac{2V_S}{v_f} + \frac{v_f}{8\pi^{3/2}D} \left(-\frac{1}{3} + d^2 - \frac{1}{2}d^4\right)(0)\right] = I_{ss} \frac{V_S}{v_f}. \qquad \text{(IV-70)}$$

This result is identical to Equation IV-41. Since the solution of Q_p is independent of V_R and K, Q_p is predicted to be independent of dispersion and of the factors which affect dispersion.

C. Experimental

1. Instrumentation and apparatus

The instrumentation and apparatus used in this study were discussed in Chapter II. Most experiments were performed with Flow System II using Electrode II as a detector. Flow System III was substituted for Flow System II in a few of the later experiments.

2. Measurement of the volume of the sample and the volume of the flow system

The volume of the sample, V_S, and the volume of the flow system, V_R, were varied by changing the length of the tubing in the sample loop of the sample-injection valve (for V_S) and the length of the tubing between the sample-injection valve and the detector (for V_R). A series of tubes was prepared by cutting Teflon tubing into sections of various lengths and fitting each with a set of Altex Tube End Connectors.

The volume of each tube was measured by acid-base titrimetry. Solutions of 2.5 N H_2SO_4 and 0 10 N NaOH were used in the measurement of volume. The strengths of the solutions were compared by diluting 25.00 mL of the acid solution to 500.0 mL and then titrating a 25.00 mL aliquot of the dilute acid with the NaOH solution to a phenolphalein end point. The volume of the NaOH solution used in the titration represents the volume of the NaOH solution required to neutralize

1.250 mL of the stock solution of H_2SO_4. A simple flow system consisting of Teflon tubing and a sample-injection valve was constructed. One end of the flow system was connected to a container of triply distilled water (TDW) and the other end was placed in a 250-mL Erlenmeyer flask. A tube, the volume of which was to be measured, was connected to the sample-injection valve as a sample loop and filled with 2.5 N H_2SO_4. A stream of TDW was trickled through the flow system by applying air pressure to the container of TDW. The contents of the sample loop were then injected into the stream of TDW and collected in the Erlenmeyer flask. TDW was passed through the sample loop to flush all the acid from the sample loop. An approximate volume of a tube was calculated from the length ($\sim 7 \times 10^{-3}$ mL cm^{-1}). Based on these calculations, injections were repeated for tubes of low volume until approximately 1 mL of acid solution had been collected. Regardless of the number of injections, the total volume of acid and wash water collected was approximately 50 mL. The contents of the Erlenmeyer flask was then titrated with the NaOH solution to a phenolphalein end point. The volume of the tube was calculated from Equation IV-71.

$$V_T = \frac{[1.25\ mL][V_{NaOH,Inj}]}{[N][V_{NaOH,Std}]} \qquad \text{(IV-71)}$$

In Equation IV-71:

V_T = the volume of the tube (mL);

$V_{NaOH,Inj}$ = the volume of NaOH required to titrate the 2.5 N H_2SO_4 collected from the injections (mL);

$V_{NaOH,Std}$ = the volume of NaOH required to titrate 1.25 mL of 2.5 N H_2SO_4 (mL);

N = the number of injections collected for titration.

The volume of the tube, V_T, was designated as either V_S or V_R depending on where the tube was placed in the flow system.

3. Preparation of solutions

Solutions of 0.10 M H_2SO_4 and 0.10 M H_2SO_4 containing 5.00×10^{-4} M KI were used in this study. The preparation of these solutions was discussed in Chapter III. The solution of KI was kept under a nitrogen atmosphere to prevent oxidation by air throughout each experiment.

4. Procedures

At the beginning of each experiment, the electrode was polished with 1-μm Metadi diamond paste as described in Chapter III, rinsed with distilled water, and connected to the flow system. The desired flow rate was set and the solution of 5.00×10^{-4} M KI was pumped through the flow system. The potential of the electrode was then scanned for several minutes between the limits of +1.3 V and -0.3 V *vs* SCE at a rate of 3.0 V min^{-1}. The potential of the electrode was then set to +0.800 V *vs* SCE; the pulse dampener was adjusted to minimize pulsations, and the steady-state current was measured.

The solution in the eluent reservior was changed to 0.10 M H_2SO_4 and pumped through the flow system. After a constant baseline was achieved, injections of 5.00×10^{-4} M KI were made. The amperometric response (i-t) of the electrode to the injections was recorded on a

strip chart recorder. V_S and V_R were easily changed during the experiment without disturbing the characteristics of the fluid stream. Changing v_f was more difficult. Each time v_f was changed, the pulse dampener had to be readjusted and the steady-state current had to be measured at the new flow rate. Usually, v_f was held constant throughout an experiment. At the end of an experiment, the steady-state current was measured again, the flow system was flushed with distilled water, and the electrode was dried and stored under vacuum in a desiccator.

There were several variations on the above procedure. For pulse amperometric detection, the potential applied to the electrode was a square wave generated by holding the potential of the electrode at +0.425 V vs SCE for 1.0 s and then stepping the potential to +0.800 V vs SCE for 0.1 s. The electrical current was measured at +0.800 V over a 1 ms interval after a 90 ms delay. The configuration of the tube connecting the sample-injection valve with the detector was also varied. Connecting tubes were either pulled straight, intentionally coiled, or allowed to coil in a random fashion.

Peak currents were calculated from measurements of peak height made with a ruler. Peak heights were estimated to the nearest 0.02 in. The areas under current-time peaks were measured either with an electronic integrator or with a planimeter (Keuffel & Esser Co., Germany).

D. Results and Discussion

1. The shape of the current-time curve as a function of V_S, V_R, and v_f

The effects of varying V_R, V_S, and v_f on the current-time response of a tubular electrode are shown in Figures IV-7 through IV-11. General statements concerning the relationship between the parameters and the amperometric response of the electrode are made by explaining the trends observed in the figures in light of the theoretical considerations presented in Section B of this chapter and in Section B of Chapter III. In all of the following discussions, statements pertaining to the effects of varying V_R and V_S are valid only if the changes in V_R and V_S reflect changes in the length of the tubing.

The amperometric response of a tubular electrode as a function of V_R for a constant V_S and v_f is shown in Figure IV-7. Curve A in Figure IV-7, given by the dashed lines, represents the response predicted for $V_R = 0$ in the absence of dispersion. The maximum signal in Curve A is the steady-state current, I_{ss}. For $V_R > 0$ (Curves B-E), the height of the peaks decreased from the steady state value as V_R was increased, while the width of the peaks increased. The increase in dispersion with increasing V_R is related to the residence time of the sample in the fluid stream. As the length of the flow stream becomes longer, the length of time that the sample is in the fluid stream and, consequently, the length of time that a sample is subjected to dispersive forces is increased. This leads to a greater dispersion of the sample. The inverse relationship between V_R and i_p is clearly shown by Equations IV-37B and IV-39D. The relationship between the width of the peak and

Figure IV-7. Current-time curves as a function of V_R

V_R:

A - 0.00 mL (hypothetical)
B - 0.259 mL
C - 0.509 mL
D - 1.149 mL
E - 2.363 mL

Other parameters:

V_S = 0.226 mL

v_f = 0.50 mL min^{-1}

C_o = 5.00 x 10^{-4} M KI

Electrode II

Flow System II

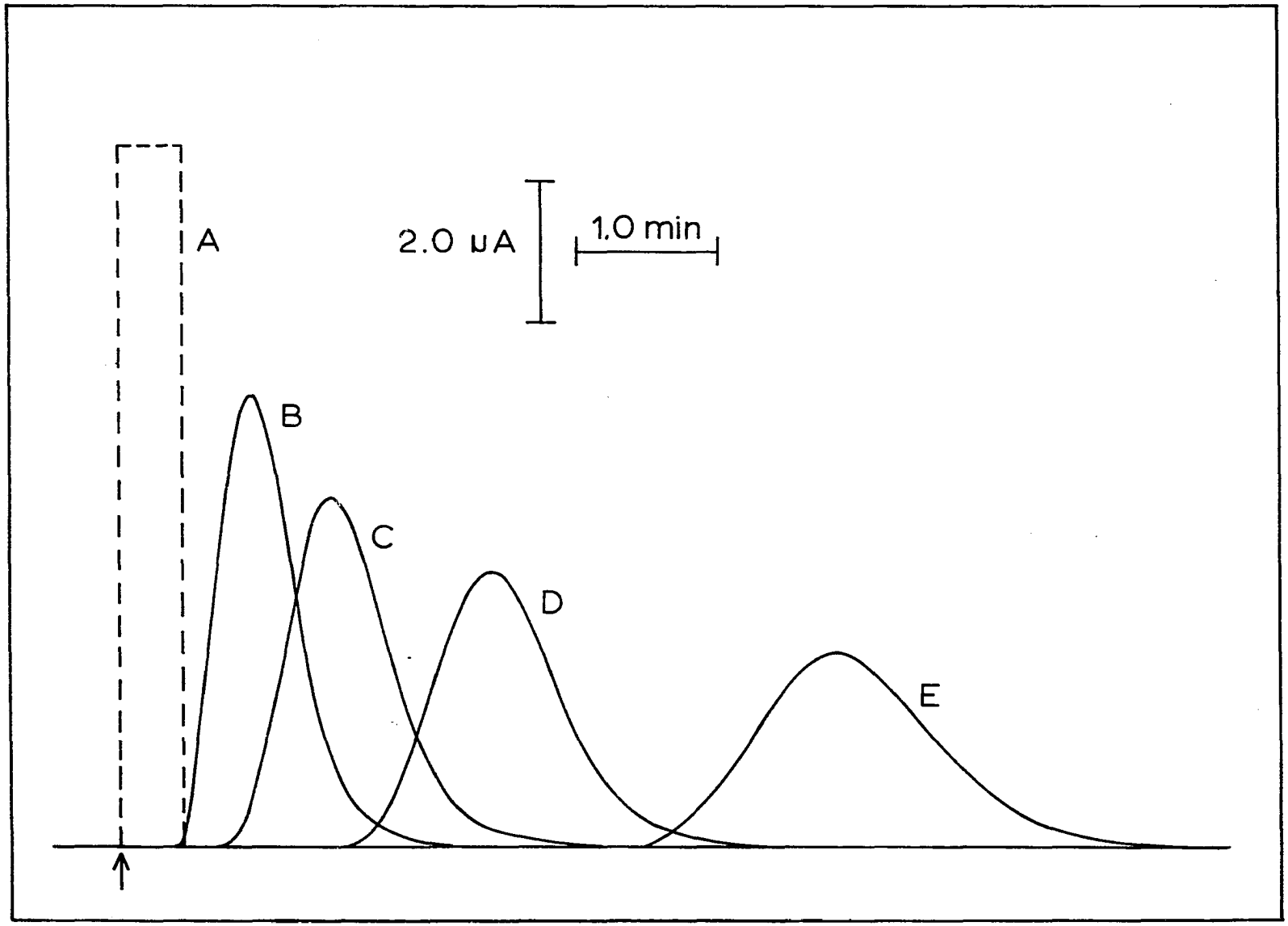
A
2.0 uA
1.0 min
B
C
D
E

V_R is expressed in Equation IV-72 if the width of the peak at one-half the peak height, $W_{1/2}$, is assumed to be equal to the area of the peak, A, divided by the peak height, H.

$$W_{1/2} = \frac{A}{H} = \frac{Q_p}{i_p} = \frac{V_S}{v_f \, \mathrm{erf}\{\frac{V_S}{4\pi a^2}\sqrt{\frac{v_f}{K(0.5\,V_S + V_R)}}\}} \qquad \text{(IV-72)}$$

Since the peak area is independent of V_R, changes in $W_{1/2}$ are inversely proportional to changes in i_p.

The symmetry of the current-time curve is also affected by the residence time of the sample in the fluid stream. Often, signal-time curves in chromatography and flow injection analysis are assumed to have symmetrical shapes. This would be true if all points on the signal-time curve were recorded at the same time (Figure IV-2). In practice, however, this is not the case. Detection occurs at a particular point along the flow system and not at a particular time. The portion of the sample which arrives at the detector early in the signal-time curve spends less time in the fluid stream than the other portions of the sample and is consequently dispersed to a lesser degree. The leading edge of the signal-time curve is, therefore, sharper than the trailing edge. With a tubular electrode, the effect of radial variations in concentration, as described in Section IV.B.3, also contributes to the asymmetric shape of the current-time curve.

The relationship between V_S and the degree of dispersion of a sample for a constant V_R and v_f is shown in Figure IV-8. As V_S increases, the effect of dispersion decreases. The maxima in the

Figure IV-8. Current-time curves as a function of V_S

V_R:

A - 1.663 mL

B - 0.955 mL

C - 0.419 mL

D - 0.226 mL

E - 0.145 mL

Other parameters:

V_R = 0.569 mL

v_f = 0.50 mL min^{-1}

C_o = 5.00 x 10^{-4} M KI

Electrode II

Flow System II

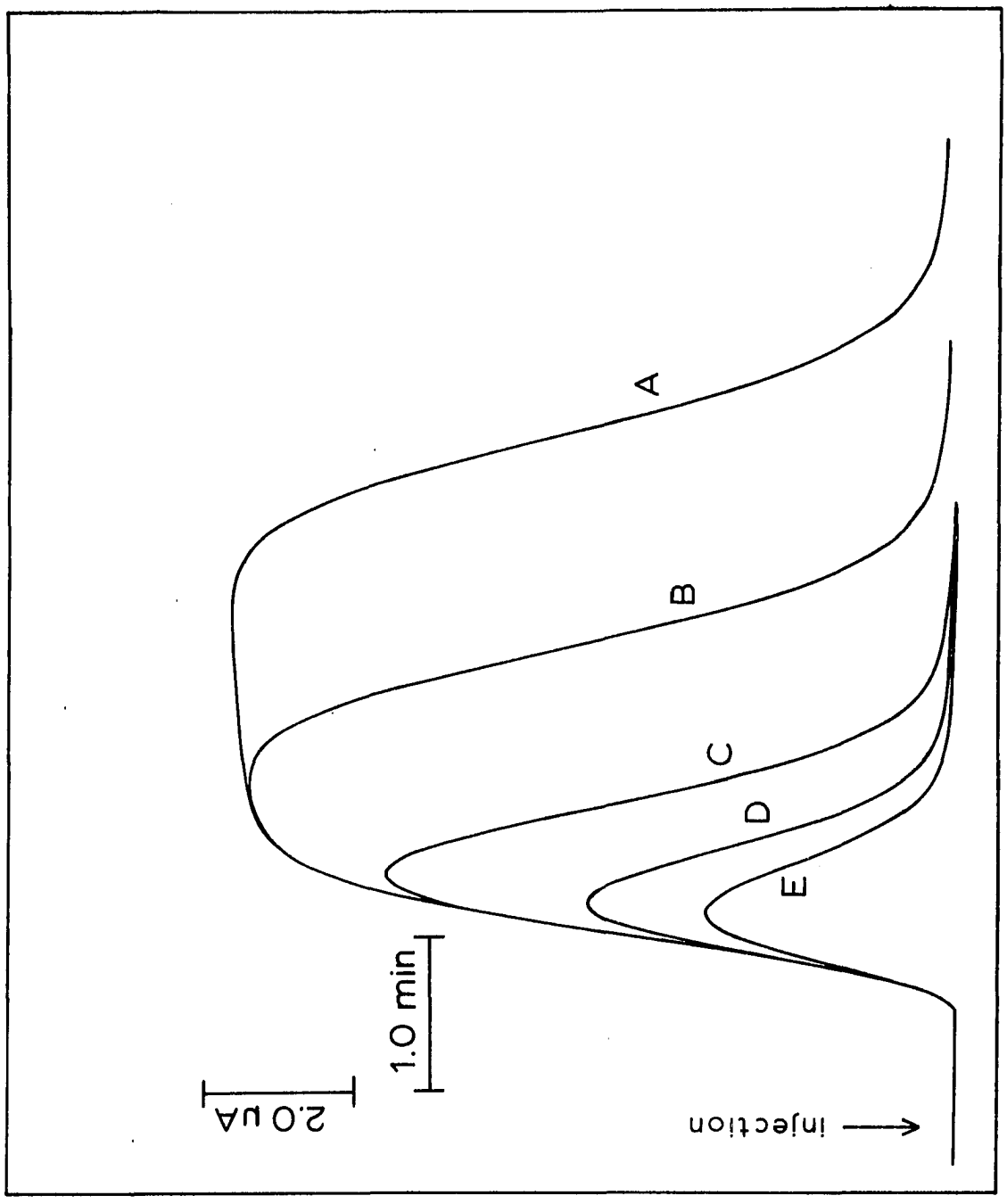
A
B
C
D
E
injection
1.0 min
2.0 uA

current-time curve reaches the value of I_{ss} for large values of V_S (Curve A) while being substantially less than I_{ss} for small values of V_S (Curves C-E). The degree of dispersion of a sample is more limited with a large sample loop than with a small sample loop because of the length of the sample zone. The sample zone can be thought of as a series of line sources of mass moving downstream at the mean fluid velocity. Under the influence of the dispersive forces, each line source loses mass at a uniform rate in both the upstream and downstream direction. The line sources at the end of the sample zone lose mass to the fluid stream while lines sources in the center of the sample zone lose mass to and gain mass from neighboring line sources at an equal rate. As the effects of dispersion move inward, outer regions of the sample zone can no longer supply the center region with enough mass to balance the loss and the center region experiences a net loss of mass. The dispersion of the sample zone, therefore, begins at the end of the sample zone and moves toward the center. Consequently, for a constant residence time, the center region of a long sample zone is affected less by dispersion than the center region of a short sample zone. This results in a higher peak current for a larger sample loop. V_S also contributes to the length of the flow stream which affects the residence time of the sample. In terms of the relationship between the degree of dispersion and V_S, the effect of V_S on the residence time of the sample is antagonistic, but secondary, to the effect of V_S on the length of the sample zone. This is shown by substituting $V_R = 0$ into Equation IV-37B (Equation IV-73).

$$i_p = I_{ss}\ \mathrm{erf}\left\{\frac{V_S}{4\pi a^2}\sqrt{\frac{v_f}{K(0.5\ V_S + V_R)}}\right\} = I_{ss}\ \mathrm{erf}\left\{\frac{V_S^{1/2}}{4\pi a^2}\sqrt{\frac{v_f}{0.5\ K}}\right\} \quad \text{(IV-73)}$$

Thus, the overall effect of increasing V_S is to increase the peak current. The width of the peak also increases with increasing V_S because of the dependence of the peak area on V_S (Equation IV-72). Although the dependence of the error function term on V_S tends to decrease $W_{1/2}$ with increasing V_S, the dependence of the peak area on V_S in the numerator is the dominant term. The increase in peak width resulting from increases in V_S represents an increase in the residence time of the sample zone in the detector due to the increased length of the sample zone.

The relationship between the height of the current-time curve and v_f is complex because of the variety of ways in which v_f influences the mass-distribution of the sample and the sensitivity of the electrode. The flow rate influences the height of the current-time curve in three ways:

1. The coefficient of dispersion, K, is a function of v_f. K is proportional to v_f^2 in a straight flow system (Equation IV-4) while being proportional to the function $\sum_{n=0}^{\infty} a_n v_f^{2(n+1)}$ in a curved flow system. Dispersion in a curved flow system is discussed in more detail in a later section. In either case, an increase in v_f increases the value of K. This reflects an increase in the dispersion and a lower current-time curve.

2. v_f affects the residence time of the sample in the fluid stream. The length of time that a sample is in the fluid stream is inversely related to v_f. The decrease in residence time with increasing v_f tends to reduce the effects of dispersion on the sample and to increase the height of the current-time curve.

3. The sensitivity of the tubular electrode is theoretically proportional to $v_f^{1/3}$ (Equation III-1). The amperometric response of a tubular electrode, therefore, increases with increasing v_f for a constant concentration. The increase in sensitivity with increasing v_f tends to increase the height of the current-time curve even though dispersion is decreasing the concentration of the analyte at the electrode.

The effects of change in v_f noted above in 1 and 2 are expressed in Equation IV-74 in the argument of the error function. Effect 1 dominates effect 2, and the value of the error function decreases with increasing v_f.

$$i_p = kv_f^{1/3} C_o \operatorname{erf}\left\{\frac{V_S}{4\pi a^2}\sqrt{\frac{v_f}{K(0.5\,V_S + V_R)}}\right\} \qquad \text{(IV-74)}$$

Effect 3 is expressed in Equation IV-74 by $v_f^{1/3}$. Since the exponent is a positive number, the change in the $v_f^{1/3}$ term with v_f is always in the direction opposite to the change in the error function. The extent

of dominance of one term over the other depends, of course, on the specific values of V_S and V_R. The value of erf{x} approaches 1.00 for $x > 3$ and changes very little for $x > 2.5$. If V_S and V_R are chosen for a low degree of dispersion, ($V_S >> V_R$), x becomes large and the value of erf{x} approaches 1.00. Changes in the value of erf{x} with changes in v_f are negligible and the $v_f^{1/3}$ term dominates the relationship between i_p and $v_f^{1/3}$. Peak height becomes approximately proportional to $v_f^{1/3}$. This is illustrated in Figure IV-9. The results in Figure IV-9 are from an early experiment in which V_R was small. The dependence of the peak height on v_f was the same for both the large sample loop ($\sim$ 3 mL) and the small sample loop ($\sim$ 0.23 mL) even though a steady-state current was not obtained with the small sample loop. Apparently, erf{x} was large enough in both cases not to be greatly influenced by a change in v_f. This experiment was performed before the effect of dispersion and the role of V_R was understood. The results of this experiment and similar experiments performed by previous workers reinforced erroneous ideas about the relationship between i_p and v_f in dispersive systems. At the other extreme, if V_S and V_R are chosen for a high degree of dispersion ($V_S << V_R$), erf{x} becomes directly proportional to x (Equation IV-38) and, consequently, proportional to $v_f^{-1/2}$ for a straight flow system. In this case, the v_f dependence of the error function term becomes dominant and i_p is proportional to $v_f^{-1/6}$. The peak height decreases with an increase in v_f (Figure IV-10). The examples above illustrate the v_f dependence of i_p for limiting cases. In practice, all values of the v_f exponent between 1/3 and -1/6 are possible. Conditions can also be

Figure IV-9. Current-time curves as a function of v_f for low dispersion

A. Steady state

$V_S \approx 3.0$ mL

B. Nonsteady state

$V_S \approx 0.23$ mL

Parameters

Au tubular electrode - 1/8 in x 0.031-in. i.d.

E_w = +0.65 V *vs* SCE

C_o = 1.0 mM NaI in 1.0 M H_2SO_4

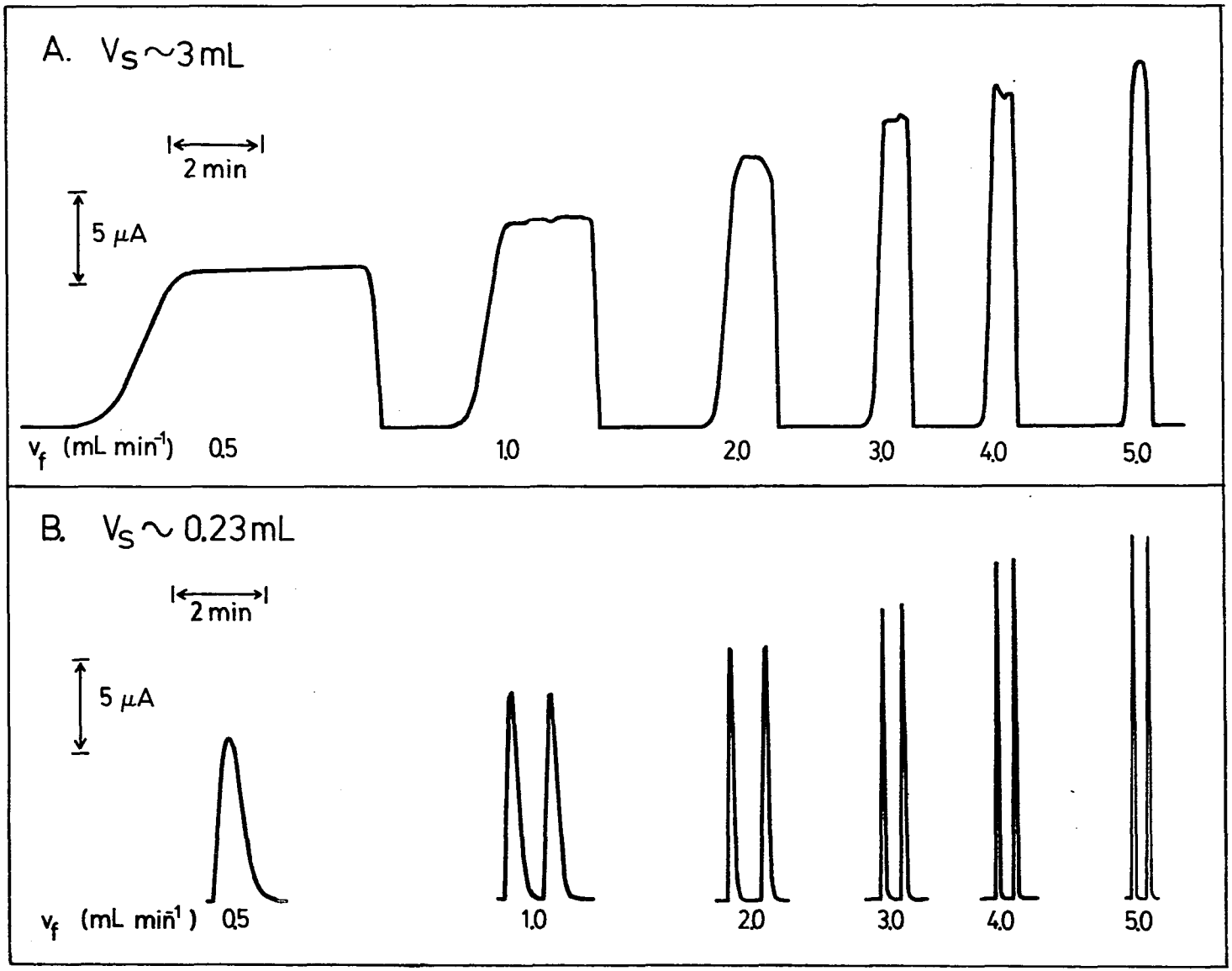
A. $V_S \sim 3$ mL
2 min
5 μA
v_f (mL min^{-1}) 0.5 1.0 2.0 3.0 4.0 5.0
B. $V_S \sim 0.23$ mL
2 min
5 μA
v_f (mL min^{-1}) 0.5 1.0 2.0 3.0 4.0 5.0

Figure IV-10. Current-time curves as a function of v_f for high dispersion

V_S = 0.226 mL

V_R = 1.168 mL

C_o = 5.00 x 10^{-4} M KI

Electrode II

Flow System II

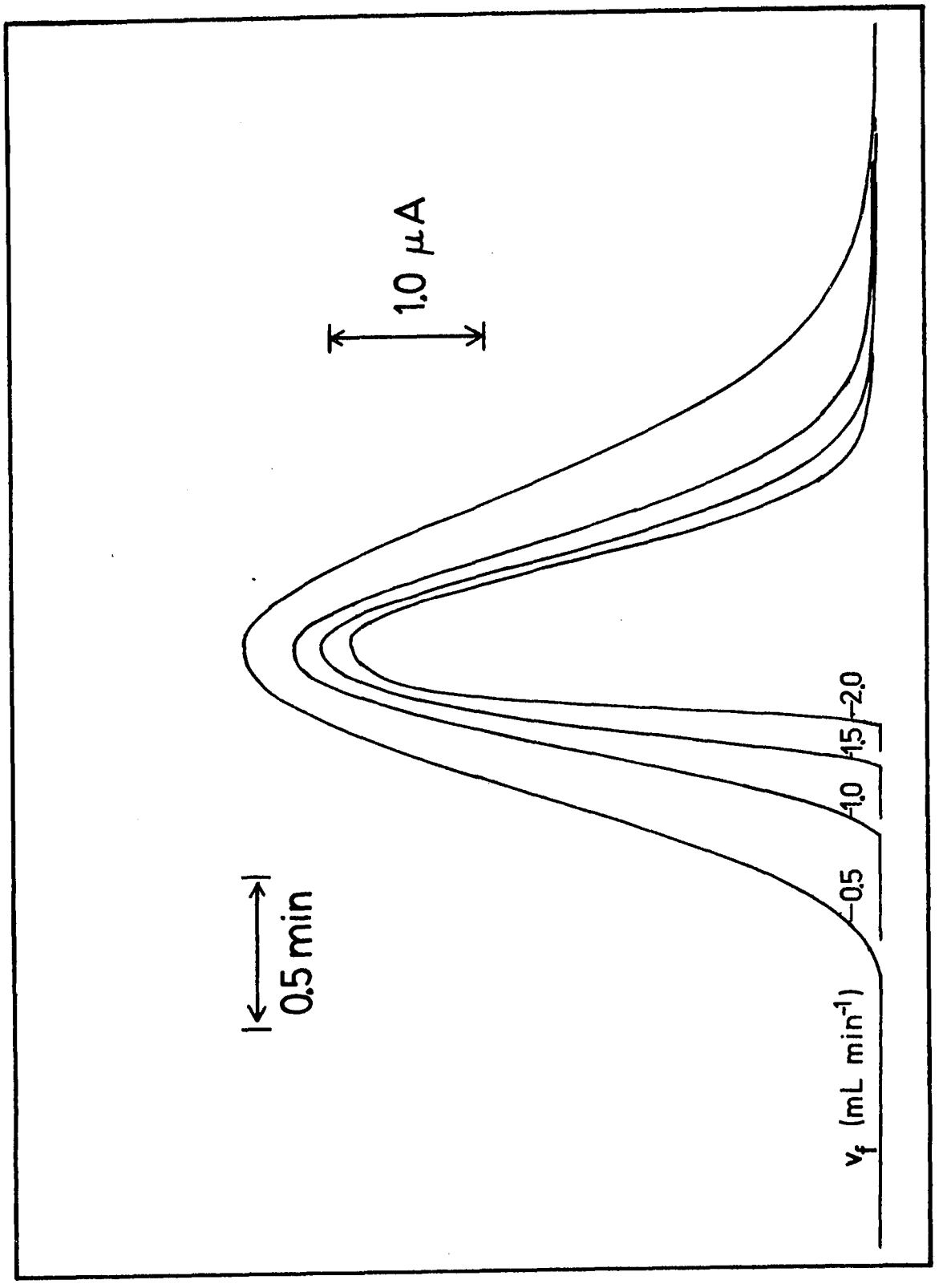
1,0 μA
0,5 min
0.5
1.0
1.5
2.0
v_f (mL min^{-1})

chosen such that the exponent is close to zero and i_p is nearly independent of v_f over a limited range of v_f (Figure IV-11).

The relationship between the width of the current-time curve and v_f is not as complex as the relationship between i_p and v_f. Since the area of the peak decreases with increasing v_f because of a decreased residence time of sample in the electrode and since the sensitivity of the electrode is not a factor, the width of the current-time curve will always decrease with increasing v_f (Equation IV-72, Figures IV-9, IV-10, IV-11).

2. The amperometric response of a tubular electrode in FIA

The validity of using the model of dispersion described in Section B to predict the current-time response of a tubular electrode is demonstrated by comparing the results of the mathematical analysis to the experimental amperometric response of a tubular electrode. In Figure IV-12, a tracing of an experimental current-time curve is compared to theoretical values of the current calculated for various times in the current-time curve. The experimental current-time curve (solid line) represents the response of the electrode to a sample of a KI solution which has been dispersed in a straight flow system. Experimental parameters are listed in the legend. The theoretical response of the electrode is denoted in Figure IV-12 by circles: The open circles represent a response to the mean concentration of the analyte, $C_m(X_D,t)$, and the filled circles represent a response to the concentration of the analyte at the outer boundary of the diffusion layer, $C(X_D,d,t)$. Current values for the filled circles were calculated using Equation IV-30B.

Figure IV-11. Current-time as a function of v_f for intermediate dispersion

V_S = 0.145 mL

V_R = 2.254 mL

C_o = 5.00 x 10^{-4} M KI

Electrode II

Flow System III

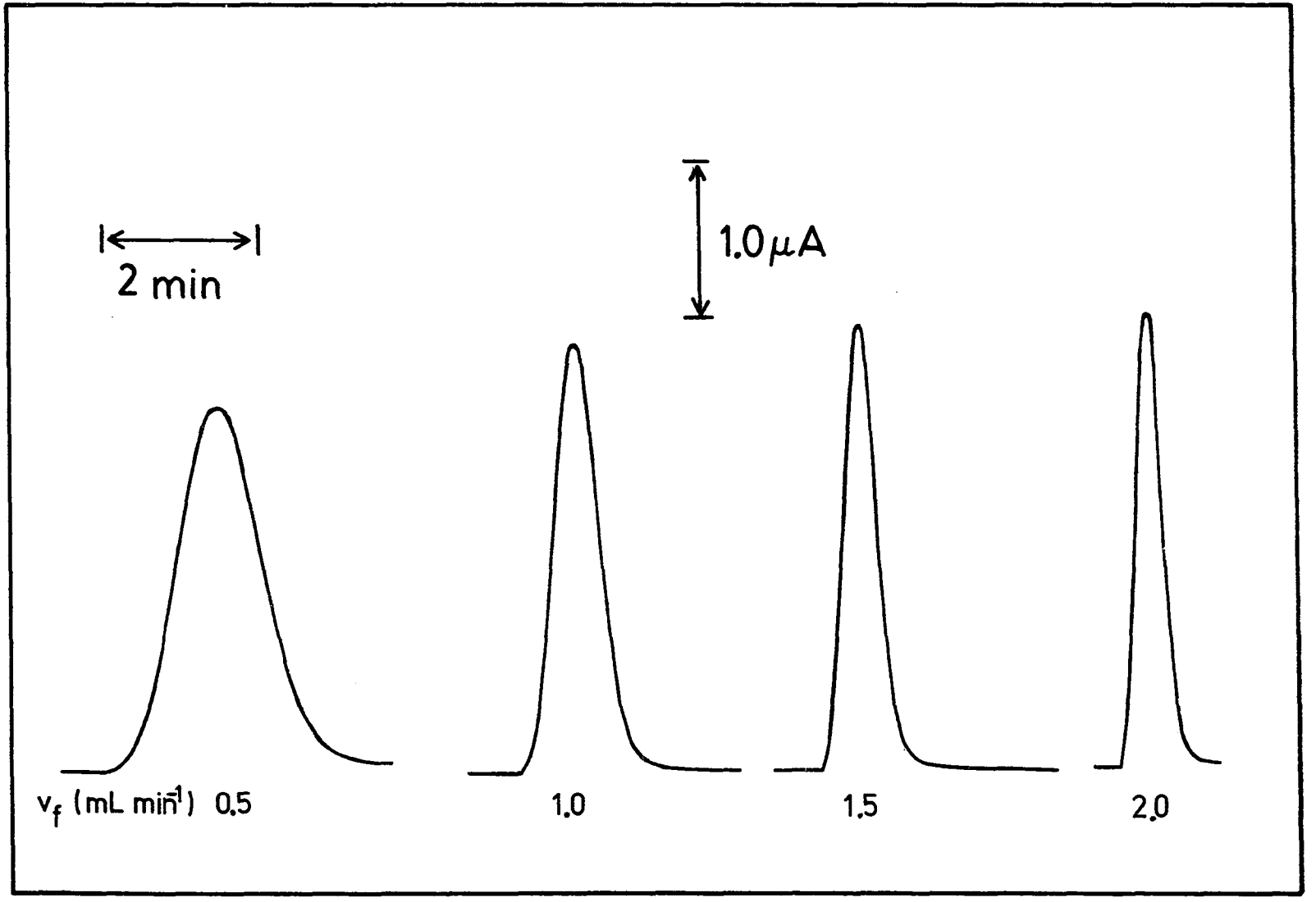
2 min
1.0 μA
v_f (mL min^{-1}) 0.5
1.0
1.5
2.0

Figure IV-12. Experimental and calculated current-time curves for dispersion in a straight flow system

Curves:

—— - Experimental current-time curve

o - Current-time curve calculated for $C_m(X_D,t)$

• - Current-time curve calculated for $C(X_D,d,t)$

Parameters:

V_R = 2.254 mL

V_S = 0.145 mL

v_f = 0.50 mL min^{-1}

K = 220 cm^2 min^{-1}

D_I = 1.74 x 10^{-5} cm^2 s^{-1}

C_o = 5 x 10^{-4} M KI

I_s = 10.34 μA

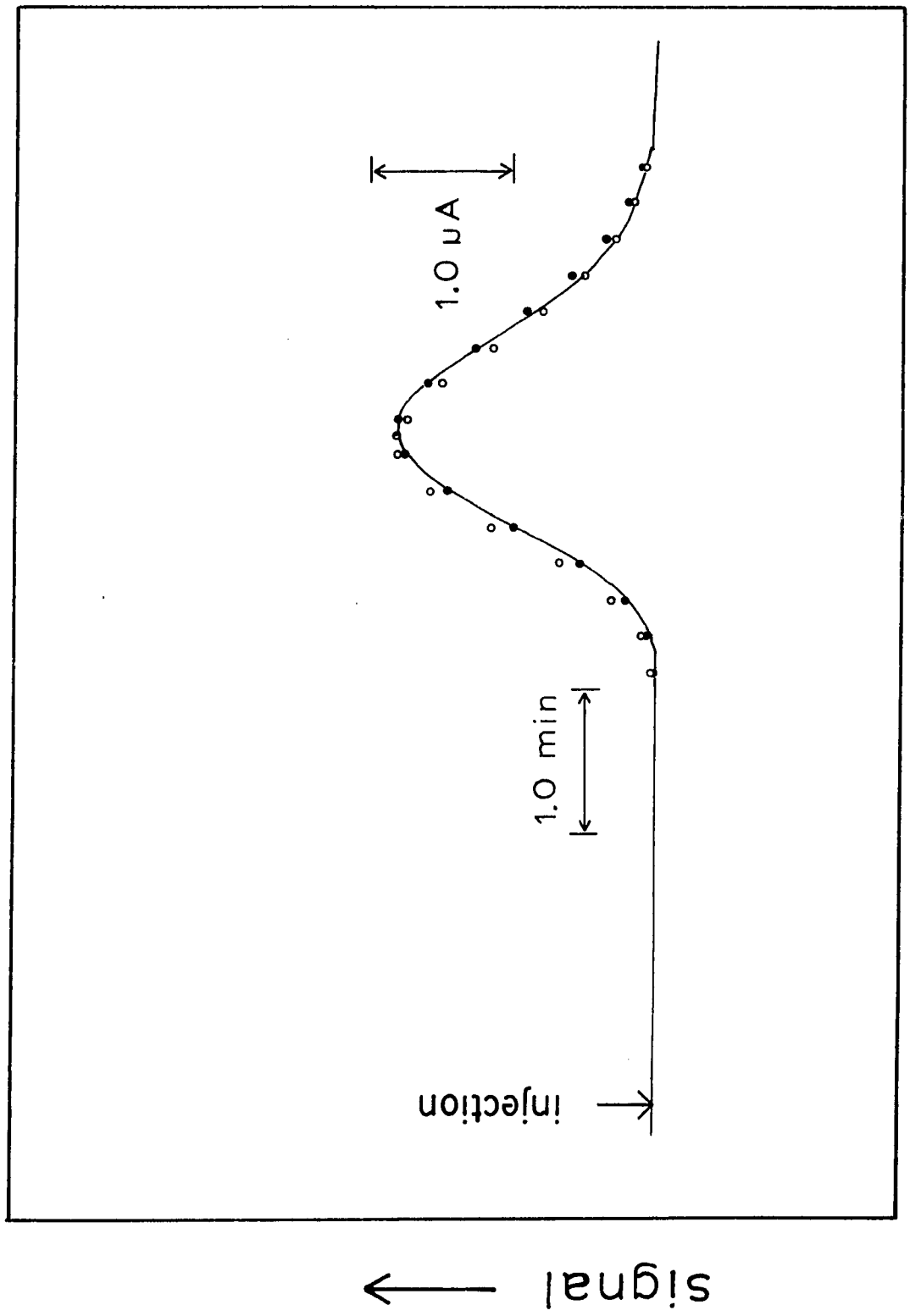
signal
1.0 uA
1.0 min
injection
time

Values for the open circles were obtained from Equation IV-75 where $C_m(X_D,t)$ is given by Equation IV-24.

$$i(t) = I_{ss}\ C_m(X_D,t)/C_o \qquad \text{(IV-75)}$$

The value of I_{ss} used to calculate i(t) in Equations IV-30B and IV-75 was measured just prior to recording the current-time curve. All parameters affecting dispersion were measured in independent experiments. Values of V_S, V_R, and v_f were obtained by the procedures described in Section C of this chapter; D, the coefficient of diffusion for I^-, was determined from data obtained by measuring the steady-state current produced by the oxidation of I^- at a Rotating Disc Electrode; and a, the radius of the tubing, was calculated from measurements of the volume and length of the tubing. K and d were calculated from Equation IV-4 and Equation IV-28, respectively, using the parameters mentioned above. Since all the parameters affecting dispersion were obtained by procedures independent of FIA, the theoretical current-time curves represented by the circles are independent of the experimental current-time curve and depict an a priori prediction of the shape of the current-time curve.

An examination of Figure IV-12 shows the excellent agreement between theory and experiment. As predicted, the experimental current-time curve correlates best with the theoretical current-time values corresponding to the concentration of the analyte at the outer boundary of the diffusion layer $C(X_D,d,t)$. The lower portion of the trailing edge of the experimental current-time curve deviates from the theoretical current-time values corresponding to $C(X_D,d,t)$ and follows more closely

the theoretical current-time values corresponding to the mean concentration, $C_m(X_D,t)$. This may indicate better radial mixing at the end of the sample zone than predicted by the dispersion theory. The deviation is, however, not significant and does not indicate a major flaw in the theory. This excellent agreement between theoretical and experimental results proves the viability of the theory describing the dispersion of mass in a fluid stream and the amperometric response of a tubular electrode to the dispersed mass.

The theoretical expression for peak current is Equation IV-37B.

$$i_p = I_{ss} \text{ erf} \left\{ \frac{V_S}{4\pi a^2} \sqrt{\frac{v_f}{K(0.5\ V_S + V_R)}} \right\} \qquad \text{(IV-37B)}$$

In general, the expression for the peak current is more useful in analytical chemistry than the expression for the complete current-time curve. To test the validity of Equation IV-37B, experimental values of the normalized peak current, i_p/I_{ss}, are compared to values of i_p/I_{ss} derived from Equation IV-37B. The ratio i_p/I_{ss} is used instead of i_p so that the effect of dispersion on the peak current can be studied without interference from changes in the sensitivity of the electrode. In the comparison, Equation IV-37B is evaluated as a function of V_S, V_R, and v_f over a range of values that is typical for FIA. As before, only dispersion in a straight tube is being considered and parameters used to calculate i_p/I_{ss} are measured using procedures that are independent of FIA.

The comparison is made in Figures IV-13, IV-14, and IV-15, and the data are summarized in Table IV-2. In the figures, filled circles represent experimental values of i_p/I_{ss} while solid lines indicate values of i_p/I_{ss} calculated from Equation IV-37B. For plots of i_p/I_{ss} as a function of V_S (Figure IV-13) and of V_R (Figure IV-14), experimental values of i_p/I_{ss} are in excellent agreement with theory. The greatest relative deviation is 2.8%. Most of the experimental values of i_p/I_{ss} are greater than the values predicted by Equation IV-37B. This is to be expected. Equation IV-37B describes a current that slightly precedes the peak current, rather than describing the peak current, because of an approximation made in the derivation of the equation. The relative error due to this approximation is less than 3% in most cases and is not significant compared to the relative error inherent in the measurement of i_p/I_{ss}.

In the case of i_p/I_{ss} as a function of v_f (Figure IV-15), experimental values of i_p/I_{ss} are in good agreement with theory at the lower flow rates, but deviate at the higher flow rates because of approximations in Taylor's solution to the problem of dispersion. Taylor's solution is a limiting case that applies only to large values of residence time (54,58,60,78). The process of dispersion, as depicted by Taylor's solution, is established after a finite period of time and not immediately upon the injection of the sample. During the interim, the dispersion of the sample is still diffusive in nature but with a coefficient of dispersion, K, that is smaller than predicted by Taylor's approximation. The value of K during this period is

Figure IV-13. i_p/I_{ss} as a function of V_S

Straight flow system:

• - Experimental values of i_p/I_{ss}

—— - Theoretical values of i_p/I_{ss} calculated from Equation IV-37B

Curved flow system:

o - Experimental values of i_p/I_{ss}

--- - Fitted values of i_p/I_{ss} calculated from Equation IV-37B for $K = 1.32 \times 10^2$ cm^2 min^{-1}

Parameters:

V_R - 2.254 mL

v_f - 0.50 mL min^{-1}

D_I - 1.74×10^{-5} cm^2 s^{-1}

C_o - 5.00×10^{-4} M KI

Electrode II

Flow System III

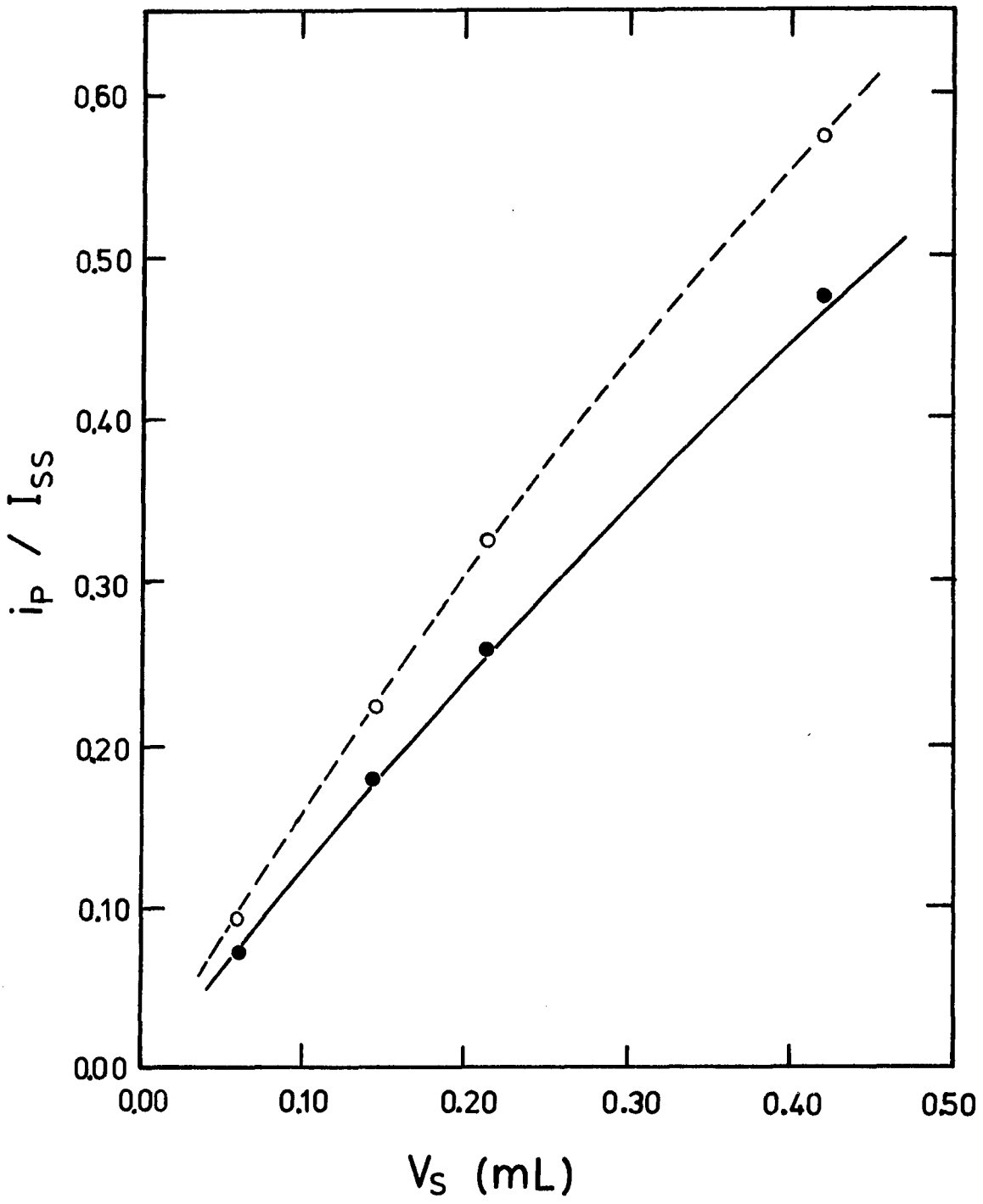
0.60
0.50
0.40
0.30
0.20
0.10
0.00
i_P / I_{SS}
0.00
0.10
0.20
0.30
0.40
0.50
V_S (mL)

Figure IV-14. i_p/I_{ss} as a function of V_R

Straight flow system:

● - Experimental values of i_p/I_{ss}

—— - Theoretical values of i_p/I_{ss} calculated from Equation IV-37B

Curved flow system:

o - Experimental values of i_p/I_{ss}

--- - Fitted values of i_p/I_{ss} calculated from Equation IV-37B for $K = 1.42 \times 10^{2}$ cm^2 min^{-1}

Parameters:

V_S = 0.145 mL

v_f = 0.50 mL min^{-1}

D_I = 1.74×10^{-5} cm^2 s^{-1}

C_o = 5.00×10^{-4} M KI

Electrode II

Flow System III

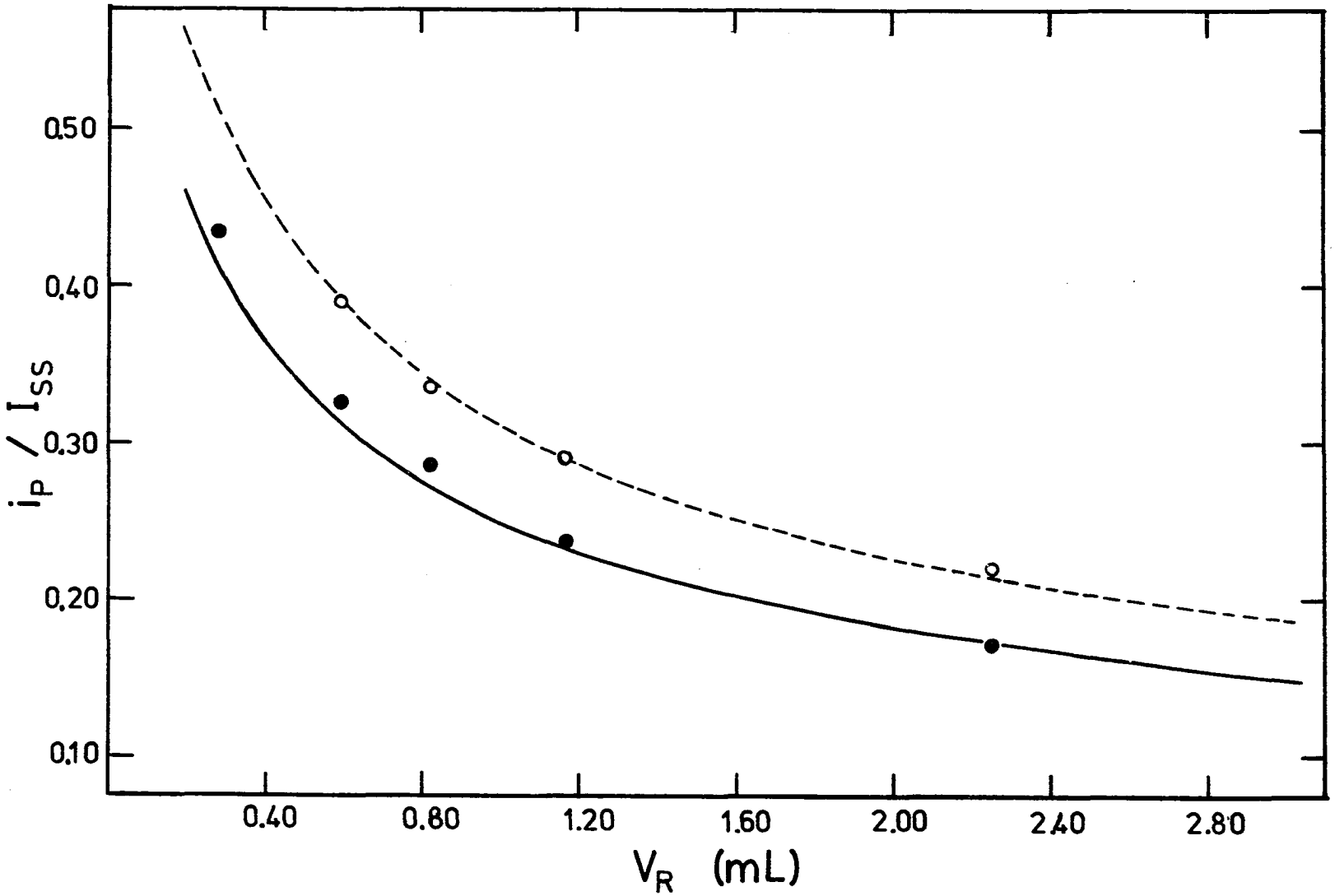
0.50
0.40
0.30
0.20
0.10
i_P / I_{SS}
0.40
0.80
1.20
1.60
2.00
2.40
2.80
V_R (mL)

Figure IV-15. i_p/I_{ss} as a function of v_f for a straight flow system

● - Experimental values of i_p/I_{ss}

—— - Theoretical values of i_p/I_{ss} calculated from Equation IV-37B

V_S = 0.226 mL

V_R = 1.168 mL

D_I = 1.74×10^{-5} cm^2 s^{-1}

C_o = 5.00×10^{-4} M KI

Electrode II

Flow System II

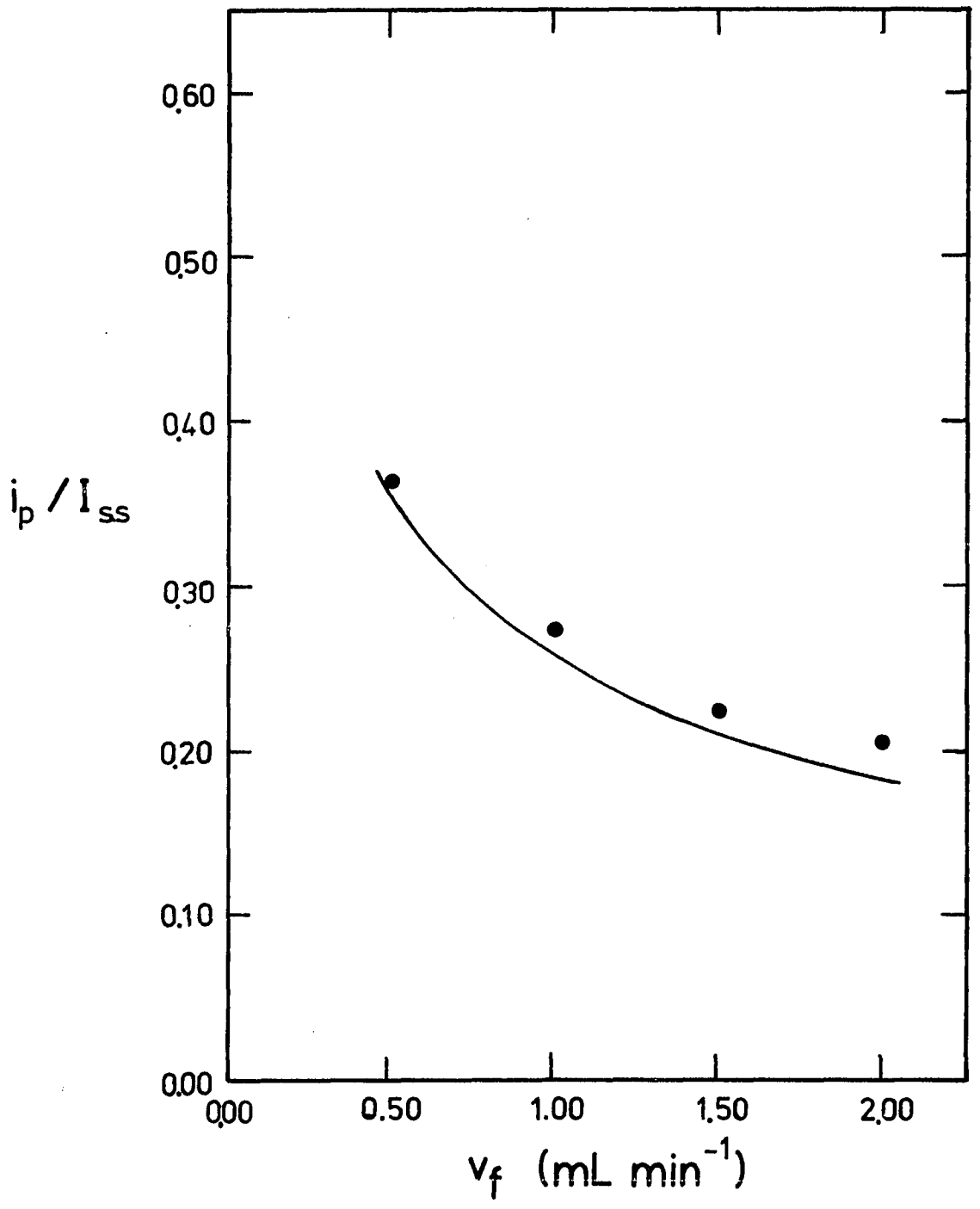
0.60
0.50
0.40
0.30
0.20
0.10
0.00
i_p / I_{ss}
0.00
0.50
1.00
1.50
2.00
v_f (mL min^{-1})

Table IV-2. Comparison of experimental values of i_p/I_{ss} to theoretical values of i_p/I_{ss} as calculated from Equation IV-37B for dispersion in a straight tube

V_S (mL)	V_R (mL)	v_f (mL min^{-1})	Exper. i_p/I_{ss}	Theor. i_p/I_{ss}	% difference
0.060	2.254	0.50	0.072	0.073	+1.4
0.145	2.254	0.50	0.179	0.174	-2.8
0.214	2.254	0.50	0.257	0.252	-1.9
0.419	2.254	0.50	0.475	0.462	-2.7
0.145	0.286	0.50	0.435	0.424	-2.5
0.145	0.594	0.50	0.326	0.319	-2.1
0.145	0.821	0.50	0.285	0.277	-2.8
0.145	1.168	0.50	0.238	0.236	-0.8
0.145	2.254	0.50	0.173	0.174	+0.6
0.226	1.168	0.50	0.362	0.356	-1.7
0.226	1.168	1.00	0.273	0.256	-6.2
0.226	1.168	1.50	0.224	0.210	-6.3
0.226	1.168	2.00	0.205	0.182	-11.2

time-dependent and increases until K becomes constant and equal to Taylor's value. Taylor's solution, therefore, overestimates the extent of dispersion at small values of time.

The accuracy of Taylor's solution in FIA depends on the residence time of the sample in the flow system which, in turn, depends primarily on V_R and v_f. Gill and Sankarasubramanian state in their analysis (54) that K becomes essentially constant and approximately equal to Taylor's value at $t = 0.5\ a^2/D$. If their criterion is applied to this study, Taylor's solution becomes applicable when the residence time of the sample is greater than 1.12 minutes. In terms of V_S, V_R, and v_f, the criterion is met when

$$t = T = \frac{0.5\ V_S + V_R}{v_f} = 1.12 \qquad \text{(IV-76)}$$

Thus, deviations from Equation IV-37B can be expected for values of v_f greater than 1.14 mL min^{-1}. The time-dependency of K can also affect i_p/I_{ss} as a function of V_R for values of V_R less than 0.490 mL in Figure IV-14. However, the effect appears to be more prevalent at higher values of v_f.

Equation IV-39D, a simplified expression for i_p, was offered in Section B of this chapter.

$$i_p = I_{ss} \frac{V_S}{2\pi^{3/2} a^2} \sqrt{\frac{v_f}{K(0.5\ V_S + V_R)}} \qquad \text{(IV-39D)}$$

Equation IV-39D was derived from Equation IV-37B and from an expression which approximates the error function. The advantage of Equation IV-39D is that i_p can be calculated without having to evaluate

the value of an error function. Experimental values of i_p/I_{ss} and values of i_p/I_{ss} calculated from Equation IV-39D, both shown in Table IV-3, are in excellent agreement for moderate to high dispersion of the sample at low rates of flow. The difference between the experimental values of i_p/I_{ss} and the theoretical values of i_p/I_{ss} are expressed in Table IV-2 and Table IV-3 as "% difference" which is a relative difference based on the experimental value. A comparison of the % difference for Equation IV-37B (Table IV-2) to the % difference for Equation IV-39D (Table IV-3) shows that the results of Equation IV-37B and Equation IV-39D are in good agreement when the dispersion of the sample is moderate to high (i.e., $i_p/I_{ss} < 0.45$). Under this condition, Equation IV-39D can be used instead of Equation IV-37B to predict values of i_p/I_{ss}. As in the case of Equation IV-37B, Equation IV-39D does not accurately predict values of i_p/I_{ss} for the higher rates of flow. This is attributed to the time-dependency of K.

On the basis of Equation IV-39D, i_p and i_p/I_{ss} are predicted to be proportional to $v_f^{-1/6}$ and $v_f^{-1/2}$, respectively. However, because of the time-dependency of K, experimental values determined for the exponent of flow rate are less than predicted. This is shown in Figure IV-16 where the log of the experimental values of i_p/I_{ss} (open circles) are plotted as a function of log v_f. The exponent of the flow rate, represented in Figure IV-16 as the slope of the dashed line, is -0.426. The solid line represents values of log i_p/I_{ss} as a function of log v_f as calculated from Equation IV-39D. The experimental values of i_p/I_{ss} appear to converge with the theoretical values of i_p/I_{ss} at the

Table IV-3. Comparison of experimental values of i_p/I_{ss} to theoretical values of i_p/I_{ss} as calculated from Equation IV-39D for dispersion in a straight tube

V_S (mL)	V_R (mL)	v_f (mL min^{-1})	Exper. i_p/I_{ss}	Theor. i_p/I_{ss}	% difference
0.060	2.254	0.50	0.072	0.073	+1.4
0.145	2.254	0.50	0.179	0.175	-2.2
0.214	2.254	0.50	0.257	0.256	-0.3
0.419	2.254	0.50	0.475	0.492	+3.6
0.145	0.286	0.50	0.435	0.447	+2.8
0.145	0.594	0.50	0.326	0.327	+0.3
0.145	0.821	0.50	0.285	0.283	-0.7
0.145	1.168	0.50	0.238	0.240	+0.4
0.145	2.254	0.50	0.173	0.175	+1.2
0.226	1.168	0.50	0.362	0.369	+1.9
0.226	1.168	1.00	0.273	0.261	-4.4
0.226	1.168	1.50	0.224	0.213	-4.9
0.226	1.168	2.00	0.205	0.185	-9.8

Figure IV-16. Dependence of i_p/I_{ss} on v_f for case of high dispersion in a straight flow system

o - Experimental values of i_p/I_{ss}

--- - Linear fit of data

—— - Theoretical values of i_p/I_{ss} from Equation IV-39D

V_S = 0.226 mL

V_R = 1.168 mL

D_I = 1.74×10^{-5} cm^2 s^{-1}

C_o = 5.00×10^{-4} M KI

Electrode II

Flow System II

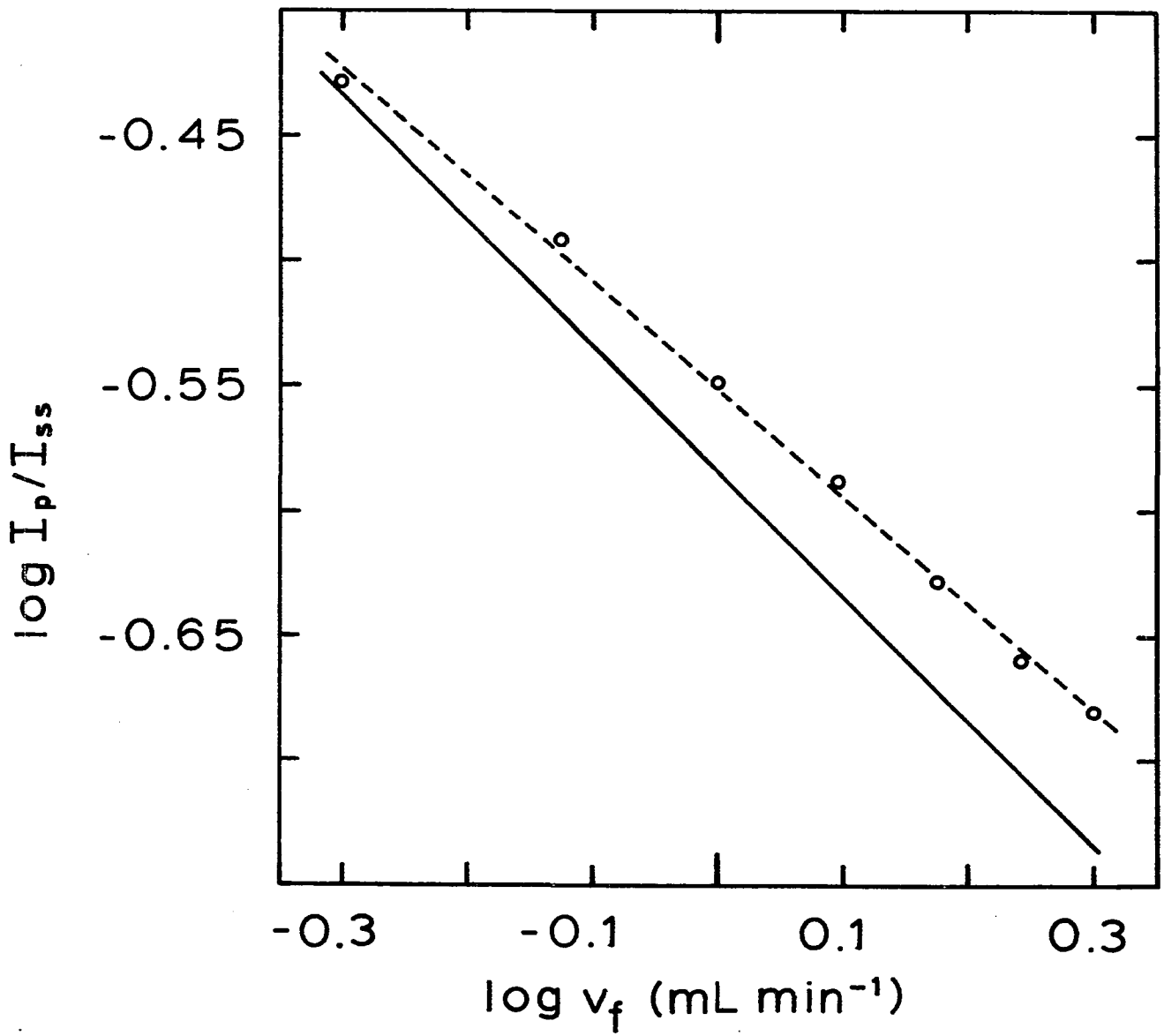
-0.45
-0.55
-0.65
log I_p/I_{ss}
-0.3
-0.1
0.1
0.3
log v_f (mL min^{-1})

lower flow rates. This indicates that the relation $i_p/I_{ss} \propto v_f^{-1/2}$ is a limiting case which describes the relationship between dispersion and flow rate for large values of retention time.

In most flow systems used in FIA, tubing is curved rather than straight. Although the study of dispersion in a straight flow system is important to the verification of the dispersion model, the practicability of such a study would be questionable if the dispersion model was not applicable to a curved system. Several workers (79,80) have addressed the problem of dispersion in a curved tube and have concluded that Taylor's theory of dispersion, that the distribution of the average concentration in a complex three-dimensional system can be described by the solution of a one-dimensional dispersion equation, also applies to dispersion in curved tubes. The major difference between the description of dispersion in a curved tube and dispersion in a straight tube is the expression for the coefficient of dispersion. The motion of fluid flowing through a curved tube is more complex than the motion of fluid flowing through a straight tube. The Poiseuille Equation no longer applies, and radial and angular components of convection exist. The motion of fluid in the curved tube affects the value of the coefficient of dispersion. Radial convection is more efficient than diffusion at decreasing values of the radial concentration gradient. Thus, under the same experimental conditions, the extent of axial dispersion in a curved tube is less than in a straight tube. The difference is expressed as a smaller value of K for dispersion in a curved tube. Theoretical expressions for K have been proposed for curved tubes. However, since

these expressions are derived for tubes having a constant radius of curvature and are based on approximate solutions for the equations of fluid motion, the expressions are not directly applicable to flow systems used in FIA even though the general form of the equations and the results of the analyses are helpful in qualitatively understanding dispersion in curved tubes.

Equations describing the distribution of the mean concentration in a straight tube can be applied to a curved tube if the coefficient of dispersion is determined experimentally. In Figure IV-17, a tracing of an experimental current-time curve from a curved flow system (solid line) is compared to values of current that were calculated from Equations IV-24 and IV-75 using an experimentally determined value of the coefficient of dispersion (open circles). K was calculated by Equation IV-37B from the experimental values of i_p and I_{ss}. The calculated values of current represent a response of the electrode to the mean concentration of the analyte, $C_m(X_D,t)$. Unfortunately, the response of the electrode to the concentration of the analyte at the outer boundary of the diffusion layer, $C(X_D,d,t)$, cannot be calculated for dispersion in a curved tube because an expression for the radial distribution of the concentration is not available. As in the case of dispersion in a straight flow system (Figure IV-12), the calculated values of current corresponding to $C_m(X_D,t)$ describe well the general shape of the current-time curve except that the calculated values of current slightly precede the corresponding values of current on the current-time curve. This is due to the difference between $C_m(X_D,t)$, the concentration used

Figure IV-17. Experimental and fitted current-time curves for dispersion in a curved flow system

Curve:

—— - Experimental current-time curve

o - Fitted current-time curve calculated for $C_m(X_D,t)$ with $K = 1.32 \times 10^2$ cm^2 min^{-1}

● - Theoretical current-time curve calculated for $C_m(X_D,t)$ for dispersion in a straight tube ($K = 2.20 \times 10^2$ cm^2 min^{-1})

Parameters:

V_R = 2.254 mL

V_S = 0.145 mL

v_f = 0.50 mL min^{-1}

D_I = 1.74×10^{-5} cm^2 s^{-1}

C_o = 5×10^{-4} M KI

I_{ss} = 10.38 μA

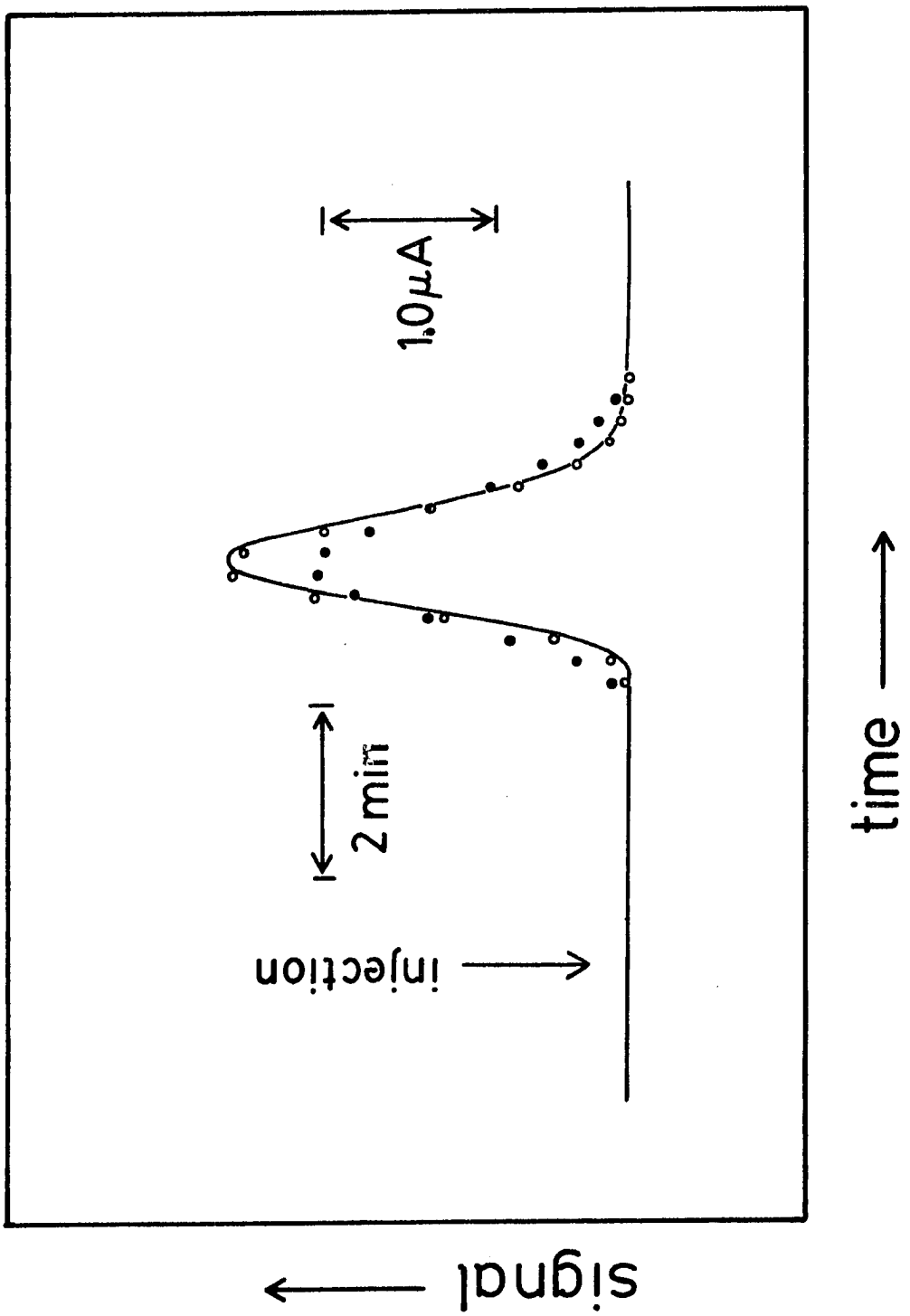
signal
time
injection
2 min
1.0μA

in the calculation, and $C(X_D,d,t)$, the actual concentration to which the electrode is responding. In spite of this discrepancy, the similarity between the shape of the experimental current-time curve and the shape of the current-time curve represented by the calculated values of current illustrates that the experimentally determined values of K pertain to the dispersion of the total sample and not just to the dispersion in the region of the peak current from which K was calculated. Calculated values of current for the dispersion of a sample in a straight flow system having the same values of V_S, V_R, and v_f are shown for comparison (filled circles).

Since equations describing the amperometric response of an electrode to $C_m(X_D,t)$ are valid for both curved and straight flow systems, equations describing the peak current are also valid for both types of flow systems. This is illustrated in Figures IV-13 and IV-14 for Equation IV-37B as a function of V_S and V_R, respectively. The open circles in these figures represent the peak current for samples which were dispersed in a curved flow system. To insure a uniform curvature, the flow system was constructed by coiling the tubing which connected the injection valves and the electrode around a cylindrical form. The diameter of the form was approximately 3.75 inches. The coefficient of dispersion was calculated for the data in each figure from a value of the peak current and Equation IV-37B. The ratio i_p/I_{ss} was then calculated as a function of V_S and V_R using Equation IV-37B and the experimentally determined value of K. These values are indicated in the appropriate figure by a dashed line. The applicability of

Equation IV-37B to dispersion in a curved tube is demonstrated by how well the dashed lines fit the experimental points. An examination of Figures IV-13 and IV-14 shows that the values of i_p/I_{ss} calculated from Equation IV-37B agree very well with the experimental values of i_p/I_{ss}. Although the experimental results above are based on data obtained from a flow system that has uniform curvature, the results apply to any flow system regardless of configuration. The coefficient of dispersion is a characteristic of a flow system for a particular flow rate and can be used to predict values of i_p/I_{ss} for changes in V_S and V_R as long as the nature of the curvature is not changed with the length of the flow system. These data are summarized in Table IV-4.

Although the effect of changes in curvature upon i_p is not as significant as changes in V_S, V_R, and v_f, it is important and has, until recently, gone unnoticed. The effect of curvature was particularly a problem in studies where peak height is taken as an indication of the activity of the surface of the electrode, and in studies where calibration curves based on i_p are not prepared daily. Typically, an electrode is removed from a flow system at the end of an experiment to be dried and stored. When the electrode is reattached, the configuration of the tubing may not be the same as before because of a change in the position of the electrode or a change in the route of the tubing. The change in the configuration results in a change in the coefficient of dispersion which affects the observed value of i_p. When compared to data obtained earlier, the change in i_p may be misinterpreted and attributed to an electrochemical phenomenon. A change in the

Table IV-4. Comparison of experimental values of i_p/I_{ss} to fitted values of i_p/I_{ss} as calculated from Equation IV-37B for dispersion in a curved tube

V_S (mL)	V_R (mL)	v_f (mL min^{-1})	Exper.[a] i_p/I_{ss}	Theor. i_p/I_{ss}	% difference
0.060	2.254	0.50	0.092	0.083	+1.1
0.145	2.254	0.50	0.223*	0.223	0.0
0.214	2.254	0.50	0.325	0.321	-1.2
0.419	2.254	0.50	0.572	0.573	+0.2
0.145	0.594	0.50	0.390	0.390	0.0
0.145	0.821	0.50	0.337	0.341	+1.2
0.145	1.168	0.50	0.291**	0.291	0.0
0.145	2.254	0.50	0.221	0.215	+2.7
0.145	2.254	0.51	0.218	---	---
0.145	2.254	1.00	0.205	---	---
0.145	2.254	1.49	0.187	---	---
0.145	2.254	1.97	0.175	---	---

[a]The experimental value of i_p/I_{ss} used to calculate K for each set is denoted by the asterisks:

* K for the first set is 1.32×10^2 xm^2 min^{-1};

** K for the second set is 1.42×10^2 cm^2 min^{-1}.

coefficient of dispersion may also lead to an error in the results of an analysis if the calibration curve is prepared from data obtained earlier. The solution to the problem is to recognize the effect of curvature. In experiments where the configuration of the flow system may change, the sensitivity of the electrode should be checked by measuring the steady-state current, and calibration curves should be prepared after a change in the configuration of the flow system In experiments where a consistent dispersion is necessary, the components of the flow system should be firmly mounted to the frame of the instrument to fix the position of the tubing. The change in position does not have to be great to affect significantly the observed value of i_p. In one case, a 9% increase in i_p was observed when the position of an injection valve was rotated 180°.

The effect of dispersion in a curved tube as a function of v_f is shown in Figure IV-18. Experimental values of i_p/I_{ss} are represented by open circles. For comparison, theoretical values of i_p/I_{ss} for dispersion in a straight tube are represented by the solid line. The verification of Equation IV-37B as a function of v_f is difficult because the coefficient of dispersion is also a function of v_f. Before Equation IV-37B can be verified, an expression for K as a function of v_f is required. Two theoretical equations for the coefficient of dispersion for a curved tube, K_{curved}, have been derived and are expressed in general terms as a function of v_f by Equation IV-77 (79)

$$K_{curved} = K_{str}[1 + kv_f^4] \qquad \text{(IV-77)}$$

and by Equation IV-78 (80)

$$K_{curved} = K_{str}[1 + k_1 v_f^4 + k_2 v_f^2 + k_3] \qquad \text{(IV-78)}$$

In the equations above, K_{str} is the coefficient of dispersion for a straight tube (Equation IV-4); and k, k_1, k_2, and k_3 are constants. The differences between Equation IV-77 and Equation IV-78 are the result of difference between the equations used to describe the motion of the fluid and to simplifying assumptions made in the derivation of Equation IV-77. In general, the solution for K_{curved} is a series expansion in λ^{-2} (Equation IV-79) where λ is a dimensionless curvature parameter (80).

$$K_{curved} = K_{str} + K_2\lambda^{-2} + K_4\lambda^{-4} + K_6\lambda^{-6} + \cdots \qquad \text{(IV-79)}$$

Equations IV-77 and IV-78 represent only a one-term correction, $(K_2\lambda^{-2})$, for the effect of curvature. Solutions containing higher orders of λ, i.e., $K_4\lambda^{-4}$, $K_6\lambda^{-6}$, etc., have not been obtained. The completeness of the solutions cannot be verified by the convergence of the series because higher-order terms of the expansion are not available. In an attempt to fit the experimental values of i_p/I_{ss} to Equation IV-37B, neither solution was found to be applicable and the development of an empirical expression for K was tried. Equation IV-78 contains a more complete solution for the second term than does Equation IV-77. Each λ-term in the series expansion is apparently a series of v_f^2 since the second term in Equation IV-78 is a function of v_f^4, v_f^2, and v_f^0. A reasonable assumption is that subsequent λ-terms would include higher orders of v_f^2 and the expression for K_{curved} would have the form shown in Equation

IV-80, where a_n is a constant:

$$K_{curved} = K_{str} \sum_{n=0}^{\infty} a_n v_f^{2n} \qquad \text{(IV-80)}$$

With four experimental values of i_p/I_{ss}, values of a_n can be evaluated up to a_3. The expression for K_{curved} becomes Equation IV-81 which has one term of v_f^{2n} beyond Equation IV-78.

$$K_{curved} = K_{str}[a_3 v_f^6 + a_2 v_f^4 + a_1 v_f^2 + a_0] \qquad \text{(IV-81)}$$

Equation IV-37B was fitted to experimental values of i_p/I_{ss} by using Equation IV-81 as the expression for K. This is shown in Figure IV-18 as a dashed line. Although the experimental values of i_p/I_{ss} can be fitted to Equation IV-37B using this approach, the overall form of the function, as depicted by the dashed line in Figure IV-18, does not appear to represent a likely solution. If Equation IV-80 is a valid expression, then perhaps orders of v_f^2 higher than v_f^6 are required to express K_{curved} accurately. More study is required in this area. Data for i_p/I_{ss} as a function of v_f for dispersion in a curved flow system are summarized in Table IV-4. Calculated values of i_p/I_{ss} for v_f are omitted from Table IV-4 due to the lack of a reasonable theoretical expression for K.

Values of i_p/I_{ss} for dispersion in a curved tube have also been calculated as a function of V_S and V_R using Equation IV-39D and an experimentally determined value of K. Experimental values of i_p/I_{ss} and calculated values of i_p/I_{ss} are compared in Table IV-5. As in the case of dispersion in a straight flow system, the results of Equation

Figure IV-18. i_p/I_{ss} as a function of v_f for a curved flow system

o - Experimental values of i_p/I_{ss}

--- - Fitted values of i_p/I_{ss} calculated from Equations IV-37B and IV-81

—— - Theoretical values of i_p/I_{ss} calculated for dispersion in a straight flow system

V_S = 0.145 mL

V_R = 2.254 mL

$C_o = 5.00 \times 10^{-4}$ M KI

Electrode II

Flow System III

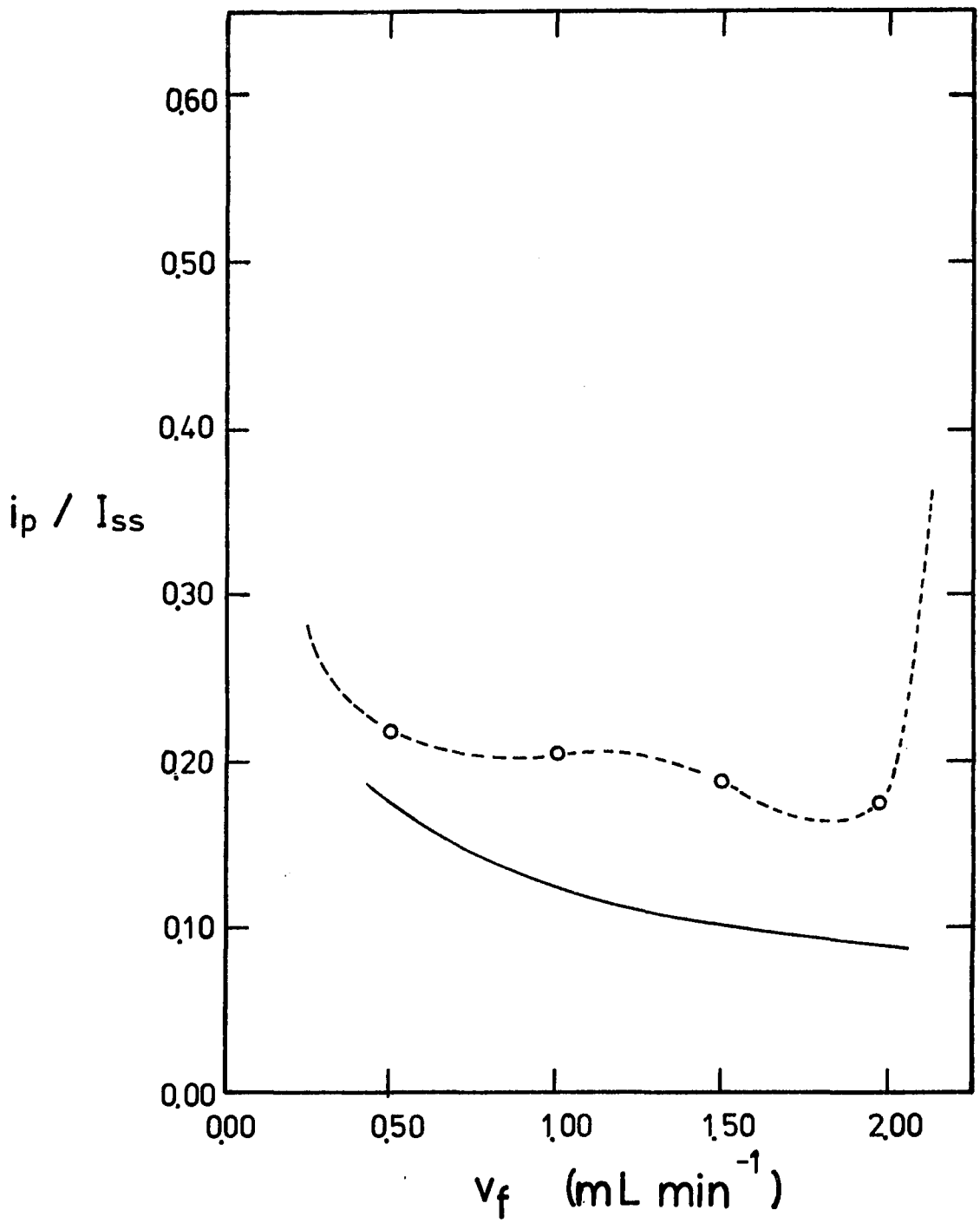
0.60
0.50
0.40
0.30
0.20
0.10
0.00
i_p / I_{ss}
0.00
0.50
1.00
1.50
2.00
v_f (mL min^{-1})

IV-39D are in good agreement with the results of Equation IV-37B and with the experimental values of i_p/I_{ss} when the degree of dispersion is moderate to high. Again, values of i_p/I_{ss} as a function of v_f have been omitted from Table IV-5 due to the lack of a reasonable theoretical expression for K.

3. Coulometric response of a tubular electrode in FIA

In spite of the complex effect dispersion has on the mass distribution of a sample in a fluid stream and on the shape of the current-time curve, the expression for the charge passed through the electrode during the electrolysis of a sample, Q_p, i.e., the area under the current-time curve, is represented by a simple equation (Equation IV-70).

$$Q_p = \frac{I_{ss} V_S}{v_f} \qquad \text{(IV-70)}$$

The result is the same whether the expression for Q_p is derived by the involved integration of the current-time equation (Equations IV-44 through IV-70) or deduced through a simplistic model (Equation IV-41). The charge is neither dependent on V_R nor on K which indicates that Q_p is independent of the resident time of the sample in the fluid stream and independent of dispersion. The dependence of Q_p on V_S and v_f reflects the dependence of Q_p on the residence time of the sample in the detector. Thus, while the shape of the current-time curve and the peak current are very dependent on what happens to the sample as it passes from the injection valves to the electrode, the integrated

Table IV-5. Comparison of experimental values of i_p/I_{ss} to fitted values of i_p/I_{ss} as calculated from Equation IV-39D for dispersion in a curved tube

V_S (mL)	V_R (mL)	v_f (mL min^{-1})	Exper.[a] i_p/I_{ss}	Theor. i_p/I_{ss}	% difference
0.060	2.254	0.50	0.092	0.093	+1.1
0.145	2.254	0.50	0.223*	0.223	0.0
0.214	2.254	0.50	0.325	0.327	+0.6
0.419	2.254	0.50	0.572	0.626	+9.4
0.145	0.594	0.50	0.390	0.397	+1.8
0.145	0.821	0.50	0.337	0.343	+1.8
0.145	1.168	0.50	0.291**	0.291	0.0
0.145	2.254	0.50	0.221	0.213	+3.6

[a]The experimental value of i_p/I_{ss} used to calculate K for each set is denoted by the asterisks:

* K for the first set is 1.35×10^{-2} cm^2 s^{-1};

** K for the second set is 1.48×10^{2} cm^2 s^{-1}.

signal, Q_p, is dependent only on what happens to the sample while in the electrode.

The data presented in this section, unless otherwise noted, were obtained using a curved flow system in which the tubing connecting the injection valve to the electrode was coiled in an arbitrary and random manner with no particular attention being given to day-to-day variations in configuration. Although Equation IV-70 was derived from the current-time equation for dispersion in a straight tube, the results apply equally as well to a curved tube. The difference between dispersion in a straight and curved flow system is reflected in the expression for K. Since Q_p is not dependent on K, the value of Q_p is not affected by the curvature of the flow system. Experimental data from both straight and curved flow systems are given in Table IV-6 for various values of V_R with V_S = 0.145 mL and v_f = 0.50 mL min^{-1}. The experimental values of Q_p presented in Table IV-6 have been normalized with division by $I_{ss}V_S v_f^{-1}$ to eliminate the effects of day-to-day variations in the analytical concentration of KI or in the electrochemical sensitivity of the electrode. The normalized value is then the fraction of the theoretical value for Q_p, as predicted by Equation IV-70, which is achieved experimentally. Values of I_{ss} used in each calculation were measured a short time before or after the coulometric experiment to insure that the value of I_{ss} measured reflected the conditions at the electrode during the experiment. Values of V_S and v_f were measured by the procedures given in Section C of this chapter. A comparison of data from a straight flow system to data from a curved flow system shows that

Table IV-6. Comparison of coulometric results for straight and curved flow systems

Straight flow system		Curved flow system	
V_R[a] (mL)	$\frac{Q_p}{I_{ss}V_S v_f^{-1}}$	V_R[a] (mL)	$\frac{Q_p}{I_{ss}V_S v_f^{-1}}$
0.286	0.982	0.286	0.984
0.594	0.966	0.596	0.963
0.820	0.989	---	---
1.168	0.970	1.176	0.966
2.254	0.959	2.390	0.980
Average	0.973±0.012		0.973±0.011

[a]Other parameters: V_S = 0.145 mL, v_f = 0.50 mL min^{-1}.

the response of the systems are virtually identical and that Q_p is not dependent on the configuration of the flow system. Also, in each series, the normalized values of Q_p show no change as a function of V_R outside of variations due to uncertainties in the measurement. This absence of a trend in the values of Q_p is an indication that Q_p is independent of V_R, as predicted. The experimental values of Q_p were slightly less than the theoretical values because of a systematic tendency to terminate integration of each current-time curve prematurely when the net signal was very close to the background signal. This was particularly true under conditions of high dispersion when the current-time curves were very broad, and the leading and trailing edges were difficult to discern from the background signal.

The theoretical dependence of Q_p on V_S and v_f, according to Equation IV-70, is verified by data given in Table IV-7. Experimental values of Q_p/I_{ss} are presented in Table IV-7 for V_S = 0.145, 0.226, 0.419, 0.955, and 1.663 mL and for v_f = 0.50, 1.00, 1.50, and 2.00 mL min^{-1}. The experimental values of Q_p were divided by I_{ss} to eliminate variations in the results due to changes in the sensitivity of the electrode or in the concentration of KI. The values of Q_p/I_{ss} presented in the table are averages taken from values of Q_p/I_{ss} for V_R = 0.289, 0.596, 1.168, and 2.390 mL for each pair of values of V_S and v_f. Hence, the data in Table IV-7 represent the integration of 80 current-time curves and a wide range of experimental conditions. The slopes of log-log plots of Q_p/I_{ss} versus V_S, and Q_p/I_{ss} versus v_f, are given and are in excellent agreement with the theoretical predictions given below.

Table IV-7. Values of Q_p/I_{ss} as a function of V_S and v_f

Q_p/I_{ss}[a] (s)

		v_f (mL min^{-1}) 0.50	1.00	1.50	2.00	$\left(\frac{\partial \log Q_p/I_{ss}}{\partial \log v_f}\right)_{V_S}$
V_S (mL)	0.145	16.93	8.52	5.73	4.19	-1.00
	0.226	26.19	13.15	8.78	6.52	-1.00
	0.419	49.02	24.84	16.51	12.27	-1.00
	0.955	115.6	56.95	37.54	28.15	-1.02
	1.663	199.7	99.24	64.99	49.08	-1.01
$\left(\frac{\partial \log Q_p/I_{ss}}{\partial \log V_S}\right)_{v_f}$		1.02	1.01	1.00	1.01	

[a]Values tabulated are averages for V_R = 0.286, 0.596, 1.176 and 2.390 mL.

$$\left(\frac{\partial \log Q_p/I_{ss}}{\partial \log V_S}\right)_{v_f} = 1.0 \qquad \text{(IV-82A)}$$

$$\left(\frac{\partial \log Q_p/I_{ss}}{\partial \log v_f}\right)_{V_S} = -1.0 \qquad \text{(IV-82B)}$$

A comparison of experimental values of Q_p to theoretical values of Q_p for ninety current-time curves is shown in Figure IV-19. The values of $Q_p/I_{ss}V_S v_f^{-1}$ are presented as a function of dispersion which is represented by i_p/I_{ss}. These data were obtained over a period of several months and represent all combinations of the values of V_S, V_R, and v_f listed in the preceding paragraph. Overall, the data in Figure IV-19 are in good agreement with theory. The average value of $Q_p/I_{ss}V_S v_f^{-1}$ is 0.992 with a relative standard deviation of 2%. As mentioned before, the single greatest cause for the uncertainty is the integration of the current-time curves; however, normalized values of Q_p also reflect the uncertainty in the measurement of I_{ss}. The problem of accurate integration is particularly evident in the integration of highly dispersed current-time curves. In Figure IV-19, as dispersion increases to an extent that $i_p/I_{ss} < 0.50$, experimental values of Q_p tend to deviate more from theoretical values. This is due to the degree of dispersion, as discussed previously, and to the size of the current-time curve. Data for higher dispersion are dominated by small values of V_S. Small values of V_S produce not only current-time curves of highly dispersed samples, but also curves which contain a small area

Figure IV-19. Coulometric response as a function of dispersion

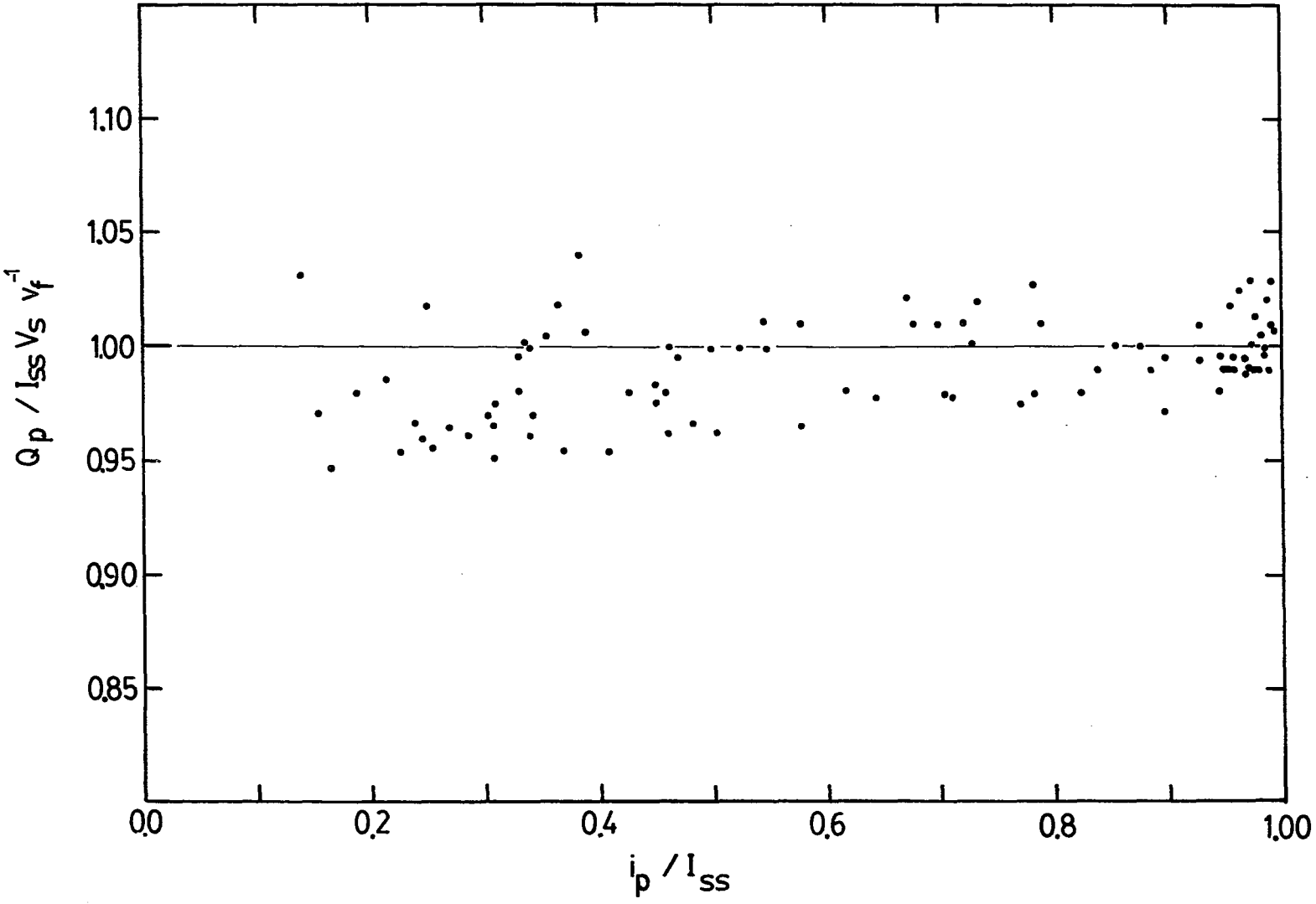
1.10
1.05
1.00
0.95
0.90
0.85
0.0
0.2
0.4
0.6
0.8
1.00
$Q_p / I_{ss} V_s v_f^{-1}$
i_p / I_{ss}

(i.e., 65 μcoul for a 0.145 mL injection at 2.0 mL min^{-1} compared to 750 μcoul for a 1.663 mL injection under the same conditions). A small area is more difficult to measure accurately than a large area. This contributes to greater uncertainty in the measurement and to greater variations in the results. Hence, the combination of high dispersion and small area produces results which tend to be lower than predicted and more scattered than results for lower dispersion and large area.

4. Comparison of the measurement of i_p to the measurement of Q_p

Analytical information can be obtained in FIA from either the measurement of the peak current, i_p, or from the measurement of the area under the current-time curve, Q_p. When comparing the relative merit of each measurement, the ease of making the measurement, the error in the measurement, and experimental factors that affect the measurement should be considered.

The measurement of i_p is straightforward. The height of the current-time curve is measured from the baseline to the peak with a ruler. Measurements can be made to the nearest 0.02 in or 0.5 mm depending on the scale. The relative standard deviation for the measurement of i_p for repetitive injections is less than ±1%. Variation in i_p from day to day is typically ±3% after corrections for changes in the sensitivity of the electrode. Without correcting for changes in the sensitivity of the electrode, i_p can vary as much as ±9% from day to day. i_p is dependent upon V_S, V_R, v_f, the curvature of the flow system, and the sensitivity of the electrode. To insure reproducible results,

values of V_S, V_R, v_f and the configuration of the flow system must remain constant, and the sensitivity of the electrode must be measured before each experiment. If the operating parameters of the flow system remain constant, the sensitivity of the electrode can be measured by the injection of a standard solution. A calibration curve from a previous experiment can then be used after correcting the data for a change in the sensitivity of the electrode. If the flow system is changed relative to V_S, V_R, v_f or the configuration, a new calibration curve must be prepared.

The effort required in measuring Q_p depends on the technique of integration. Measurement with a planimeter of the area under a current-time curve is tedious and time-consuming. Practice is required before reproducible and accurate measurements can be made; however, once the technique is mastered, good results can be obtained. A simple electronic integrator constructed from operational amplifiers is more convenient to use than a planimeter and results of similar quality can be obtained. Unfortunately, the electronic integrator has several drawbacks: The area of a peak can only be measured once, the initiation and termination of the integration is performed manually by the operator, and a simple analog integrator cannot compensate for a shift in the baseline. Sophisticated electronic integrators designed for chromatographic systems are commercially available, but none were used in this study.

The relative standard deviation for the measurement of Q_p for repetitive injections is less than 1%. Day to day variations in Q_p can

be as much as ±4%, although typically the variation is closer to ±2%. The value of Q_p depends upon V_S, v_f, and the sensitivity of the electrode. Q_p does not depend on V_R or on the configuration of the flow system; hence, these parameters can be changed from experiment to experiment without affecting the value of Q_p. If V_S and v_f are the same in each experiment, the sensitivity of the electrode can be checked by the injection of a standard solution and the calibration curve from the previous experiment can be used after the data are corrected for the change in sensitivity. If either V_S or v_f is changed, a new calibration curve must be prepared.

The ease of measurement and the error in the measurement of i_p is comparable to the ease of measurement and the error in the measurement of Q_p. The real comparison of i_p and Q_p is in how experimental factors affect the measurement of each. In this respect, the measurement of Q_p has the advantage over the measurement of i_p because the value of Q_p is independent of dispersion which eliminates the problem of changes in the configuration of the flow system in FIA. This conclusion has particular significance for the application of flow-through electrode as detectors in Liquid Chromatograph. At a constant value of v_f, Q_p is predicted to be independent of band broadening and the retention time. This is in definite contrast to i_p which decreases with increasing retention time because of an increase in the dispersion. Consequently, addition of a single internal standard to the sample should suffice for obtaining a calibration constant for the detector which will be applicable for all peaks regardless of the band width or retention time.

5. Pulse amperometric response of a tubular electrode in FIA as a function of flow rate

One undesirable characteristic of flow-through amperometer detectors is the dependence of the signal upon the flow rate. Several workers have employed pulse amperometric and differential pulse amperometric detectors in Liquid Chromatography and Segmented Flow Analysis in an effort to develop an electrode whose response is independent of flow rate (34,82). The rationale for using pulse techniques to eliminate the effects of flow rate on the response of the electrode lies in the pulse amperometric response of the electrode to the continuous passage of a solution that contains a uniform concentration of an analyte. The behavior of the electrode under these conditions will be from this point on referred to as pulse amperometric detection for continuous flow.

In pulse amperometry, the potential of the electrode alternates between a potential at which no electrolysis of the analyte occurs and a potential at which the electrolysis of the analyte occurs at a rate determined by the mass transport of the analyte to the surface of the electrode. The length of time at each potential varies typically from several milliseconds to several seconds, depending on the application. Unlike the amperometric response of an electrode, the response of an electrode in pulse amperometry is time-dependent as shown in Figure IV-20. Initially, after the application of the electrolyzing potential, the response of the electrode is controlled by diffusion. The analyte nearest the surface of the electrode is electrolyzed first resulting

Figure IV-20. Pulse amperometric response of a tubular electrode as a function of time

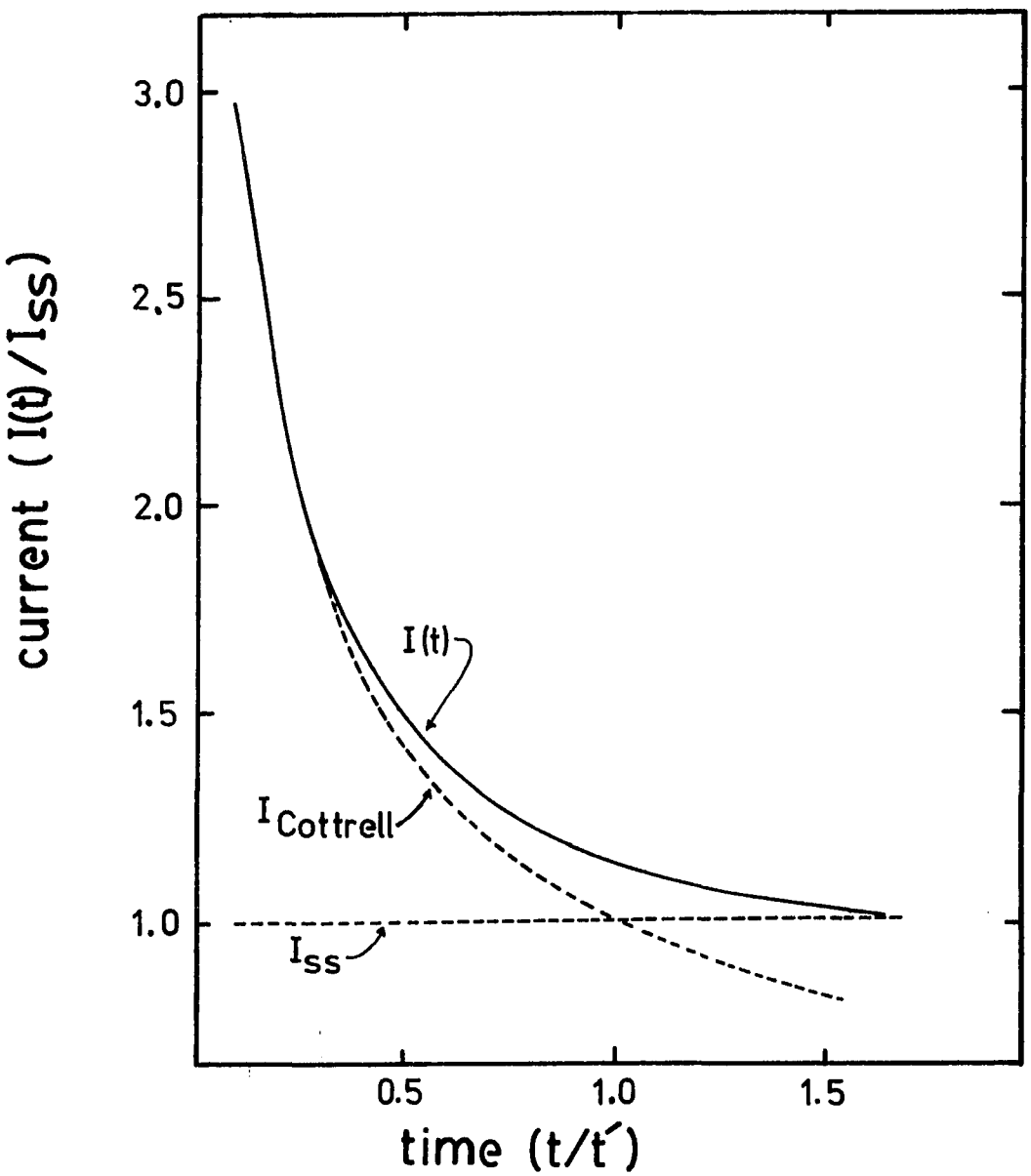
3.0
2.5
2.0
1.5
1.0
current (I(t)/Iss)
I(t)
I Cottrell
Iss
0.5
1.0
1.5
time (t/t')

in a large instantaneous flow of current. After the analyte near the surface of the electrode is depleted, analyte from the solution begins to diffuse to the surface of the electrode. As the electrolysis continues, the region of depletion, the diffusion layer, extends further and further into the solution. The current decreases as the diffusion layer grows because of the increase in the time required to transport the analyte across the diffusion layer to the surface of the electrode. The contribution of convection to the mass transport of the analyte becomes more important as the diffusion layer extends further into the fluid stream. Eventually, the rate at which convection brings the analyte to the outer boundary of the diffusion layer is equal to the rate at which diffusion carries the analyte to the surface of the electrode. At this point, a steady state is reached: The diffusion layer ceases to grow. The current of electrolysis becomes constant, i.e., independent of time, and, for a tubular electrode, is the steady-state current as described by Equation III-1. The potential of the electrode is then returned to the nonelectrolyzing potential and a uniform concentration of the analyte is once again established throughout the solution in contact with the electrode. The potential of the electrode is then stepped to the electrolyzing potential and the process described above is repeated.

The pulse amperometric response of the electrode immediately after the application of the electrolyzing potential is described by the Cottrell Equation (Equation IV-83)

$$i(t) = nFA\left(\frac{D}{\pi t}\right)^{1/2} C_o \qquad \text{(IV-83)}$$

In Equation IV-83, A is the area of the electrode (cm^2), and all other symbols have their usual significance. The Cottrell Equation was derived for linear diffusion to a planar electrode. This is a good approximation for diffusion to the walls of a tubular electrode early in the electrolysis when the radius of the electrode is much greater than the thickness of the diffusion layer. Flanagan and Marcoux (12) used the computational technique of digital simulation to study the pulse amperometric response of a tubular electrode. According to the results of their study, the Cottrell Equation describes the pulse amperometric response of a tubular electrode when $t < 0.4t'$ where t is time measured from the beginning of the electrolysis and t' is a computation parameter known as the equivalent time. t' is defined by Equation IV-84.

$$t' = 0.4259R^2L^{2/3}D^{-1/3}v_f^{-2/3} \qquad \text{(IV-84)}$$

Flanagan and Marcoux also predicted that the pulse amperometric response of a tubular electrode reaches a steady-state value at $t > 2.0t'$.

In pulse amperometry, the current is sampled at a given time after the application of the electrolyzing potential rather than monitored continuously. If the current is sampled during the time in which the Cottrell Equation is applicable, the response of the electrode will be dependent on the time at which the current is sampled and the concentration of the analyte, but will not be dependent on the flow rate.

Thus, under the conditions of continuous flow, the pulse amperometric response of an electrode is constant and independent of flow rate if the current is sampled at a set time interval soon after the initiation of the electrolyzing potential.

When pulse amperometric detection was applied to Liquid Chromatography (82) and Segmented Flow Analysis (34), the following assumption was made: If timing parameters can be chosen such that the pulse amperometric detection of a continuously flowing sample is independent of flow rate, then the response of the detector will also be independent of flow rate in applications where samples are injected into a fluid stream if the same timing parameters are used. MacDonald and Duke (34) reported that the use of pulse techniques in their experience had minimized the effect of flow rate on current measurements. Swartzfager (82) claimed that the "application of pulse techniques may remove or sharply decrease the flow rate dependence of the measured current from an electrochemical detector." A detailed study of the response of an electrode to an injected sample as a function of flow rate was offered in neither publication. MacDonald and Duke based their claim of flow-rate independence on the relative response of the electrode to periodic fluctuations in the flow rate due to the action of the peristalic pump. Their results are semi-quantitative at best and only hint at the relationship between current and flow rate without offering any substantial information. Swartzfager reported data for pulse amperometric detection for continuous flow to support his argument, but provided no data from the chromatographic

system to substantiate his claims. Actually, Swartzfager's claims are misleading. The response of his electrochemical detector was independent of flow rate only after the response of the electrochemical detector was divided by the response of a UV detector, which simultaneously monitored the eluent stream, to correct for the flow-rate dependence of the column parameters. This implies that the response of his electrode was not totally independent of the flow rate.

Experiments were conducted in this laboratory to determine if the pulse amperometric response of a tubular electrode is independent of flow rate when the electrode is used as a detector in FIA. Prior to these experiments, the assumption had been made that if the response of the electrode is independent of flow rate for the continuous flow of sample, then the response of the electrode will also be independent of flow rate in FIA. This assumption proved not to be valid in the majority of cases.

As in amperometry, the flow-rate dependence of pulse amperometric detection for continuous flow reflects changes in the sensitivity of the electrode due to changes in the thickness of the diffusion layer. When considering the response of an electrode in FIA, the effect of dispersion on the mass distribution of the sample must be considered in addition to the sensitivity of the electrode. Since changes in the flow rate affect the rate of dispersion and the residence time of the sample in the fluid stream, the response of the electrode can vary with flow rate even though the sensitivity of the electrode is constant. Hence, because of dispersion, the behavior of an electrode under the

conditions of continuous flow is not a good model for the behavior of an electrode in FIA or in other dispersive systems.

Whether or not the response of an electrode is independent of flow rate depends on the design of the flow system and on the mode of detection. If a system is designed for low dispersion, i.e., when V_S is approximately equal to V_R and v_f is large, the degree of dispersion changes very little with changes in the flow rate and the response of the electrode appears to be independent of flow rate when pulse amperometric detection is used. This is shown in Figure IV-21 where the flow-rate dependency of the response of the electrode under the conditions of continuous flow (large sample loop) is compared to the flow-rate dependence of the peak current (small sample loop). Although some variation in peak current is seen because of changes in dispersion, the response of the electrode is relatively constant especially when compared to the amperometric response shown in Figure IV-9 which, except for the mode of detection, was recorded under the same experimental conditions. The data in Figure IV-21 are from an early experiment. The values of V_S and V_R were chosen arbitrarily. It is only coincidental that the conditions were such that the pulse amperometric response for the peak currents are nearly independent of flow rate. Unfortunately, data of this nature obtained early in a study tend to reinforce erroneous ideas which lead to misconceptions when used as the basis for general conclusions.

Data for a more typical flow system are shown in Figure IV-22 as a comparison of peak currents for amperometric and pulse amperometric

Figure IV-21. Pulse amperometric detection of injected samples as a function of v_f for low dispersion

A. Continuous flow

$V_S \approx 3.0$ mL

B. Flow Injection Analysis

$V_S \approx 0.23$ mL

Parameter:

Au tubular electrode - 1/8 in x 0.031-in i.d.

E_W - Initial potential = +0.40 V vs SCE (28 ms)

Pulse potential = +0.65 V vs SCE (4 ms)

Sample time = 2 ms at +0.65 V after 2 ms delay

C_o = 1.0 mM NaI in 1.0 M H_2SO_4

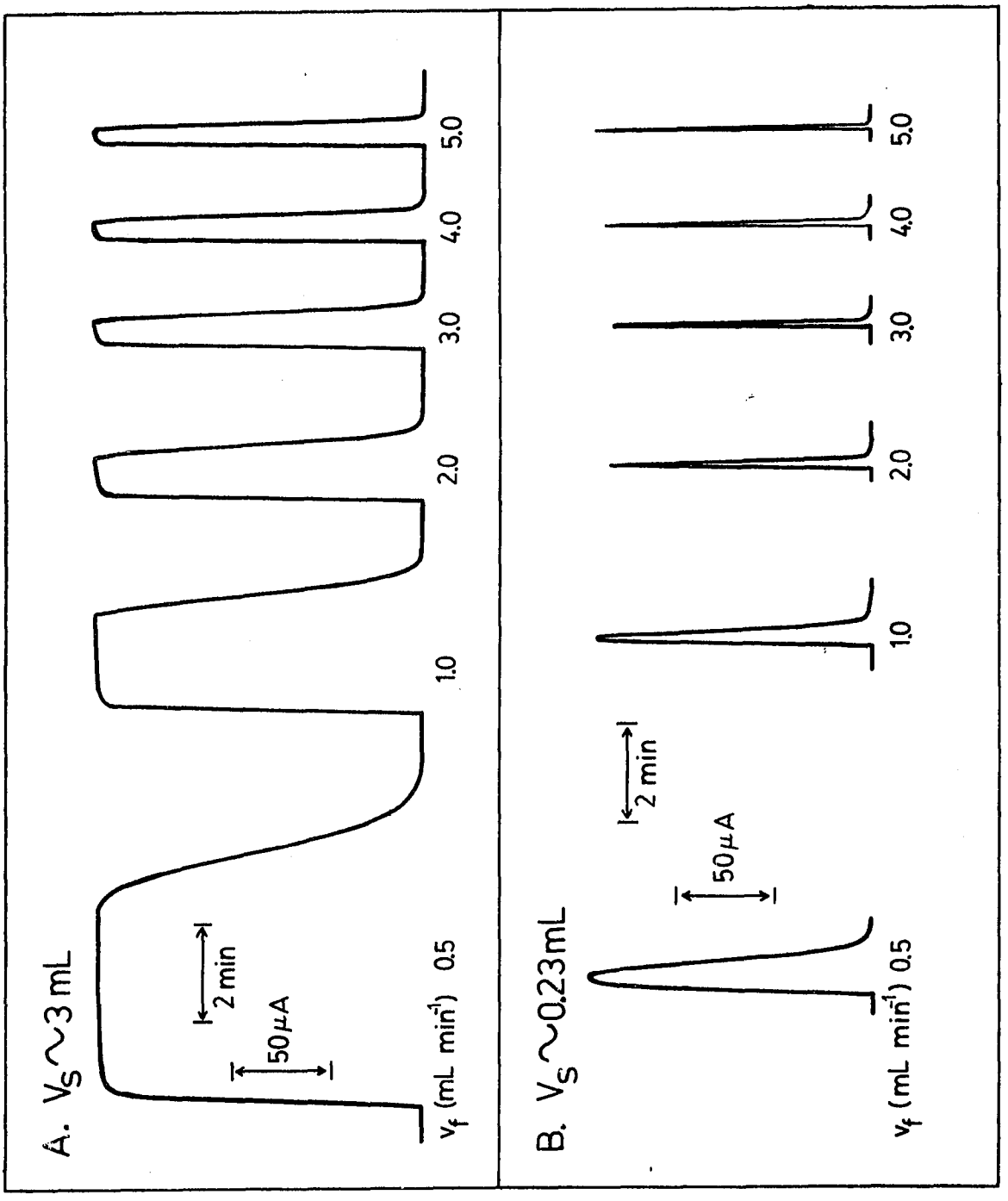
A. $V_S \sim 3$ mL
2 min
50 μA
v_f (mL min^{-1}) 0.5
1.0
2.0
3.0
4.0
5.0
B. $V_S \sim 0.23$mL
2 min
50 μA
v_f (mL min^{-1}) 0.5
1.0
2.0
3.0
4.0
5.0

Figure IV-22. Comparison of amperometric and pulse amperometric detection in FIA as a function of v_f

o - Pulse amperometric detection

● - Amperometric detection

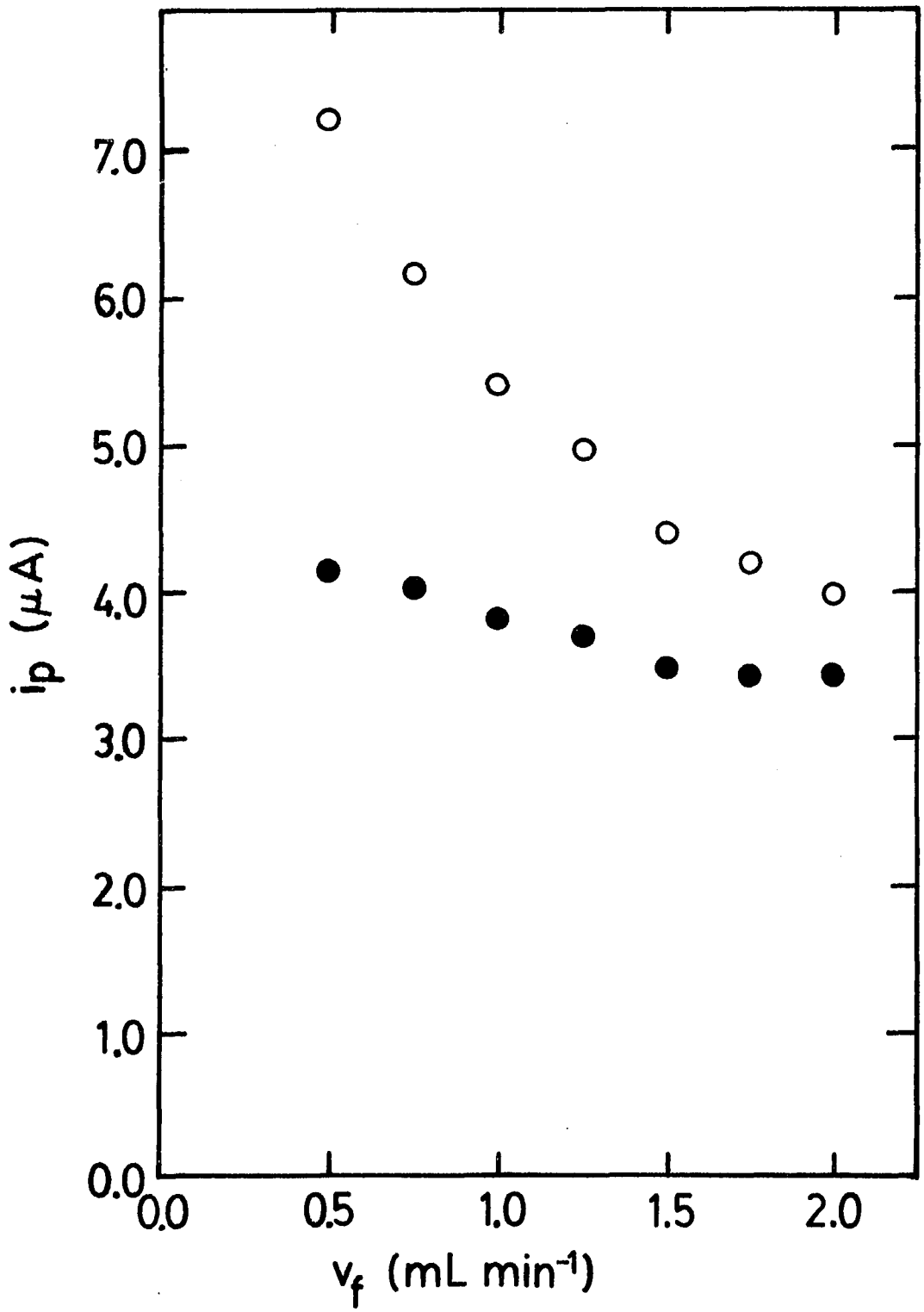
7.0
6.0
5.0
4.0
3.0
2.0
1.0
0.0
i_p (μA)
0.0
0.5
1.0
1.5
2.0
v_f (mL min^{-1})

detection. In this case, V_R was greater than V_S and v_f was moderate. Under these conditions, the pulse amperometric response of the electrode was not only more dependend on the flow rate than the amperometric response, but the amperometric response was nearly independent of flow rate at the higher values of v_f. In amperometric detection, the sensitivity of the electrode increases with increasing flow rate which tends to offset the effect of dispersion. Since the degree of dispersion can be controlled by the selection of values of V_S and V_R, and the degree of curvature, a flow system can be designed such that the amperometric response of an electrode is flow rate independent over a limited range of v_f. In pulse amperometric detection, the sensitivity of the electrode is constant; thus, the response of the electrode reflects the effect of dispersion on the mass distribution of the sample.

The results above show that the pulse amperometric response of a tubular electrode in FIA is not inherantly more independent of flow rate than the amperometric response even though the sensitivity of the electrode is independent of flow rate. The flow-rate independence of each mode of detection depends on the design of the flow system. Pulse amperometric detection tends to be independent of flow rate when the degree of dispersion is low, while amperometric detection can be independent of flow rate when the degree of dispersion is moderate to high. In all of the discussions above, the response of the electrode refers solely to the peak current. The area under the current-time curve is always dependent on flow rate regardless of the design of the flow system or the mode of detection. Although FIA was studied

specifically, the conclusion of the study also applies to the response of electrochemical detectors in Liquid Chromatography and in other dispersive systems.

E. Summary

G. I. Taylor's treatment for the dispersion of mass in a fluid stream is applied to Flow Injection Analysis for the amperometric detection of an injected sample by a flow-through, tubular electrode. Equations describing the current-time response of the electrode, $i(t)$, the maxima of the current-time curve, i_p, and the area under the current-time curve, Q_p, are derived as a function of the volume of the sample, V_S, the volume of the flow system, V_R, the flow rate of the fluid stream, v_f, the coefficient of dispersion, K, and the steady-state current, I_{ss}, for the dispersion of a sample in a straight tube under the conditions of laminar flow. Based on the results of the mathematical analysis, the following conclusions were drawn:

(1) Since the tubular electrode responds only to the concentration of the analyte close to the surface of the electrode, the effect of the nonuniform radial concentration gradient caused by dispersion must be considered when describing the current-time response of a tubular electrode.

(2) The maxima of the current-time curve, i.e., the peak current, i_p, are dependent upon the dispersion of the sample and, consequently, factors which affect the dispersion of the sample. An increase in the value of V_S increases the value

of i_p, while an increase in the value of V_R decreases the values of i_p. The relationship between i_p and v_f is complex because of the relationships between v_f and the sensitivity of the electrode, the retention time of the sample in the fluid stream, and the coefficient of dispersion. For high dispersion, i_p decreases with increasing v_f and is proportional to $v_f^{-1/6}$. For low dispersion, i_p increases with increasing v_f and is proportional to $v_f^{1/3}$. The exponents of v_f above are for limiting cases and values of the exponent between 1/3 and -1/6 are possible.

(3) The coulometric response of the tubular electrode in FIA, i.e., the area under the current-time curve, Q_p, depends on I_{ss}, V_S, and v_f, but is independent of dispersion. Q_p is proportional to V_S and $v_f^{-2/3}$.

The agreement of experimental results with theory is excellent for i(t) and i_p for moderately low values of flow rate. A comparison of an experimental current-time curve to theoretical values of i(t) shows that, as predicted by theory, the electrode responds to the concentration of the analyte at the outer boundary of the diffusion layer and not to the mean concentration of the analyte evaluated across the radius of the tube. Equations describing i_p predict the correct relationship between i_p and the parameters V_S and V_R. However, the experimental values of i_p are greater than the theoretical values of i_p for the higher values of v_f. This is attributed to the time-dependency of the coefficient of dispersion K. The effect of the time-dependency of K

on dispersion becomes apparent only when the retention time of the sample in the fluid stream is short.

The dispersion of a sample in a curved flow system was also studied, and found to be less than the dispersion of a sample in a straight flow system for the same values of V_S, V_R, and v_f. A mathematical expression for the value of K for a curved flow system is not available; however, equations for i_p for a straight flow system can be used to calculate i_p as a function of V_S and V_R for a curved flow system if an experimentally determined value of K is used in the calculation. Values of i_p as a function of v_f cannot be calculated for a curved flow system, even with an experimentally determined value of K, because the value of K is a function of v_f and no suitable general expression for K as a function of v_f has been found.

Experimental and theoretical values of Q_p are in excellent agreement. The relationship between Q_p, V_S and v_f is as predicted by theory. Experiments verify that Q_p is independent of V_R and of the curvature of the flow system which proves that Q_p is independent of dispersion. Both i_p and Q_p are linear functions of I_{ss} and, therefore, a linear function of the concentration of the sample injected. In comparing the relative merits of i_p and Q_p for analytical measurements, the ease of measurement and the error in the measurement of i_p is comparable to the ease of measurement and the error in the measurement of Q_p. The measurement of Q_p, however, is more advantageous than the measurement of i_p in that the measurement of Q_p is independent of dispersion.

Pulse amperometric detection with a tubular electrode was studied in an attempt to develop a detector whose response is independent of flow rate. The use of pulse amperometry to develop a detector whose response is independent of flow rate is not feasible in that, even though the sensitivity of the electrode is independent of flow rate in pulse amperometry, the dispersion of the sample is dependent on flow rate and affects the response of the electrode regardless of the mode of detection.

V. SUGGESTIONS FOR FUTURE WORK

At the beginning of the dispersion study, I had not anticipated the effect of the curvature of the flow system on the dispersion of the sample. The existence of the relationship between curvature and dispersion became apparent toward the end of the study; consequently, the effect of curvature on dispersion was not investigated to the extent that this important relationship should have been investigated. The change in dispersion with a change in curvature is assumed to be due to a change in the value of the coefficient of dispersion, K. For applications in FIA, the dependence of K on the flow rate of the fluid stream in a curved flow system, v_f, and on the extent of the curvature is very important in the design of the flow system. These relationships, however, are not well understood. Experiments studying K as a function of v_f and the curvature should be conducted and a mathematical expression for K in a curved flow system should be developed.

The approach used in describing the dispersion of a sample in FIA can also be adapted to Liquid Chromatography. In chromatography, the mechanism of dispersion would be different, but the process could still be described as "diffusive" in nature. K would be a function of chromatographic parameters (e.g., distribution coefficients) and parameters of the flow system (e.g., flow rate). Each component of a sample would have a value of K unique for the component for a particular column. The value of the approach described above is a more complete description of the chromatographic peak.

The theory of dispersion could also be extended to multi-sample analyses in FIA. The theory would have to be developed to include the rate of sampling and the cross-contamination of samples in the fluid stream. The extended theory could be used to predict the maximum rate of sampling for a flow rate.

VI. BIBLIOGRAPHY

1. Ruzicka, J.; Stewart J. W. B. Anal. Chim. Acta 1975, 79, 79.
2. Ruzicka, J.; Hansen, E. H. Anal. Chim. Acta 1980, 114, 19.
3. Lewis, E. C. Ph.D. Dissertation, Iowa State University, Ames, Iowa, 1977.
4. Larochelle, J. H. Ph.D. Dissertation, Iowa State University, Ames, Iowa, 1977.
5. Whitmore, J. Analog Dialogue 1974, 8, 17.
6. Koile, R. C. Ph.D. Dissertation, Iowa State University, Ames, Iowa, 1979.
7. Blaedel, W. J.; Iverson, D. G. Anal. Chem. 1977, 49, 1563.
8. Levich, V. G. "Physiochemical Hydrodynamics"; Prentice Hall: Englewood Cliffs, New Jersey, 1962; pp 112-116.
9. Blaedel, W. J.; Olson, C. L.; Sharma, L. R. Anal. Chem. 1963, 35, 2100.
10. Blaedel, W. J.; Klatt, L. N. Anal. Chem. 1966, 38, 879.
11. Blaedel, W. J.; Boyer, S. L. Anal. Chem. 1973, 45, 258.
12. Flanagen, J. B.; Marcoux, L. J. Phys. Chem. 1974, 78, 718.
13. Aoki, K.; Matsuda, H. J. Electroanal. Chem. 1978, 94, 157.
14. Blaedel, W. J.; Yim, Z. Anal. Chem. 1978, 50, 1722.
15. Sharma, L. R.; Dutt, J. Indian J. Chem. 1968, 6, 593.
16. Sharma, L. R.; Dutt, J. Indian J. Chem. 1969, 7, 485.
17. Sharma, L. R.; Dutt, J. Indian J. Chem. 1970, 8, 170.
18. Blaedel, W. J.; Iverson, D. G. Anal. Chem. 1976, 48, 2027.
19. Blaedel, W. J.; Iverson, D. G. Anal. Chem. 1977, 49, 523.
20. Pungor, E.; Feher, Zs.; Nagy, G. Anal. Chim. Acta 1970, 51, 417.
21. Feher, Zs.; Pungor, E. Anal. Chim. Acta 1974, 71, 425.

22. Oesterling, T. O.; Olson, C. L. Anal. Chem. 1967, 39, 1543.

23. Blaedel, W. J.; Olson, C. Anal. Chem. 1964, 36, 343.

24. Easty, D. B.; Blaedel, W. J.; Anderson, L. Anal. Chem. 1971, 43, 509.

25. Bomstein, J.; Shepp, J. M.; Dawson, S. T.; Blaedel, W. J. J. Pharm. Sci. 1966, 55, 94.

26. Mason, W. D.; Olson, C. L. Anal. Chem. 1970, 42, 548.

27. Seitz, W. R.; Jones, R.; Klatt, L. N.; Mason, W. D. Anal. Chem. 1973, 45, 840.

28. Lieberman, S. H.; Zirino, A. Anal. Chem. 1974, 46, 20.

29. Blaedel, W. J.; Boyer, S. L. Anal. Chem. 1971, 43, 1538.

30. Mason, W. D.; Olson, C. L. Anal. Chem. 1970, 42, 488.

31. Andrews, R. W.; Johnson, D. C. Anal. Chem. 1976, 48, 1056.

32. Davenport, R. J.; Johnson, D. C. Anal. Chem. 1974, 46, 1971.

33. Lewis, E. C.; Johnson, D. C. Clin. Chem. 1978, 24, 1711.

34. MacDonald, A.; Duke, P. D. J. Chromatogr. 1973, 83, 331.

35. Armentrout, D. N.; McLean, J. D.; Long, M. W. Anal. Chem. 1979, 51, 1039.

36. Stulik, K.; Pacakova. V. J. Chromatogr. 1980, 192, 135.

37. Morris, V. L. M.S. Thesis, Iowa State University, Ames, Iowa, 1976.

38. Maitoza, P. Ph.D. Dissertation, Iowa State University, Ames, Iowa, 1980.

39. Stulik, K.; Hova, V. J. Electroanal. Chem. 1976, 70, 253.

40. Snider, B. G.; Johnson, D. C. Anal. Chim. Acta 1979, 105, 25.

41. Lindstrom, T. R. Ph.D. Dissertation, Iowa State University, Ames, Iowa, 1980.

42. Andrews, R. W. Ph.D. Dissertation, Iowa State University, Ames, Iowa, 1975.

43. Davenport, R. J. Ph.D. Dissertation, Iowa State University, Ames, Iowa, 1974.

44. Snider. B. G.; Johnson, D. C. Anal. Chim. Acta 1979, 106, 1.

45. Karger, B. L.; Snyder, L. R.; Horvath, C. "An Introduction to Separation Science"; Wiley-Interscience: New York, New York, 1973; Chapter 5.

46. Johnson, E. L.; Stevenson, R. "Basic Liquid Chromatography"; Varian Associates, Inc.: Palo Alto, California, 1978; Chapter 2.

47. Ruzicka, J.; Hansen, E. H. Anal. Chim. Acta 1978, 99, 37.

48. Betteridge, D. Anal. Chem. 1978, 50, 832A.

49. Snyder, L. R. Anal. Chim. Acta 1980, 114, 3.

50. Poppe, H. Anal. Chim. Acta 1980, 114, 59.

51. Tijssen, R. Anal. Chim. Acta 1980, 114, 71.

52. van der Berg, J. H. M.; Deelder, R. S.; Egberink, H. G. M. Anal. Chim. Acta 1980, 114, 91.

53. Reijn, J. M.; van der Linden, W. E.; Poppe, H. Anal. Chim. Acta 1980, 114, 105.

54. Gill, W. N.; Sankarasubramanian, R. Proc. R. Soc. London, Ser. A 1970, 316, 341.

55. Bournia, A.; Coull, J.; Houghton, G. Proc. R. Soc. London, Ser. A 1961, 261, 227.

56. Evans, E. V.; Kenney, C N. Proc. R. Soc. London, Ser. A 1965, 284, 540.

57. Gill, W. N.; Ananthakrishnan, V. AIChE J. 1967, 13, 801.

58. Taylor, G. I. Proc. R. Soc. London, Ser. A 1953, 219, 186.

59. Taylor, G. I. Proc. R. Soc. London, Ser. A 1954, 223, 446.

60. Taylor, G. I. Proc. R. Soc. London, Ser A 1954, 225, 473.

61. Lighthill, M. J. J. Inst. Maths. Applics. 1966, 2, 97.

62. Caro, C. G. J. Physiol. 1966, 185, 501.

63. Bate, H.; Rowlands, S.; Sirs, J. A.; Thomas, H. W. Brit. J. Appl. Phys., Ser. 2 1969, 2, 1447.

64. Bate, H.; Rowlands, S.; Sirs, J. A. J. Appl. Physiol. 1973, 34, 866.

65. Levenspeil, O.; Smith, W. K. Chem. Eng. Sci. 1957, 6, 227.

66. Levenspeil, O. Ind. Eng. Chem. 1958, 50, 343.

67. Aris, R. "Introduction to the Analysis of Chemical Reactors"; Prentice Hall: Englewood Cliffs, New Jersey, 1965; pp 297-303.

68. Levenspeil, O. "Chemical Reaction Engineering", 2nd ed.; John Wiley & Sons: New York, New York, 1972; Chapter 9.

69. Froment, G. F.; Bischoff, K. B. "Chemical Reactor Analysis and Design"; John Wiley & Sons: New York, New York, 1979; pp 617-630.

70. Golay, M. J. E. In "Gas Chromatography 1958"; Desty, D. H., Ed.; Academic Press: New York, New York, 1958; pp 36-53.

71. Hofman, K.; Halasz, I. J. Chromatogr. 1979, 173, 211.

72. Halasz, I. J. Chromatogr. 1979, 173, 229.

73. Crank, J. "The Mathematics of Diffusion"; Clarendon Press: Oxford, England, 1956; pp 9-14.

74. Bailey, H. R.; Gogarty, W. B. Proc. R. Soc. London, Ser. A 1962, 259, 352.

75. Ananthakrishnan, V.; Gill, W. N ; Barduhn, A. J. AIChE J. 1965, 11, 1063.

76. Gill, W. N.; Ananthakrishnan, V. AIChE J. 1966, 12, 906.

77. Aris, R. Proc. R. Soc. London, Ser. A 1956, 235, 67.

78. Gill, W. N. Chem. Eng. Sci. 1967, 22, 1013.

79. Erdogan, M. E.; Chatwin, P. C. J. Fluid Mech. 1967, 29, 465.

80. Nunge, R. J.; Lin, T.-S.; Gill, W. N. J. Fluid Mech. 1972, 34, 363.

81. Weast, R. C., Ed. "Handbook of Chemistry and Physics", 49th ed.; The Chemical Rubber Co.: Cleveland, Ohio, 1968; p A-228, No. 529.

82. Swartzfager, D. G. Anal. Chem. 1976, 48, 2189.

VII. ACKNOWLEDGEMENTS

"Knowledge is good."
Emil Faber
The National Lampoon's Animal House Book

The experience of graduate school can at times be trying. It was at those times when the inspirational words expressed above gave me the courage, direction, and drive to continue.

I wish to thank Dr. Dennis C. Johnson for his help and guidance throughout my graduate studies. One of Dennis' greatest virtues is probably patience. To varying degrees, a graduate student becomes a paranoid schizophrenic at some point in his career and the major professor receives the brunt of the student's aberrant behavior. I was no exception. All I can say is "I'm glad you didn't take it personally, Denny."

The financial support through grants GP-40646X and CHE 76-17826 from the National Science Foundation, a summer grant from the Pine Instrument Co., and funds from the Graduate College are gratefully acknowledged. The nontraditional financial support I received from Mr. Nick's, the Ames Country Club, Palmas Restaurant & Lounge, Stumpy's Lounge, and several American Legion posts in central Iowa is also appreciated.

The people that follow are the supporting cast. I mean, of course, the group responsible for my emotional support. First of all, I am grateful to my wife, Jean, for her patience and understanding. She has earned this degree as much as I have. I thank my parents, Peter and

Anna, for their support. I have always found comfort in their love and concern for me. A note of appreciation goes to my sister, Maryann, who has shared the experience of graduate school with me and from whom I have learned about myself. I would also like to thank Gwynn and Archie Coyle for giving me a family in Ames. They are dear people who have made my stay in Ames more pleasant and are mentioned here because I promised to get their names into this thesis.

My last thanks go to all the graduate students and members of the staff, past and present, who have shared the experience of graduate school with me. The number of friends I have made during graduate school is too numerous to mention here, but the times spent with them are the most cherished memories I have of Iowa State University.